DEFENCE S&T TECHNICAL BULLETIN

VOL. 8 NUM. 2 YEAR 2015 ISSN 1985-6571

CONTENTS

Classification of Airborne Radar Signals Based on Pulse Feature Estimation Using Time-Frequency Analysis 103 - 120
Ashraf Adamu Ahmad & Ahmad Zuri Sha'ameri

Evaluation of the Accuracy of Global Positioning System (GPS) Speed Measurement via GPS Simulation 121 - 128
Dinesh Sathyamorthy, Shalini Shafii, Zainal Fitry M Amin, Asmariah Jusoh & Siti Zainun Ali

A Review of Electrodeposition Techniques and Variables for Production of Nickel-Cobalt / Alumina (Ni-Co/Al_2O_3) Composite Coatings 129 - 140
Nik Hassanuddin Nik Yusoff, Othman Mamat & Mahdi Che Isa

A Review of Soot Particle Measurement in Lubricating Oil 141 - 152
Fadzli Ibrahim, Wan Mohd Faizal Wan Mahmood, Shahrir Abdullah & Mohd Radzi Abu Mansor

The Importance of Forensic Microbiology in CBRNe Investigations 153 - 161
Gian Marco Ludovici, Orlando Cenciarelli, Mariachiara Carestia, Andrea Malizia, Annalaura Tamburrini, Valentina Gabbarini, Alessandro Sassolini, Daniele Di Giovanni, Sandro Mancinelli, Leonardo Palombi, Pasquale Gaudio, Carlo Bellecci & Teresa Rinaldi

STRIDE

SCIENCE & TECHNOLOGY RESEARCH INSTITUTE FOR DEFENCE

AIMS AND SCOPE

The Defence S&T Technical Bulletin is the official technical bulletin of the Science & Technology Research Institute for Defence (STRIDE). The bulletin, which is indexed in, among others, Scopus, Index Corpenicus, ProQuest and EBSCO, contains manuscripts on research findings in various fields of defence science & technology. The primary purpose of this bulletin is to act as a channel for the publication of defence-based research work undertaken by researchers both within and outside the country.

WRITING FOR THE DEFENCE S&T TECHNICAL BULLETIN

Contributions to the bulletin should be based on original research in areas related to defence science & technology. All contributions should be in English.

PUBLICATION

The editors' decision with regard to publication of any item is final. A manuscript is accepted on the understanding that it is an original piece of work that has not been accepted for publication elsewhere.

PRESENTATION OF MANUSCRIPTS

The format of the manuscript is as follows:

a) Page size A4
b) MS Word format
c) Single space
d) Justified
e) In Times New Roman ,11-point font
f) Should not exceed 20 pages, including references
g) Texts in charts and tables should be in 10-point font.

Please e-mail the manuscript to:

1) Dr. Dinesh Sathyamoorthy (dinesh.sathyamoorthy@stride.gov.my)
2) Dr. Mahdi bin Che Isa (mahdi.cheisa@stride.gov.my)

The next edition of the bulletin (Vol. 9, Num 1) is expected to be published in April 2016. The due date for submissions is 17 February 2016. **It is strongly iterated that authors are solely responsible for taking the necessary steps to ensure that the submitted manuscripts do not contain confidential or sensitive material.**

The template of the manuscript is as follows:

TITLE OF MANUSCRIPT

Name(s) of author(s)

Affiliation(s)

E-mail:

ABSTRACT

Contents of abstract.

Keywords: *Keyword 1; keyword 2; keyword 3; keyword 4; keyword 5.*

1. TOPIC 1

Paragraph 1.

Paragraph 2.

1.1 Sub Topic 1

Paragraph 1.

Paragraph 2.

2. TOPIC 2

Paragraph 1.

Paragraph 2.

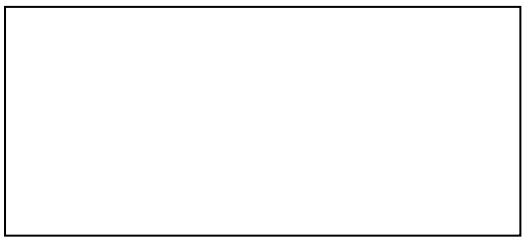

Figure 1: Title of figure.

Table 1: Title of table.

Content	Content	Content
Content	Content	Content
Content	Content	Content
Content	Content	Content

Equation 1 (1)
Equation 2 (2)

REFERENCES

Long lists of notes of bibliographical references are generally not required. The method of citing references in the text is 'name date' style, e.g. 'Hanis (1993) claimed that...', or '…including the lack of interoperability (Bohara *et al.*, 2003)'. End references should be in alphabetical order. The following reference style is to be adhered to:

Books

Serra, J. (1982). *Image Analysis and Mathematical Morphology*. Academic Press, London.

Book Chapters

Goodchild, M.F. & Quattrochi, D.A. (1997). Scale, multiscaling, remote sensing and GIS. *In* Quattrochi, D.A. & Goodchild, M.F. (Eds.), *Scale in Remote Sensing and GIS*. Lewis Publishers, Boca Raton, Florida, pp. 1-11.

Journals / Serials

Jang, B.K. & Chin, R.T. (1990). Analysis of thinning algorithms using mathematical morphology. *IEEE T. Pattern Anal.*, **12**: 541-550.

Online Sources

GTOPO30 (1996). *GTOPO30: Global 30 Arc Second Elevation Data Set*. Available online at: http://edcwww.cr.usgs.gov/landdaac/gtopo30/gtopo30.html (Last access date: 1 June 2009).

Unpublished Materials (e.g. theses, reports and documents)

Wood, J. (1996). *The Geomorphological Characterization of Digital Elevation Models*. PhD Thesis, Department of Geography, University of Leicester, Leicester.

CLASSIFICATION OF AIRBORNE RADAR SIGNALS BASED ON PULSE FEATURE ESTIMATION USING TIME-FREQUENCY ANALYSIS

Ashraf Adamu Ahmad[1] & Ahmad Zuri Sha'ameri[2*]

[1]Department of Electrical and Electronic Engineering, Federal University of Technology, Nigeria
[2]Faculty of Electrical Engineering, Universiti Teknologi Malaysia (UTM), Malaysia

[*]E-mail: zuri@fke.utm.my

ABSTRACT

This paper describes the realization of an airborne radar signal type analysis and classification (ARTAC) system that uses spectrograms to obtain time-frequency representation ((t,f) representation) and then apply the related analysis tools, such as the instantaneous energy and frequency, and time-frequency marginal, to estimate the various signal characteristics. The estimated parameters are used as input to a rule-based classifier that classifies the signal appropriately. Monte-Carlo simulation is then conducted to quantify the accuracy of signal classification at various signal-to-noise ratios (SNRs) in additive white Gaussian noise (AWGN). The methodology used achieves 90% classification accuracy at SNR of 6 dB irrespective of the identity of the signal. The performance and computational complexity (CC) of the system are also addressed in an electronic support (ES) operating scenario.

Keywords: *Airborne radar signal type analysis and classification (ARTAC) system; time-frequency representation ((t,f) representation); spectrogram; Monte-Carlo simulation; low probability of intercept (LPI) radar.*

1. INTRODUCTION

Electronic support (ES) is a part of electronic warfare (EW) that deals with signal interception in order to determine the adversary's electromagnetic order of battle (EOB) (Neri, 2006). Besides communications, ES also covers the estimation and classification of radar signals. This paper focuses on airborne radars that operate at frequency range of 8 to 12 GHz (X-band), and typically used as weapon control and weather radars by military and civil aviation aircrafts respectively. Most radar systems have pulses that are modulated at the carrier frequency. A radar signal can be characterized by its carrier frequency, pulse repetition period (PRP) and pulse width (PW). Advanced radar systems use radar pulses of different pulse repetition frequencies (PRFs), also known as staggered pulses, with pulse compression to improve the ability to detect a moving target in clutter for air surveillance applications, improve range resolution, prevent of eclipsed received signal, achieve low probability of intercept (LPI), and protect against electronic attack (EA) (Wiley, 2006). Recent trends include metric deduction of LPI waveforms (Barker coded pulse inclusive) (Fancy & Alabaster, 2010), and the use of Costas code for modern radar and multi-input multi-output (MIMO) radar waveform design (Galati & Pavan, 2013).

Due to the low peak transmit power of the LPI radar, the probability of detection typically through the side lobe of the transmitting antenna is diminished and as such, advanced signal analysis techniques have to be adopted. Time-frequency analysis is identified for this purpose due to its ability to analyze signals at low signal-to-noise ratio (SNR) (Wiley, 2006; Pace, 2009). In this paper, spectrograms are used to obtain time-frequency representation ((*t*,*f*) representation) due to its low computational complexity (CC) as compared to the Wigner-Ville distribution (WVD) and quadratic time-frequency distribution (QTFD) (Boashash, 2015). This is important for platforms with payload such as an aircraft. A detailed discussion on the CC for the various time-frequency distributions can be found in

Chee *et al*. (2012). Provided that the compromise between time and frequency resolution is clearly addressed, spectrograms can provide reasonable accuracy with a reduction in the CC by about four times as compared to QTFD. Furthermore, spectrograms do not introduce cross-terms that could result in misinterpretations of the true signal characteristics. Recent studies on the use of spectrograms for analysis of radar signals include the use of the L-statistic method on the spectrogram as part of an algorithm for micro-Doppler (m-D) effect removal in radar imaging analysis (Stankovic *et al*., 2013), extension of slanted spectrograms to non-harmonic synthetic aperture radar (SAR) chirp analysis (Agcaoglu *et al*., 2013), and spectrograms used in conjunction with the cepstrogram for discrimination of birds and small unmanned aerial vehicles (UAVs) (Harmanny *et al.*, 2014).

Since radar signals are time-varying in amplitude, frequency and phase, time-frequency analysis methods such as spectrograms provides accurate representation for these signals. Once the (t,f) representation is obtained, the instantaneous energy and frequency, and other related analysis tools can be derived directly from this representation without using other methods, such as the time series or spectrum analyses, to estimate the parameters of the radar signals. Next, the estimated parameters are used as input to a rule-based classifier. The paper is organized as follows: an overview of electronic support, signal models, and followed by the relevant fundamental theories and the realization of an airborne radar signal type analysis and classification (ARTAC) system. Lastly, various results to verify the system performance are presented at various SNRs, operational scenarios and CC, followed with the concluding remarks.

2. ELECTRONIC SUPPORT (ES)

ES together with EA and electronic protection (EP) form the pillars of EW. ES' primary function is to acquire and derive information or intelligence from the interception and identification of radiated electromagnetic energy, and also to determine the threat level, which forms the basis for further course of action (Adamy, 2001). The radiated electromagnetic energy could be information bearing from communications systems or non-information bearing such as radar. The use of ES systems could be either strategic or tactical: a strategic system considers the collection of intelligence with emphasis on accuracy over a long term (Neri, 2006); while a tactical system covers a short term for the on field command and is usually integrated as part of a weapon system (Elsworth, 2010). The block diagram of an ES system is as shown in Figure 1 and covers the basic functions, including antenna system, emitter locating, parameter estimation, classification, and signal storage and retrieval (Sha'ameri & Boashash, 2015).

Further details on the basic functions of an ES system can be described as follows:

1. Emitter locating – this is the main part of the system that determines the location of an airborne radar based on its emission. Among the basic methods used are angle of arrival estimation (AOA) (Poisel, 2012) and time-delay of arrival estimation (TDOA) (Sha'ameri *et al*., 2015). A single AOA estimate only provides direction, but combining the AOA estimates from multiple sites by triangulation (Poisel, 2012) enables position estimation of the airborne radar. The implementation of TDOA allows position estimation in 2D or 3D, with the availability of the appropriate number of receivers, high transmit power and large receiver separation (Sha'ameri *et al*., 2015).
2. For ES operations that relate to radar, the wide frequency coverage from 1 to 18 GHz requires an antenna system that receives all the signals and a radio frequency (RF) front end that allows simultaneous analysis of all the received signals. The solution is provided by using the channelized receivers (Tsui, 2004) that form the RF front of most ES systems.
3. Once the signal is downconverted to the intermediate frequency or demodulated to video, the signal processing stage of the ES system performs two types of pulse feature analysis: inter-pulse and intra-pulse analyses. Inter-pulse analysis is used to determine the timing parameters

of the signal, such as pulse width (PW) and pulse repetition period (PRP) (Wiley, 2006). Intra-pulse analysis estimates the parameters of the signal within a PW: frequency and phase.

4. The parameters estimated at the signal processing stage are then used as input to a classifier (Tan *et al.*, 2010). By matching the received parameters with the signal database, also referred to as the threat library, the classifier can determine if the received signal is a friendly, foe or unknown.
5. The decision stage is when the operator decides on the next course of action based on the output from the classifier. Possible courses of action could be to investigate further, update the signal database or activate countermeasures if the ES system is used at tactical level.
6. The signal database contains all the possible information that describes the airborne radar from the signal parameters classified from the received signal and other sources, the electronic order of battle (EOB), and the geographic information system (GIS).

The scope of this paper covers the 'signal processing' component of the ES system and targets signal sources that come from airborne radars.

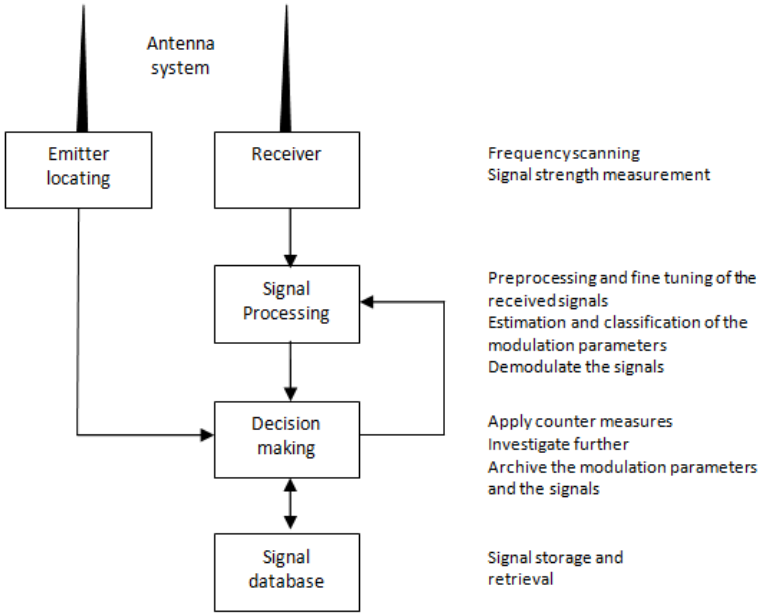

Figure 1: Block diagram of an ES system (Sha'ameri & Boashash, 2015).

3. RADAR SIGNAL PARAMETERS

The term airborne radar used in this paper refers to weapon control and weather radars used by military and civil aviation aircrafts respectively. Due to the limited space on board the aircraft, the transmit power ranges from 500 (Fred, 2010) to 20,000 W (Kopp, 2008), typically in the X-band. Unlike air defense and traffic control radars that operate at lower frequencies of 1 to 2 GHz (L-band) or 2 to 4 GHz (S-band), the higher band allows for the design of smaller antennas and lightweight RF systems (Skolnik, 2008). Also out of the scope of this paper are airborne warning and control system (AWACS) aircrafts, which forms a minority of aircrafts in use. The transmit power is in the order 1 MW with operating frequencies in the S-band (E-3 Sentry, 2015).

On most military aircrafts, the ES systems are often referred to as radar warning receivers (RWR) (Neri, 2006), whose objective is to perform fast threat detection that links to countermeasures (jammer or flares) to protect the aircraft. Specifically designed aircrafts, such as the RC 135 Rivet Joint, performs the ES operations at the strategic level where the emphasis is to provide precise technical

analysis of all signals both radar and communications. Besides being utilized for intelligence gathering, the ES systems can be used to complement existing air defense radar infrastructure to detect airborne threats (Sha'ameri *et al.*, 2015). The passive nature of the ES systems makes it invulnerable to detection and from being disabled by anti-radiation weapons. Since the ES systems are complex, as shown in Figure 1, the paper focuses on the 'signal processing' module of the system.

It is convenient to process the signals at either the intermediate frequency or at the baseband (the alternate term used for radar is video) due to advances in microelectronic and computer technology. The signal received at the X-band by the antenna system and the RF front end is down-converted to the intermediate frequency where the signal is sampled at the Nyquist rate. A sampling frequency of 40 MHz is assumed for an intermediate frequency of 10 MHz and maximum bandwidth of 20 MHz. The selection of the sampling and intermediate frequencies is based on the availability of an off-the-shelf platform suitable to implement an ES system (Keysight, 2015). The signal parameters selected for this paper are shown in Table 1. The first three signal types are defined based on pulse compression techniques (Levanon & Mozeson, 2004), while the latter two are simple pulse modulated signals. Airborne radars for weapon control systems and weather radars normally cover ranges of less than 150 km corresponding to PRP of less than 400 μs (Skolnik, 2008). The chirp ratio (α) of the linear FM pulse (LFM) is derived from the bandwidth (BW) and PW, while the Costas coded pulse (CCP) and phase coded pulse (PCP) are coded based on the eight-length Costas code and seven-length Barker code respectively. Both the simple modulated pulse (SiP) and staggered modulated pulse (StP) have the same modulation, except the latter has two PRPs. In general, all the signals are assumed to have a duty cycle (PW/PRP) range from 0.02 to 0.12. Current generation LPI radars such as the active electronically scanned array (AESA) radars have large duty cycle as compared to conventional radars, which allows for reduction in peak transmit power while maintaining similar probability of detection (Pace, 2009).

Table 1: Airborne radar signal parameters.

Signal Type	Frequency Parameters (MHz)	Time Parameters (μs)	Equations
Linear FM pulse (LFM)	f_{min}=2, BW=15	PW= 2 PRP=100	$x(t) = \cos\left(2\pi\left(f_{\min} + \frac{\alpha t}{2}\right)t\right)$ $\alpha = \frac{BW}{PW}$
Costas coded pulse (CCP)	8 frequencies f_{min}=5, f_{max}=13.75 f_{dev}=1.25	PW= 12.8 PRP= 100	$x(t) = \cos(2\pi f_m t)$ $f_m=f_{min}+kf_{dev}$ k=0,1,2....7
Phase coded pulse (PCP)	f_c=10	PW=2.8 PRP=100	$x(t) = \cos(2\pi f_c t + \phi_k)$ ϕ_k=0, k=3,4,6 $f_k = \pi$, k=0,1,2,5
Simple modulated pulse (SiP)	f_c=10	PW=1 PRP=50	$x(t) = \cos(2\pi f_c t)$
Staggered modulated pulse (StP)	f_c= 10	PW=1 PRP1=50 PRP2= 200	$x(t) = \cos(2\pi f_c t)$

Note : f_c-frequency of the signal down-converted to the intermediate frequency, f_{min}-minimum frequency, f_{max}-maximum frequency, f_{dev}-deviation frequency which the frequency difference between each frequency component, ϕ_k-the k^{th} phase component for a phase modulated signal, PRP1-first PRP, PRP2-second PRP.

Assuming that the signal is received by the antenna and then down-converted to intermediate frequency by the RF front end, the received signal is modelled as follows:

$$y(t)=x(t) + v(t) \quad (1)$$

where $x(t)$ is the airborne radar signal whose parameters are defined in Table 1, and $v(t)$ is the interference that is modelled as an additive white Gaussian noise (AWGN) with zero mean and unity variance. Sources of noise in radars systems could be thermal noise and other sources of unwanted signals, which under the worst case condition are best assumed as AWGN (Ziemer & Peterson, 2001). Noise in general introduces error in the estimation of signal parameters that subsequently results in misclassification of received signals.

Target detection from radar emission by an ES system offers a potential advantage over an air defense radar. This is because the path loss for the former is inversely proportional to the distance d^2 as compared to the later at distance d^4. Assuming the same noise floor, antenna gain, transmit power and radar cross section, the ES system could detect the target at a relatively further distance as compared to the air defense radar (Wiley, 2006). With the introduction of a LPI radar, it is possible to reduce the transmit power and with a subsequent reduction in the received signal level from either the side or back lobe of the radar transmitting antenna. The ES system has to receive signals at very close to the noise floor, and at low SNR negating the advantage in propagation loss that the ES system has over the air defense radar. Hence, the quality of the RF front end has to be improved with noise reduction and more robust processing of signals in noise. Relevant to the scope of this paper, time-frequency analysis methods have been proven to provide improved parameter estimation of signals in noise (Boashash, 2015). Furthermore, radar signals are time-varying, which means that time-frequency analysis methods provide accurate representation of signals as compared to spectrum estimation or time-series analysis.

4. RELEVANT FUNDAMENTAL THEORY

Time-frequency analysis based on spectrograms is the main method used in the ARTAC system. This section explains its fundamental theory, properties, and relationship to other signal estimation methods such as the autocorrelation and power spectrum.

4.1 Spectrogram

Consider an analytical signal $x(t)$ and a real and even window $w(t)$, a spectrogram (Boashash, 2015) is defined as:

$$S_x^w(t, f) = \left| \int_{-\infty}^{\infty} w(\tau - t) x(\tau) e^{-j2\pi f\tau} d\tau \right|^2 \quad (2)$$

The analytical signal is the complex version of the received signal. It is used in time-frequency analysis to improve the (t,f) representation by reducing artifacts and cross terms (Boashash, 2015).

Together with the Wigner-Ville distribution, spectrograms are the most basic method to implement time-frequency analysis. The origin of most time-frequency distributions can be traced to either one of the two distributions. Provided that the window function is carefully setup, spectrograms can provide a reasonably accurate (t,f) representation with no artifacts or cross terms at low computational complexity. In the ARTAC system, spectrograms are used to perform the intra-pulse analysis.

4.2 Instantaneous Energy (IE)

IE is used in the inter-pulse analysis of the system in order to determine the time parameters of the incoming radar signal. For the analytical signal, IE estimation is given by:

$$E_x(t) = x(t)x^*(t) \tag{3}$$

where * denotes the conjugate of the signal. The total energy can be obtained by:

$$E_x = \int_{-\infty}^{\infty} E_x(t)dt \tag{4}$$

Besides the direct estimation of IE as shown in Equation 2, IE can also be estimated from the time-marginal of the (*t*,*f*) representation as follows (Boashash, 2015):

$$E_x(t) = \int_{-\infty}^{\infty} S_x^w(t, f)df \tag{5}$$

Between the two methods, the direct IE estimation in Equation 3 is less complex as compared to estimation from the time-marginal as shown in Equation 5. The interval between each modulated pulse defined by the PRP is bigger than the PW, but it has zero energy and carries no information. However, the time samples of the PRP have to be maintained to represent the temporal characteristics of the signal. Thus, the lower CC is the reason for using the direct IE estimation over the time-marginal to perform the inter-pulse analysis.

4.3 Instantaneous Frequency (IF)

IF is presented in Boashash (2015) to characterize non-stationary signals. In this paper, IF is estimated from the (*t*,*f*) representation for intra-pulse analysis to reduce the CC by converting a 3D representation to a 2D representation for further analysis. The IF of mono-component signal estimated from the peak of the (*t*,*f*) representation is (Boashash, 2015):

$$f_i(t) = \max_f[S_x^w(t, f)] \qquad 0 \le t \le T \tag{6}$$

where *T* is the duration of the signal. Current work has shown that IF estimated from the (*t*,*f*) representation is efficient where the estimation error variance meets the theoretical limit defined by the Cramer Rao lower bound (CRLB) at SNR above 0 dB (Chee *et al*., 2014).

4.4 Time-Frequency Marginals and Autocorrelation Function

From the (*t*,*f*) representation, the power spectrum and IE can be estimated from the frequency and time marginals respectively. The estimation of IE from the time-marginal is defined previously in Equation 5. Normally, the power spectrum of a signal is estimated from the time-representation by using the Fourier transform (Peebles, 2001). Since the (*t*,*f*) representation is already available, it is not cost effective from a computational perspective to recalculate the power spectrum from the time representation. The availability of the frequency marginal is used to estimate the power spectrum from the (*t*,*f*) representation. Thus, the power spectrum can be obtained as follows (Boashash, 2015):

$$S_{xx}(f) = \int_{-\infty}^{\infty} S_x^w(t, f)dt \tag{7}$$

The autocorrelation function compares a signal with a time delayed version of itself. It simplifies the analysis of random signals by producing a deterministic representation. This requirement is needed for the ARTAC system to differentiate a pulse radar signal from a phase modulated radar signal. Instead

of deriving the autocorrelation function from the time representation (Peebles, 2001), the Wiener-Khinchine theorem applied to the power spectrum in Equation 7 produces the autocorrelation function:

$$R_{xx}(\tau) = \int_{-\infty}^{\infty} S_x(f) e^{j2\pi f\tau} df \tag{8}$$

The theoretical foundations described in this section enable the estimation of the power spectrum and autocorrelation function from the (*t*,*f*) representation required to perform the intra-pulse analysis. Although IE can be derived from the time-marginal of the (*t*,*f*) representation, direct estimation of IE from the time-representation is used due to the lower CC.

5. REALIZATION OF THE ARTAC SYSTEM

The use of time-frequency distribution for signal classification was reported in Lunden & Koivunen (2007) and Tan & Sha'ameri (2008a). The adaptive smooth-windowed Wigner-Ville (SWWVD) with rule-base classifier achieved 90% classification accuracy at minimum SNR of 4dB (Tan & Sha'ameri, 2008b). The Wigner-Ville and Choi-Williams time-frequency distributions are deployed to extract features from eight compression radar waveforms, which are used as input for a supervised classification system (Lunden & Koivunen,2007). The system achieved 98% classification accuracy at SNR of 6 dB. Due to the advantages of using the time-frequency distribution, this paper appropriately extends the work in signal classification to airborne radar signals.

Figure 2 describes the methodology for implementing the ARTAC system. The flow chart is divided into two sections: inter-pulse and intra-pulse analyses. Thereafter, rules are formed from the estimated parameters from both analyses to classify incoming signals appropriately. These steps are further explained in the upcoming sub-sections.

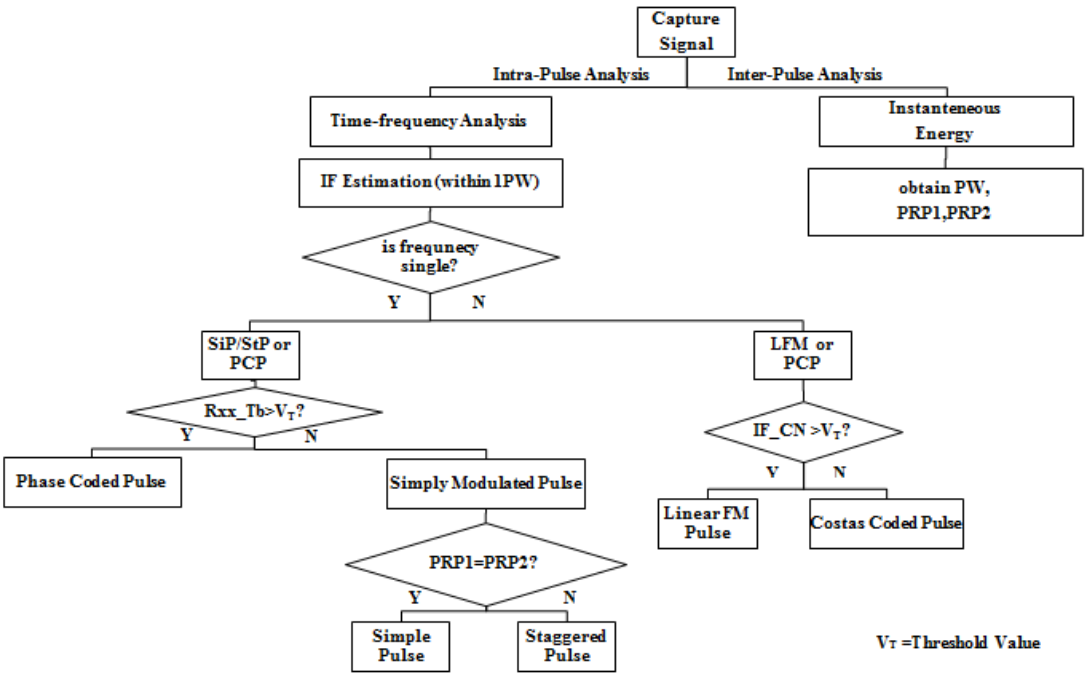

Figure 2: ARTAC system methodology.

5.1 Inter-Pulse Analysis

The inter-pulse analysis estimates the time parameters PW, PRP1 and PRP2 by using the IE estimated from Equation 3. To reduce the variance in the IE estimate due to noise, a window function is applied to the IE and the resulting smoothed estimate can be expressed as:

$$E_{x,smoothed}(t) = \int_{-\infty}^{\infty} w(\tau) E_x(\tau - t) d\tau \quad (9)$$

where $w(t)$ is the window function and $E_x(t)$ is the IE estimate.

Two windows are considered to determine the accuracy for estimating the time parameters. Since the PW is smaller than the PRP, the estimation error for the PW is more significant and thus, this section focuses only on the PW estimation. A SiP radar signal is considered under noiseless condition using both rectangular and Hamming windows. Noise is not included because it is important to estimate PW correctly. Using either one of the window function at one time, PW is estimated for various window lengths. The evaluation results are presented in Table 2.

Table 2: PW estimation for rectangular and Hamming windows.

Window length (Samples)	0	4-40	50	60	70	80	100	120	150	200
Estimated PW (Samples)	40	41	51	61	71	81	101	121	151	201

a) Rectangular window

Window length (Samples)	0	4-50	60	70	80	100	120	150	200
Estimated PW (Samples)	40	41	44	47	51	59	69	84	109

b) Hamming window

The window width of zero presented in the Tables 2 shows the default value of the estimated PW without the use of any window for smoothing. Between the two windows, it is evident that the Hamming window introduces lower PW estimation error as compared to the rectangular window. Window length (N_w) of 8 sample-points (0.2 μs) is selected to minimize the CC while still achieving a good time parameter estimate. Similar experiments to select the window length were carried out using the adaptive short time Fourier transform (STFT) on seismic electric signals (SES) (Astuti *et al.*, 2012). In the next section on intra-pulse analysis, the window function is used to localize the signal in the (t,f) representation using the spectrogram.

5.2 Intra-Pulse Analysis

Intra-pulse analysis is the process performed to obtain the properties of the radar signal within its pulse. In this section, the process includes (t,f) representation generation, IF estimation, discrimination between single frequency and frequency modulated signals, and discrimination between SiP, StP and phase modulated signals.

5.2.1 Window Length Selection for Spectrogram

The window function associated with the spectrogram as presented in Equation 2 is used to segregate the signal into various time segments and obtain their spectrum representations. Thus, the spectrogram is able to detect the frequency variation of the signal. Due to the uncertainty principle involving the reciprocal relationship between time and frequency, it is important that an optimal window length is selected (Boashash, 2015). Since the selection of window length is critical, evaluation is conducted to determine the window length (N_w=32, 64 and 128) for the spectrogram that can provide accurate (t,f)

representation for the CCP signal. The resulting (*t*,*f*) representations for the CCP signal at various window lengths are shown in Figure 3.

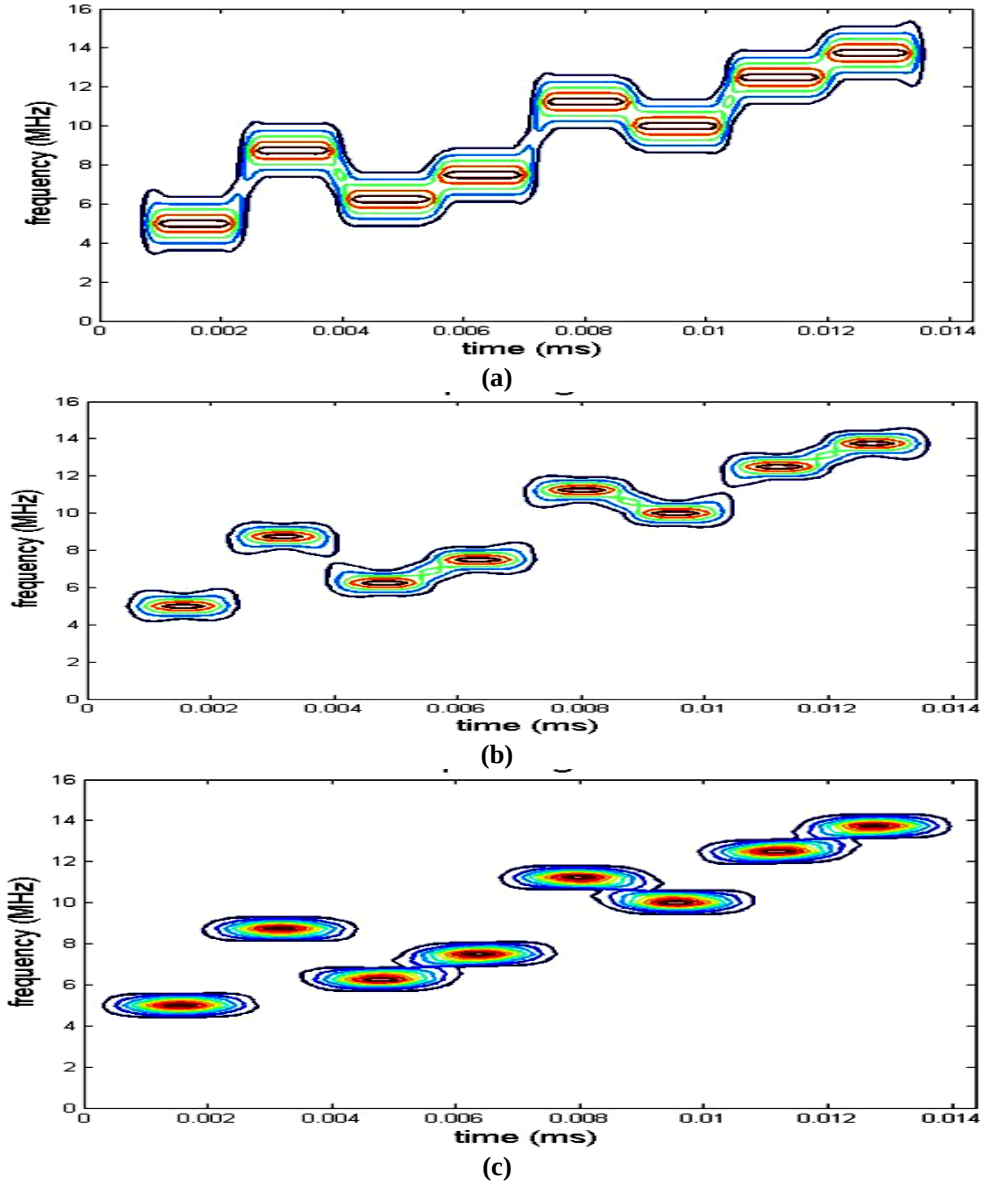

Figure 3: The (*t*,*f*) representations of a CCP signal pulse for window length (N_w)=(a) 32, (b) 64 and (c) 128.

Figure 3 shows the (*t*,*f*) representations of the CCP signal pulse at different window lengths. It is seen that the time resolution decreases as the frequency resolution increases (as indicated by the reduced main-lobe width) with the window length. However, this is at the expense of the increase in the CC. As a compromise between the time resolution, frequency resolution and CC, a moderate window length of N_w =64 samples is adopted for the spectrogram. IF is then estimated using Equation 6, as shown in Figure 4. From the IF estimate, it is possible to determine two signal types: single frequency signals (SiP, StP and PCP) and frequency modulated signals (CCP and LFM).

5.2.2 Discrimination Between CCP and LFM Signals

The CCP and LFM signals are frequency modulated signals used in pulse compression signaling. For the CCP signal, the frequency varies according to a defined pattern, while for the LFM signal, the frequency varies linearly with time. Figures 4(a) and 4(b) show the (*t*,*f*) representations for both signals. Since the two signals have distinctive IF characteristics, they can be discriminated by comparing with a linear frequency and time relationship based on the chirp ratio α as shown in Figure 4(c). A large difference with the linear frequency and time relationship means the signal is a CCP signal while minimum difference indicates that the signal is a LFM signal.

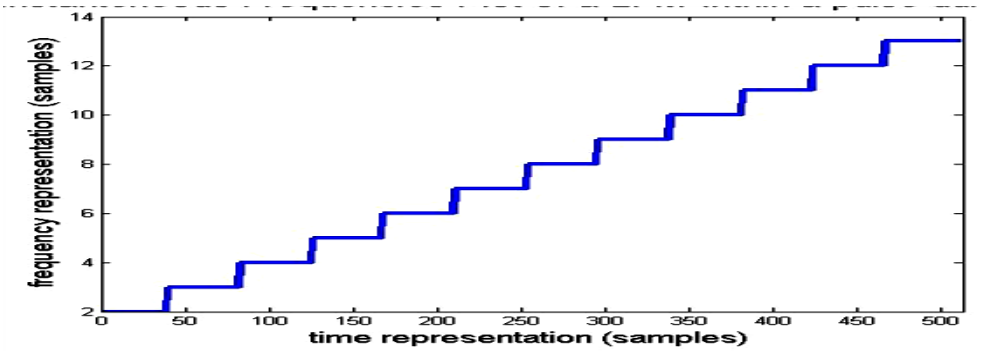

(a)

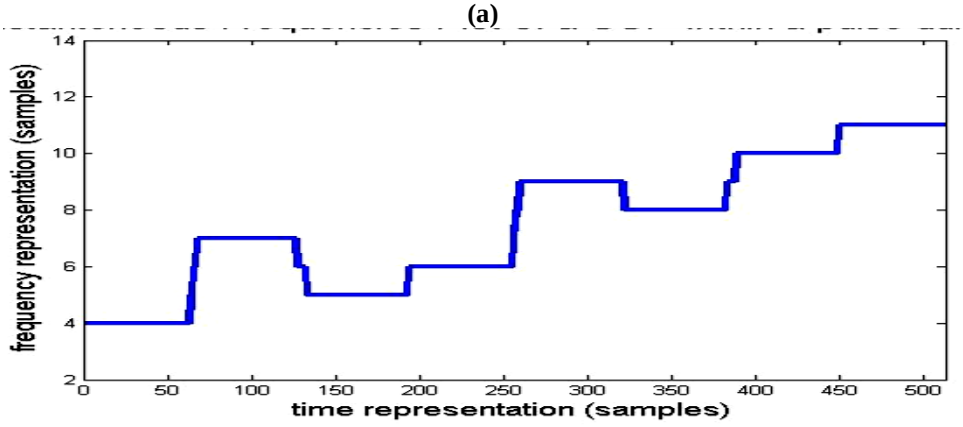

(b)

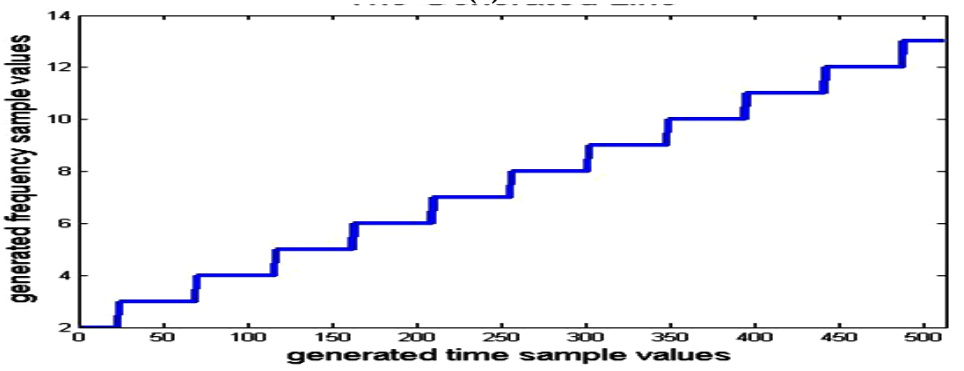

(c)

Figure 4: IF plots for (a) LFM and (b) CCP signals, and (c) the linear frequency and time relationship.

5.2.3 Discrimination between SiP / StP and PCP Signals

Since the spectrogram belongs to the class of quadratic time-frequency distribution, the phase information is not represented in the (*t*,*f*) representation. The signal parameters defined in Table 1

shows that there are three signals with single frequency - SiP, StP and PCP- and between them, PCP is phase modulated. Instead of using the (*t,f*) representation, the three signals can be discriminated from the autocorrelation function. First, the power spectrum is derived from the (*t,f*) representation in Equation 7. Next, the Wiener-Khinchine theorem is applied according to Equation 8 to obtain the autocorrelation function. To improve the representation of the autocorrelation function, the autocorrelation function is first squared and then smoothed using the Hamming window (Tan & Sha'ameri, 2008b). The width of the squared and smoothed autocorrelation is shown to be proportional to the symbol duration, which is then used to set up the lag window of the quadratic time-frequency distribution. The process to obtain the smoothed squared autocorrelation function is shown in the following equations:

$$\mathbf{R}_{xx}(\tau) = R_{xx}(\tau)R^{*}_{xx}(\tau) \tag{10}$$

$$\mathbf{R}_{xx,smoothed}(\tau) = \int_{-\infty}^{\infty} w(\lambda)\mathbf{R}_{xx}(\tau-\lambda)d\lambda \tag{11}$$

where $w(\tau)$ is the window function and $R_{xx}(\tau)$ is the autocorrelation function.

The smoothed squared autocorrelation for the SiP / StP and PCP signals are shown in Figure 5. Between the two signals, the width of the smoothed squared autocorrelation is bigger for the SiP and StP signals as compared to the PCP signal. The width of the autocorrelation function for simple modulated signals depends on the PW. Although the pulse duration for the PCP signal, as shown in Table 1, is longer, the width of the autocorrelation function is independent of the PW and rather depends on the sub-pulse duration. This characteristic is observed on the PCP signal because the Barker code modulated on the signal is a pseudo-random sequence (Peebles, 2001). In order to differentiate between the SiP and StP signals with the PCP signal, the received signal is either the SiP or StP signals if the width of the squared smoothed autocorrelation is equal to the PW estimated from the inter-pulse analysis in Section 5.1, else the received signal is PCP signal.

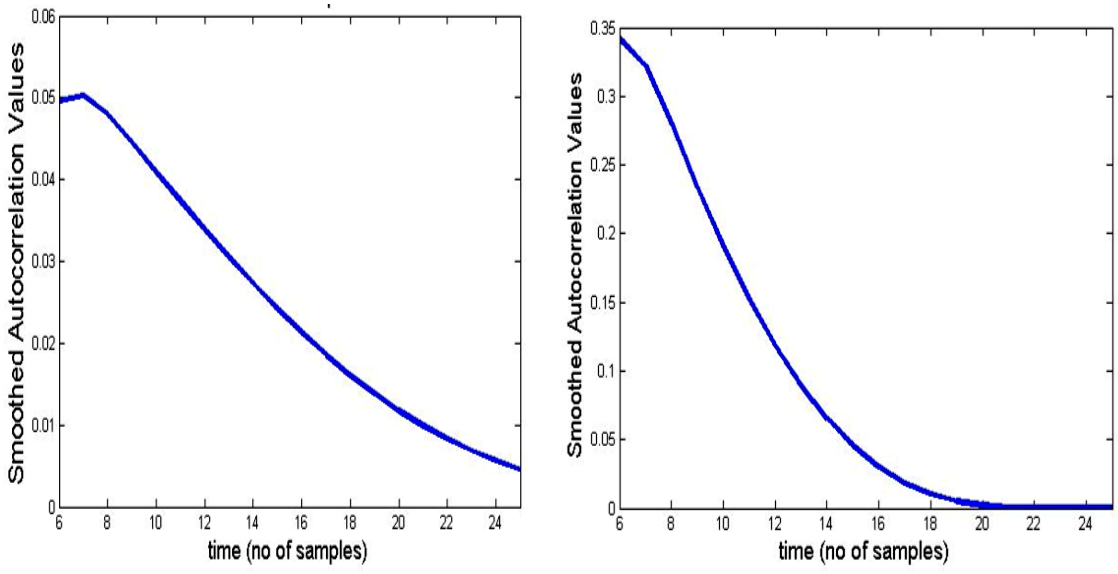

(a) **(b)**

Figure 5: The squared smoothed autocorrelation of the (a) SiP and (b) PCP signals.

5.3 Rule-Based Classifier

A rule-based classifier identifies and classifies objects based on a set of defined rules. It is enacted from the if-else syntax that leads to a type of decision tree (Witten *et al*., 2011). The rule based classifier is used in various signal processing fields, with some applications in the high frequency (HF) communications signals (Tan *et al*., 2010) and audio processing (Vavrek *et al*., 2013). The rules used in this paper to classify the various radar signal types derived from the parameters estimated from the (*t*,*f*) representation are shown in Figure 6.

[Rule 1] if Fbw>=10 and IF_count_Norm>=0.15	D=1; Linear FM Pulse
[Rule 2] if Fbw>=10 and IF_count_Norm<0.15	D=2; Costas Coded Pulse (8-FSK)
[Rule 3] if Fbw<10 and Rxx_Tb<28	D=3; Phase Coded Pulse (BPSK)
[Rule 4] if Fbw<10 and Rxx_Tb>28 and (PRP1-0.1*PRP1)<=PRP2<=(0.1*PRP1+PRP1)	D=4; Simple Pulse
[Rule 5] if Fbw<10 and Rxx_Tb>28 and (PRP1-0.1*PRP1)>PRP2>(0.1*PRP1+PRP1)	D=5; Staggered Pulse

Figure 6: Classification rules for ARTAC system.

6. RESULTS AND DISCUSSION

The performance of the ARTAC system to analyze and classify signals is verified by Monte Carlo simulation for the various SNRs. The application of the system is then evaluated in a practical ES scenario. Finally, the CC is evaluated which is critical for implementation on an embedded system.

6.1 Analysis and Classification Performance

Monte Carlo simulation is performed to verify the performance of the ARTAC system. The simulation is a risk analysis tool used to cater for elements of uncertainty and variability. It depicts the response of a designed system when faced with uncertainty parameters. As such, this work uses this simulation to examine the behavior of the classifier design from very low to high SNR. Probability of correct classification (P_{cc}) is determined by running the system for 100 trials at a given SNR range from 0 to 18dB. In relation to radar signal processing, Monte Carlo simulation has been used in the areas of precise detection statistics in radar receivers (Jahns, 2000), cluttered SAR imagery (Knowles & Parker, 2004) and automatic censoring techniques of radar interfering targets (Almarshad *et al*, 2007).

Figure 7 shows the performance of the system in terms of P_{cc} for various SNR. In general, all the signals achieved P_{cc} of 90% at SNR of 6.2 dB. Both LFM and PCP signals have more than 90% classification accuracy at SNR below 0 dB. The CCP signal also has 90% accuracy at 6.2 dB, but its performance downgraded rapidly at lower SNR as compared to the other signals. Table 3 summarizes the performance for all the signals by comparing the SNR to achieve P_{cc} of 90%.

Besides the classification accuracy shown in Figure 7, it would be of interest to look at how the signal is misclassified. This is provided by using the confusion matrix, also known as error matrix or contingency table (Stephen, 1997). Entries along the diagonals signify correct classification, while the non-diagonals signify otherwise (Wickens, 2002). Two confusion matrices are presented in Table 4 for low (0 dB) and high (6 dB) SNR.

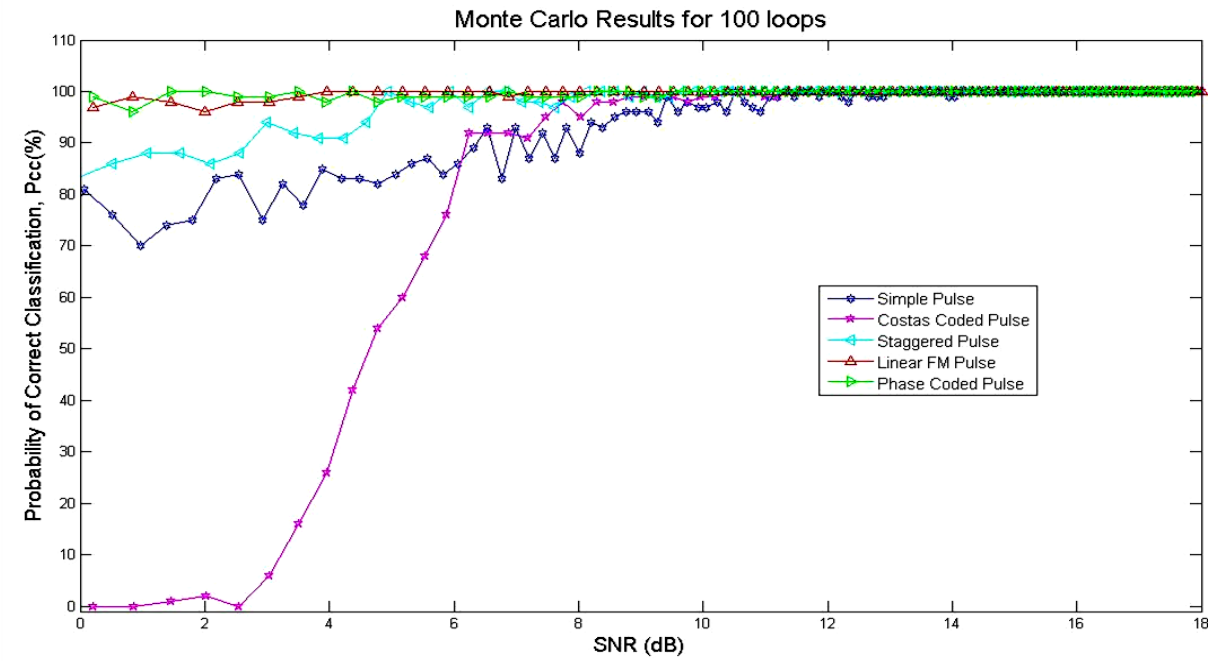

Figure 7: Classification performance of the ARTAC system for various SNRs.

Table 3: SNR at P_{cc} > 90%.

Signal	SiP	StP	CCP	LFM	PCP
SNR at P_{cc} > 90% (dB)	6.2	3	6.2	-8	-9

Table 4: Confusion matrix for the ARTAC system for SNR of 0 and 6 dB.

	LFM	**CCP**	**PCP**	**SiP**	**StP**
LFM	99	1	0	0	0
CCP	0	0	17	59	24
PCP	0	0	100	0	0
SiP	0	0	35	65	0
StP	0	0	11	0	89

(a) SNR=0 dB

	LFM	**CCP**	**PCP**	**SiP**	**StP**
LFM	100	0	0	0	0
CCP	9	77	9	5	0
PCP	0	0	100	0	0
SiP	0	0	11	89	0
StP	0	0	1	0	99

(b) SNR=6 dB

At low SNR (0 dB), the CCP signal performed the poorest due to the need to estimate most of its frequencies before proper classification is performed. This is also the main reason why it is misclassified as single-frequency signal (SiP, StP or PCP). Next in terms of poor performance is the SiP signal, which is misclassified as the PCP signal at times due to the phase shift introduced by the noise. The StP signal performed better than the SiP signal despite using the same modulation type due to its longer PRP2. Hence, more samples representing the interval makes it less susceptible to misclassification error.

At high SNR (6 dB), it is observed that the CCP signal is correctly classified, and at times misclassified as a LFM signal or single frequency signal. This means that the system has on average estimated the frequencies of the CCP signal correctly, which is used as input to the classifier. In general, the system achieved 100% correct classification for all signals at SNR ≥ 13 dB.

6.2 Practical Classification Performance of the ARTAC System

The ARTAC system described in this paper is an ES system suitable for implementation either on a land, marine or airborne platform. Based on the simulation results from the previous section, it would be of interest to evaluate its performance as an ES system close to a practical scenario. First, let us assume that the receiver is based on the system described in Keysight (2015) with the following receiving parameters:

- Receiving frequency range: 8 to 12 GHz
- Intermediate frequency: 10 MHz
- Sampling frequency: 40 MHz
- Receiver bandwidth: 20 MHz.
- Noise figure (NF): 5 dB
- Received antenna gain: 12 dBi
- Received antenna height: 10 m
- Antenna site: 200 m above mean sea level
- Sensitivity: -95 dBm

The scenario for the ARTAC system assumes that the target flies at a minimum altitude of 300 m (approximately 1,000 ft), which allows for minimum line of sight of 150 km. The system receives the signal either from the main or side lobe. Since the radar scans over a specific volume of the airspace, most of the received signal comes from either the side or back lobe. The analysis is simplified by assuming that the side and back lobes have the same gain. The parameters of the weapon control and weather radars are as follows:

Weapon Control Radar

- Transmit antenna gain at main lobe: 35 dBi
- Transmit antenna gain at side lobe: -15 dBi
- Peak transmit power: 10 or 20 kW.
- Duty cycle: 0.01, 0.2 and 0.5
- Losses due to matching, beam width and shape, and other losses: 2 dB

Note: The radar is characterized with a low side lobe and could go into LPI mode by changing the duty cycle.

Weather Radar

- Transmit antenna gain at main lobe: 30 dBi
- Transmit antenna gain at side lobe: -2 dBi
- Peak transmit power: 0.5 kW.
- Duty cycle: 0.01
- Losses due to matching, beam width and shape, and other losses: 2 dB

Note: The radar has a fixed and small duty cycle, and the side lobe is not reduced.

Since line of sight is present, the propagation loss is best predicted using free space loss. The objective is now to determine the received SNR and determine if it is within 9 dB to ensure 90% classification. The analysis results based on the parameters of the weapon control and weather radars are shown in Table 5. In general, reception from the main lobe gives the highest SNR, exceeding 38 dB, which is sufficient to give classification accuracy of greater than 90%. Lower SNR is received from the side lobe with a minimum of 2.5 dB for the weapon control radar transmitting at peak power of 10 kW on LPI mode (duty cycle of 0.5). At this SNR, the classification rate for the radar signals, such as the CCP signal, is downgrade significantly to less than 10 %. For side lobe reception from a weapon

control radar with duty cycle less than 0.2 and weather radar, the received SNR is within 6 dB, which means that the classification rate is about 80% for SiP and CCP signals, while the rest of the signals can still be correctly classified at 90%. For older generation weapon control radars, the main lobe's gain and the side lobe level is similar to the weather radar described in this section. Thus, it is expected that the received SNR is close to 6 dB giving a similar classification rate to the weather radar.

Table 5: Comparison of received SNR from the main and side lobes of the transmitting radar.

Radar type	Peak T_x power (kW)	Duty cycle	Reception – main lobe (M) or side lobe (S)	Recorded SNR
Weapon control radar	20	0.01	M	58
			S	8
		0.2	M	58
			S	8
		0.5	M	55
			S	5.5
	10	0.01	M	55
			S	5.5
		0.2	M	55
			S	5
		0.5	M	52.5
			S	2.5
Weather radar	0.5	0.01	M	38
			S	6.5

6.3 Computational Complexity (CC)

The issue of CC becomes important if there is a need to implement the processing on an embedded system. The CC depends on the analysis and classification process described in Figure 2. Since the processing is done in discrete-time, the processing parameters, such as the signal length, window length, and pulse width, are defined in samples. The CC is measured as the number of instruction cycles to perform the processing of signal (Chee *et al*., 2012, 2014). Thus, the actual implementation speed depends on the duration of the instruction cycle.

For the inter-pulse analysis, the CC depends on the signal length (N) and window length (N_{w1}) to smooth the IE. The CC for the smoothed IE is:

$$CC_{SIE}=N_{w1}N \tag{12}$$

From here, the PRP and PW are calculated based on the algorithm described in Section 5.1.

The intra-pulse analysis is more complex because it involves the analysis of the signal within a pulse that is either single frequency sinusoid, frequency modulated or phase modulated. Details on the processing are described in Section 5.2. First, the spectrogram is used to generate the (t,f) representation and the analysis is then conducted based on single frequency (SFS) and frequency modulated (FMS) signals. The CC for the spectrogram is $N_pN_{w2}\log_2N_{w2}$, where N_p is the pulse width duration and N_{w2} is the window length for the spectrogram. From the (t,f) representation, the IF is estimated from the location of the peak along frequency axis of length N_{w2} for the PW duration of N_p. Thus, the CC for the IF estimation is $0.5N_{w2}N_p$.

The SFS analysis is performed first by estimating the power spectrum from the frequency marginal of the (t,f) representation which requires a CC of $N_{w2}N_p$. Calculating the autocorrelation from the power

spectrum requires a CC of $N_{w2}\log_2 N_{w2}$. Next, squaring and smoothing of the autocorrelation requires a CC of $N_{w1}N_{w2}$. Thus, the CC for SFS analysis is

$$CC_{SFS}=N_{w2}N_p+N_{w2}\log_2 N_{w2}+N_{w1}N_{w2} \quad (13)$$

To perform the FMS analysis, IF is first estimated from the (t,f) representation and an additional step is required to compare the estimated IF with the generated IF with a CC of $2N_p$. The CC for the MFS analysis is:

$$CC_{FMS}=0.5N_{w2}N_p+2N_p \quad (14)$$

The overall CC for the SFS signals – SiP, StP and PCP- is the sum of the CC of the inter-pulse analysis, spectrogram, IF estimate, frequency marginal and inverse Fourier transform to obtain the autocorrelation function, and squaring and smoothing of the autocorrelation function:

$$\begin{aligned} CC_{total,SFS} &= CC_{SIE}+CC_{SFS} \\ &= N_{w1}N+N_pN_{w2}\log_2 N_{w2}+0.5N_{w2}N_p+N_{w2}N_p+N_{w2}\log_2 N_{w2}+N_{w1}N_{w2} \end{aligned} \quad (15)$$

Next, the overall CC for FMS signals – LFM and CCP- is the sum of the CC of the inter-pulse analysis, spectrogram, IF estimate, and comparison between the estimated and generated IF:

$$CC_{total,FMS} = CC_{SIE}+CC_{FMS} = N_{w1}N +N_pN_{w2}\log_2 N_{w2}+0.5N_{w2}N_p+2N_p \quad (16)$$

The comparison between all the signals is presented in Table 6. For all signals, N_{w1} and N_{w2} are fixed at 8 and 64 samples respectively. In general, the CC obtained for the inter-pulse analysis (CC_{SIE}) is higher as compared to the intra-pulse analysis (CC_{SFS}/CC_{FMS}) due to the need to analyze a large number of time samples that represent the radar signal. For the intra-pulse analysis, the CC obtained very much depends on the signal type and pulse length, with the highest being the CCP signal at 153,686 instruction cycles, while the lowest is for the SiP and StP signals at 15,265 instruction cycles. The difference between the largest and smallest CC for the inter-pulse analysis is about 10 times. Thus, it can be concluded that the CC will be much higher for LPI radar signals, which utilize phase and frequency modulations with large PW (high duty cycle).

Table 6: Comparison of CC for all the signals.

Signal	N	N_p	CC_{SIE}	CC_{SFS}/CC_{FMS}	CC
PCP	16,000	112	128,000	41,341	169,341
SiP	16,000	40	**128,000**	**15,265**	**143,265**
StP	20,000	40	160,000	15,265	175,265
LFM	16,000	80	128,000	24,013	152,013
CCP	16,000	512	**128,000**	**153,686**	**281,686**

7. CONCLUSION

In this paper, an ARTAC system is developed based on the spectrogram time-frequency distribution to analyze and classify airborne radar signals. Estimation of the signal parameters is performed from the (t,f) representation without separate processing techniques such as time-series analysis and spectrum estimation. Based on Monte Carlo simulation, it is shown that the developed system is able to analyze and classify airborne radar type signals with 90% classification accuracy at SNR of 6 dB. Similar performance is achieved by considering the practical application in an ES environment, where the signal is received typically from the side lobe of the transmitting radar antenna. The signals are considered to operate at normal mode (low duty cycle) as well as at low LPI. The CC is also evaluated to determine the processing requirements of the system.

ACKNOWLEDGEMENT

The authors would like to thank Universiti Teknologi Malaysia (UTM) under project Vot No. Q.J130000.7823.4F188 and Ministry of Higher Education (MOHE), Malaysia for providing the resources for this research.

REFERENCES

Adamy, D. (2001). *EW101: A First Course in Electronic Warfare*. Artech House, Boston.

Agcaoglu, O., Santhanam, B. & Hayat, M. (2013). Improved spectrograms using the discrete Fractional Fourier transform. *IEEE Digital Signal Processing and Signal Processing Education Meeting (DSP/SPE)*, 11-14 August 2013, pp.80-85.

Almarshad, M.N., Barkat, M. & Alshebeili. S.A. (2007). A Monte Carlo simulation for Two Novel Automatic Censoring Techniques of Radar Interfering Targets in Log-Normal Clutter. *9th International Symposium on Signal Processing and Its Applications, 2007 (ISSPA 2007)*, 12-15 February 2007. pp. 1-4.

Astuti, W., Sediono, W., Aibinu, A.M., Akmeliawati, R. & Salami, M.J.E (2012). Adaptive Short Time Fourier Transform (STFT) analysis of seismic electric signal (SES): A comparison of Hamming and rectangular window. *IEEE Symposium on Industrial Electronics and Applications (ISIEA), 2012*, 23-26 September 2012, pp. 372-377

Boashash, B. (2015). Heuristic formulation of time-frequency distribution. *In* Boashash, B. (Ed.), *Time Frequency Signal Analysis and Processing: A Comprehensive Reference (2nd edition)*, Elsevier, Oxford, pp. 94-125. (In Press).

Chee, Y.M., Sha'ameri, A.Z. & Boashash, B. (2012), Efficient phase estimation for the classification of digitally phase modulated signals using the cross-WVD: A performance evaluation and comparison with the S-transform. *EURASIP J. Adv. Signal Proc.*, **65**: 1–22.

Chee, Y.M., Sha'ameri, A.Z. & Zabidi, M.M. A. (2014). IF estimation of FSK signals using adaptive smoothed windowed cross Wigner-Ville distribution. *Signal Proc.*, **100**: 71–84.

E-3Sentry (2015). *AWACS Surveillance Radar*. Available online at: http://www.northropgrumman.com/capabilities/awacsapy2/documents/awacs.pdf (Last access date: 31 August 2015).

Elsworth, A.T. (2010). *Electronic Warfare*. Nova Science Publishers. Inc., New York.

Fancey, C. & Alabaster, C.M. (2010). The metrication of low probability of intercept waveforms. *2010 International Waveform Diversity and Design Conference (WDD)*, 8-13 Aug. 2010, pp. 58-62.

Fred, P.R. (2010). *Airborne Weather Radar - Separating Fact from Fiction*. Available online at: http://www.helicoptermaintenancemagazine.com/article/airborne-weather-radar-separating-fact-fiction (Last access date: 15 January 2015).

Galati, G & Pavan, G. (2013). Waveforms design for modern and MIMO radar, *2013 IEEE EUROCON*., 1-4 July 2013, pp. 508-513.

Harmanny, R.I.A., de Wit, J.J.M. & Cabic, G.P. (2014). Radar micro-Doppler feature extraction using the spectrogram and the cepstrogram, *2014 11th European Radar Conference (EuRAD)*, pp. 165-168

Jahns, A. (2000). Precise detection statistics by probability transform (PT) simulation applied to a hard-limited radar receiver. *The Record of the IEEE 2000 International Radar Conference*, pp. 410-415.

Keysight (2015). N6841A RF Sensor. *Keysight Technology*. Available online at: http://www.keysight.com/en/pd-1414739-pn-N6841A/rf-sensor?cc=MY&lc=eng (Last access date: 15 January 2015).

Knowles, Z. & Parker, D. (2004). A Monte Carlo Simulation based approach to a priori performance prediction for target detection and recognition in cluttered synthetic aperture radar imagery. *IEE Target Tracking 2004: Algorithms and Applications*, 23-24 March 2004, pp. 107-114.

Kopp, C. (2008). *Assessing Russian Fighter Technology*. Available online at: http://www.ausairpower.net/APA-2008-04.html (Last access date: 15 January 2015).

Lessard, C.S. (2006), *Signal Processing of Random Physiological Signals*. Morgan & Claypool, USA.
Levanon, N. & Mozeson, E. (2004), *Radar Signals*. Wiley, New York.
Lunden, J & Koivunen, V. (2007). Automatic radar waveform recognition. *IEEE J. Sel. Top. Signal Proc.*, **1**: 124,136.
Neri, F (2006). *Introduction to Electronic Defense Systems*. SciTech Publishing Inc., North Carolina.
Pace, P.E. (2009). *Detecting and Classifying Low Probability of Intercept Radar*. Artech House, Norwood, MA.
Peebles, P.Z. (2001). *Probability, Random Variables and Random Signal Principles*. McGraw-Hill Singapore.
Poisel, R. A. (2012), *Electronic Warfare Target Location Methods*, Artech House, London.
Sha'ameri, A.Z., Shehu, Y.A. & Asuti, W. (2015). Performance analysis of a minimum configuration multilateration for airborne emitter position estimation. *Defence S&T Bull.*, **8**: 27-41.
Sha'ameri, A. Z. & Boashash, B. (2015). Time-frequency estimation of radio signal modulation parameters. *In* Boashash, B. (Ed), *Time Frequency Signal Analysis and Processing: A Comprehensive Reference (2nd Edition)*, Elsevier, Amsterdam, pp. 784-795. (In Press).
Skolnik, M. I. (2008), *Radar Handbook. (3rd Ed)*. Mc-Graw Hill, New York.
Stankovic, L., Thayaparan, T., Dakovic, M. & Bugarin, V.P. (2013). Micro-Doppler removal in the radar imaging analysis. *IEEE Trans. Aero. Elec. Syst.*, **49**: 1234-1250.
Stephen, V.S. (1997). Selecting and interpreting measures of thematic classification accuracy. *Remote Sens. Environ.*, **62**: 77-89.
Tan, J.L. & Sha'ameri, A.Z. (2008a). Signal analysis and classification of digital communication signals using adaptive smooth-windowed Wigner-Ville distribution. *6th National Conference on Telecommunication Technologies 2008 and 2008 2nd Malaysia Conference on Photonics. NCTT-MCP 2008*, 26-28 August 2008, pp. 260-266.
Tan, J. L., Sha'ameri, A. Z. (2008b). Adaptive optimal kernel smooth-windowed-Wigner-Ville distribution for digital communication. *EURASIP J. Adv. Signal Proc.*, **Vol. 2008**: Article ID 408341.
Tan, J.L., Sha'ameri A.Z. & Chee, Y.M. (2010). Signal analysis and classification of digital communication signal using time-frequency analysis techniques in the multipath fading environment. *10th International Conference on Information Sciences, Signal Processing and their Applications (ISSPA)*, 10-13 May 2010, pp. 678-681.
Tsui, J. B. (2004), *Digital Techniques for Wideband Receivers*. SciTech Publishing, Raleigh.
Vavrek, J., Juhar, J. & Cizmar, A. (2013). Audio classification utilizing a rule-based approach and the support vector machine classifier. *36th International Conference on Telecommunications and Signal Processing (TSP)*, 2-4 July 2013, pp. 512-516,
Wickens, T.D. (2002). *Elementary Signal Detection Theory*. Oxford University Press, New York.
Wiley, R. G. (2006). *ELINT: The Interception and Analysis of Radar Signals*. Artech House, Boston.
Witten, I.H., Frank, E. & Hall, M.A. (2011). *Data Mining: Practical Machine Learning Tools and Techniques (3rd Ed.)*. Morgan Kauffman, Massachusetts.
Ziemer, R.E., & Peterson, R.L. (2001). *Introduction to Digital Communication*. Prentice-Hall International, Upper Saddle River, New Jersey.

EVALUATION OF THE ACCURACY OF GLOBAL POSITIONING SYSTEM (GPS) SPEED MEASUREMENT VIA GPS SIMULATION

Dinesh Sathyamorthy*, Shalini Shafii, Zainal Fitry M Amin, Asmariah Jusoh & Siti Zainun Ali

Science & Technology Research Institute for Defence (STRIDE), Ministry of Defence, Malaysia

*E-mail: dinesh.sathyamoorthy@stride.gov.my

ABSTRACT

In this study, Global Positioning System (GPS) simulation is employed to evaluate the accuracy of GPS speed measurements. The two methods of GPS speed measurement, trackpoints and Doppler shift, are compared for two conditions of tests: 1) Normal scenario with the full range of available GPS satellites; 2) Obstruction scenario with only six GPS satellites available. For the trackpoints method, significant errors are observed, due to positioning errors caused by the GPS receiver's user equivalent ranging error (UERE). The errors increased with increasing speed due to increasing length of zig-zag lines connecting the trackpoints, which is caused by the receiver's positioning errors. The Doppler shift method generated much smaller errors for the normal scenario (maximum of 0.238 km/h for speeds of up to 1,800 km/h), as it is insensitive to the UERE of GPS receivers. Decrease of available GPS satellites in the obstruction scenario also caused increase of error for the trackpoints method due to increased position dilution of precision (PDOP) and thus, increased UERE. For the Doppler shift method, the increase of error was much smaller (maximum of 0.254 km/h for speeds of up to 1,800 km/h), indicating that change in GPS satellite geometry has limited effect on this method.

Keywords: *Global Positioning System (GPS) simulation; speed; trackpoints and Doppler shift; user equivalent ranging error (UERE); position dilution of precision (PDOP).*

1. INTRODUCTION

Global Navigation Satellites Systems (GNSS) receivers are becoming smaller, cheaper and more reliable, and hence, are being increasingly used for measurement of speed. Speed is defined as the rate of change of position, with its determination requiring measurements of distance and time components (Witte & Wilson, 2004). There are two methods for computation of GNSS speed measurement, which are trackpoints and Doppler shift.

For GNSS speed measurement via trackpoints, the GNSS receiver records a series of computed positions (trackpoints) at regular time intervals, which are then used to compute the speed. However, each trackpoint is suspect to variable errors, resulting in the computed speed being less accurate and reliable. Due to trackpoint inaccuracies, the line connecting all the trackpoints would be a zig-zag, even if the real path is a smooth or straight line. Since the length of a zig-zag line is always longer than the corresponding smooth or straight line, the accumulated distance and thus, the computed average speed is always overestimated as compared to the real speed (Chalko, 2007; Huang *et al*., 2013; Gaglione, 2015).

For GNSS speed measurement via Doppler shift, the GNSS receiver continuously tracks the carrier frequencies of the available GNSS satellites. The difference between the known satellite carrier frequency and the frequency determined at the receiver, known as the Doppler shift, is directly proportional to the speed of the receiver along the direction to the satellite. A minimum of four tracked satellites are required to determine the 3D speed vector of the receiver. A significant

advantage of Doppler speed measurement is that it is insensitive to distances from satellites, phase delays and a number of factors that are major sources of error for GNSS positioning using satellite range measurement. However, its accuracy is not constant as it is dependent on the number and geometrical distribution of available satellites (Zhang *et al*., 2006; Chalko, 2007; Huang *et al*., 2013; Gaglione, 2015).

A number of studies have been conducted to evaluate the accuracy of GNSS speed measurements (Witte & Wilson, 2004; Chalko, 2007; Huang *et al*., 2013; Little *et al*., 2013; Steinmetz *et al*. 2014; Bai *et al*., 2015). These studies were conducted via field evaluations using live GNSS signals. However, such field evaluations are subject to various error parameters, such as ionospheric and tropospheric delays, GNSS satellite clock and ephemeris errors, GNSS satellite positioning and geometry, radio frequency interference (RFI), and obstructions and multipath, which are uncontrollable by users (Aloi *et al.* 2007; Kou & Zhang 2011; Pozzobon *et al.*, 2013).

The ideal GNSS receiver evaluation methodology would be using a GNSS simulator, which can be used to generate multi-satellite GNSS configurations, transmit GNSS signals that simulate real world scenarios, and adjust the various error parameters. This would allow for the evaluations of GNSS receiver performance under various repeatable conditions, as defined by users. As the evaluations are conducted in controlled laboratory environments, they will not be inhibited by unwanted signal interferences and obstructions (Aloi *et al.* 2007; Kou & Zhang 2011; Pozzobon *et al.*, 2013). In previous studies, Global Positioning System (GPS) simulation was used to evaluate the vulnerabilities of GPS to radio frequency interference (RFI) (Dinesh *et al*., 2012, 2014a), multipath (Dinesh *et al*., 2013, 2014b), GPS satellite clock error (Dinesh *et al*., 2015a) and power consumption (Dinesh *et al*., 2015b).

In this study, GPS simulation is employed to evaluate the accuracy of GPS speed measurements. Both methods of GNSS speed measurement, trackpoints and Doppler shift, are compared for two conditions of tests: 1) Normal scenario with the full range of available GPS satellites; 2) Obstruction scenario with only six GPS satellites available.

2. METHODOLOGY

The apparatus used in the study are an Aeroflex GPSG-1000 GPS simulator (Aeroflex, 2010), a notebook running GPS Diagnostics v1.05 (CNET, 2004) and a Garmin GPSmap 60CSx handheld GPS receiver (Garmin, 2007). The GPS receiver employs the GPS L1 coarse acquisition (C/A) signal, which is an unencrypted civilian GPS signal widely used by various GPS receivers. The signal has a fundamental frequency of 1,575.42 MHz and a code structure which modulates the signal over a 2 MHz bandwidth (DOD, 2001; Kaplan & Hegarty, 2006; USACE, 2011). The study is conducted in STRIDE's mini-anechoic chamber (Kamarulzaman, 2010) to avoid external interference signals and unintended multipath errors. The test setup employed is as shown in Figure 1. Simulated GPS signals are generated using the GPS simulator and transmitted via the coupler. The following assumptions are made for the tests conducted:

i) No ionospheric or troposheric delays
ii) No GPS satellite clock and ephemeris error
iii) No obstructions or multipath
iv) No interference signals.

The tests are conducted for coordinated universal time (UTC) times of 0000, 0300, 0600 and 0900 for the routes shown in Table 1. The almanac data for the periods is downloaded from the US Coast Guard's web site (USCG, 2015) and imported into the GPS simulator. The GPS signal power level is set at -130 dBm. The speeds used for the test are 0, 30, 100, 250, 500, 1000, 1,500 and 1,800 km/h. For each reading, the trackpoints and Doppler shift speed computed by the GPS receiver are recorded for a period of 15 min.

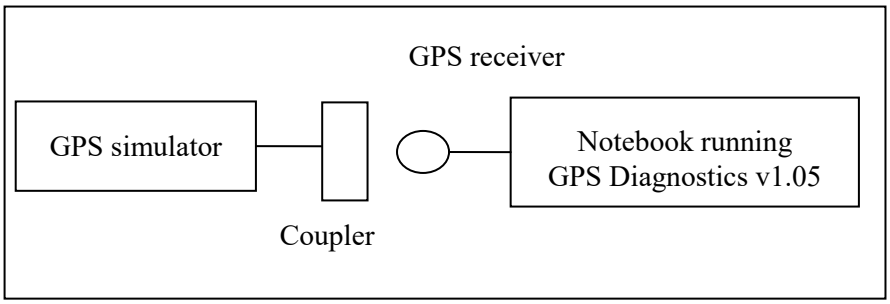

Figure 1: The test setup employed.

Table 1: The routes used for the tests conducted.

Start		Stop	
Kajang, Selangor, Malaysia	N 2° 58' E 101° 48'	Hanoi, Vietnam	N 20° 54' E 105° 49'
Denver, Colorado, US	N 39° 45' W 105° 00'	Washington D.C., Washington, US	N 38° 54' W 77° 2'
Cairns, Queensland, Australia	S 16° 55' E 145° 46'	Canberra, Australian Capital Territory (ACT), Australia	S 35° 15' E 149° 10'
Rio Gallegos, Argentina	S 51° 37' W 69° 12'	Buenos Aires, Argentina	S 34° 35' W 57° 30'

3. RESULTS & DISCUSSION

For the stationary condition, as shown in Table 2, the trackpoints method erroneously indicates that the GPS receiver is moving. This is due to the user equivalent ranging error (UERE) of the receiver, which is the total expected magnitude of position errors due to measurement uncertainties from the various error components for the receiver, such as receiver noise and antenna orientation (DOD, 2001; Kaplan & Hegarty, 2006; Worley, 2007; USACE, 2011). The errors generated result in the computed position of the receiver moving over time, depending on GPS coverage in terms of position dilution of precision (PDOP), which represents the effect of GPS satellite geometry on 3D positioning precision. A PDOP value of 1 is associated with an ideal arrangement of the satellite constellation. To ensure high-precision GPS positioning, a PDOP value of 5 or less is usually recommended. In practice, the actual PDOP value is usually much less than 5, with a typical average value in the neighbourhood of 2 (DOD, 2001; Kaplan & Hegarty, 2006; Dinesh *et al.*, 2010; USACE, 2011). Higher PDOPs would result in larger errors and hence, higher speeds. It is observed that the Doppler shift method is able to provide accurate results as it is insensitive to the UERE of GPS receivers.

For the moving condition, for the trackpoints method (Figure 2), it is observed that increase of speed causes increase of error. This is due to increasing length of zig-zag lines connecting the trackpoints, which is caused by the receiver's positioning errors. For the Doppler shift method, increase of speed also causes increase of error, but the range of error is much smaller (maximum of 0.238 km/h) (Figure 3) as compared to the trackpoints method.

For the trackpoints method, the errors computed for the obstruction scenario (Figure 4) are higher as compared to the normal scenario. This is as the decrease of number of GPS satellites causes in increase of PDOP and hence, increase of the receiver's UERE, resulting in less precise positioning. For the Doppler shift method, the increase of error is much smaller (maximum of 0.254 km/h) (Figure 5), indicating that change in GPS satellite geometry has limited effect on this method. This is consistent with the findings of Witte & Wilson (2004), who reported that the effect of satellite geometry on this method is not significant.

Table 2: Measured speeds for the stationary condition.

Location	UTC time	Average speed (km/h)			
		Normal		Obstruction	
		Trackpoints	Doppler	Trackpoints	Doppler
Kajang	0000	0.015	0	0.031	0
	0300	0.015	0	0.019	0
	0600	0.006	0	0.010	0
	0900	0.011	0	0.017	0
Denver	0000	0.015	0	0.023	0
	0300	0.015	0	0.033	0
	0600	0.005	0	0.016	0
	0900	0.012	0	0.031	0
Cairns	0000	0.015	0	0.023	0
	0300	0.018	0	0.033	0
	0600	0.007	0	0.012	0
	0900	0.012	0	0.030	0
Rio Gallegos	0000	0.017	0	0.031	0
	0300	0.014	0	0.022	0
	0600	0.012	0	0.019	0
	0900	0.016	0	0.025	0

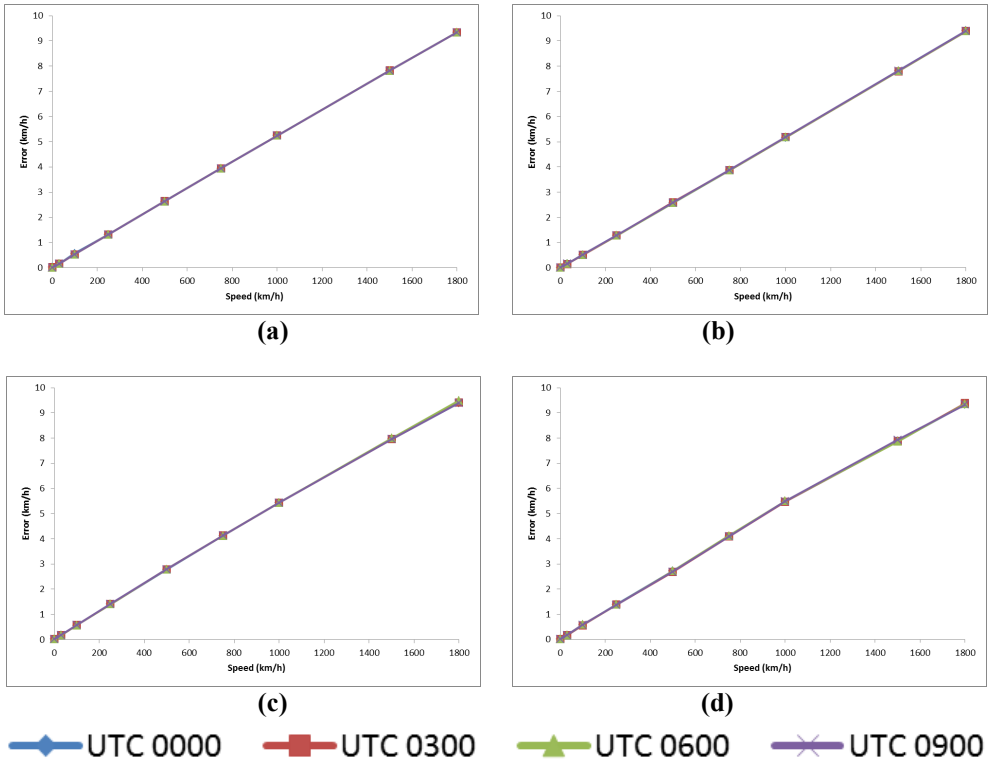

Figure 2: Errors for GPS speed measurement using the trackpoints method for the normal scenario for routes of: (a) Kajang-Hanoi (b) Denver-Washington D.C. (c) Cairns-Canberra (d) Rio Gallegos-Buenos Aires.

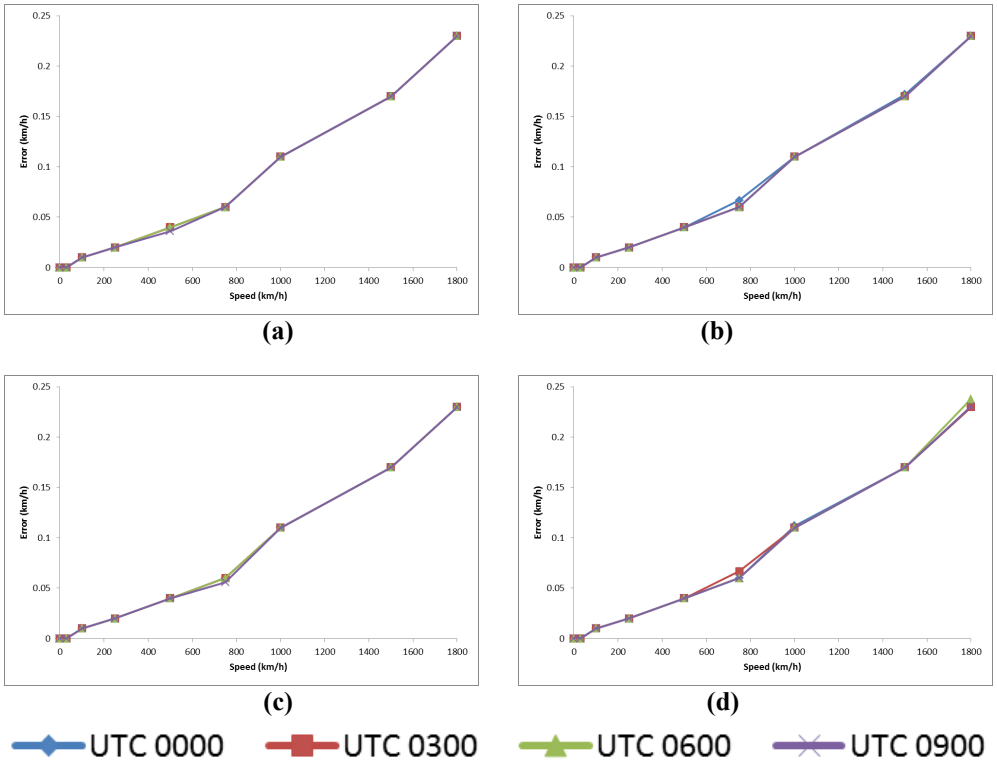

Figure 3: Errors for GPS speed measurement using the Doppler shift method for the normal scenario for routes of: (a) Kajang-Hanoi (b) Denver-Washington D.C. (c) Cairns-Canberra (d) Rio Gallegos-Buenos Aires.

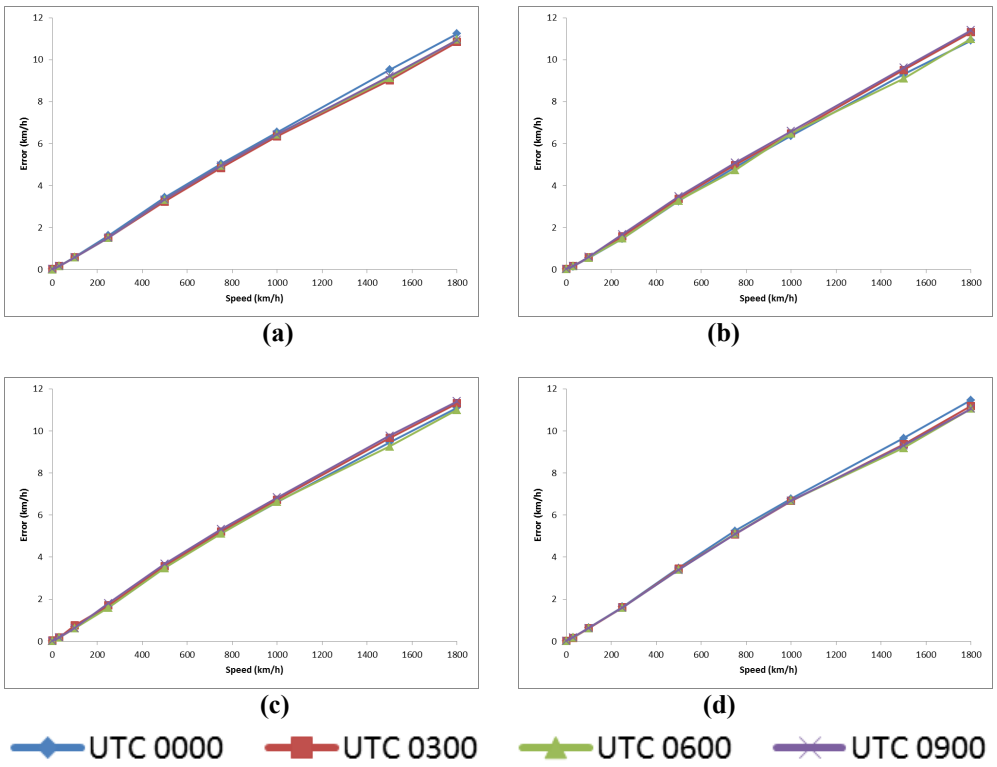

Figure 4: Errors for GPS speed measurement using the trackpoints method for the obstruction scenario for routes of: (a) Kajang-Hanoi (b) Denver-Washington D.C. (c) Cairns-Canberra (d) Rio Gallegos-Buenos Aires.

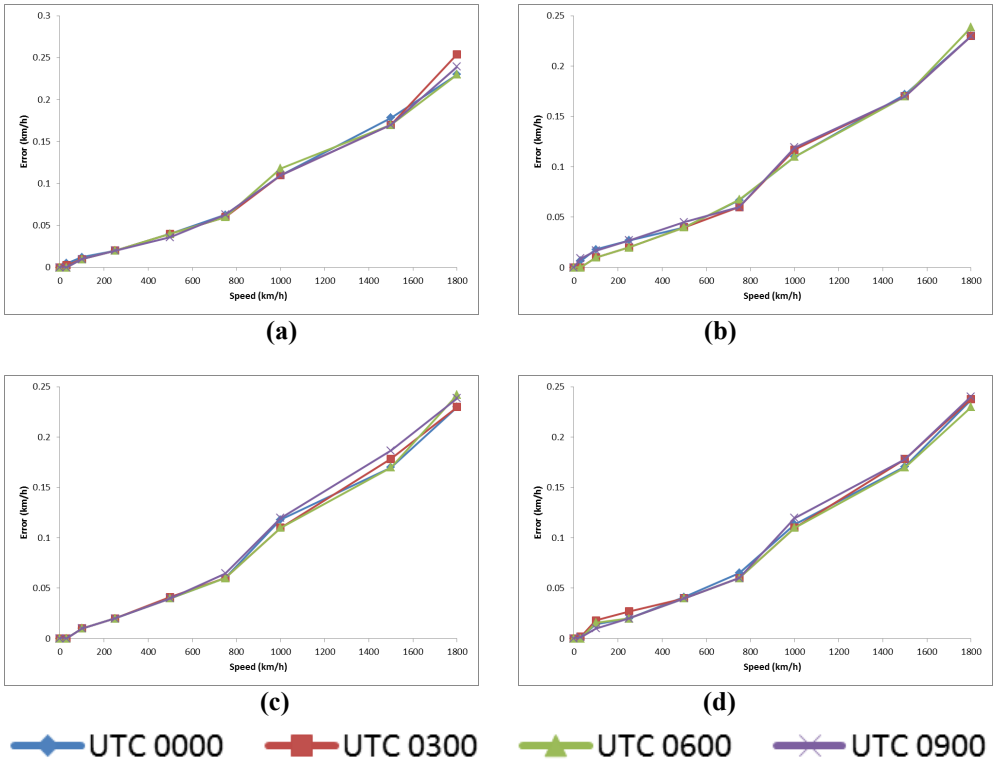

Figure 5: Errors for GPS speed measurement using the Doppler shift method for the obstruction scenario for routes of: (a) Kajang-Hanoi (b) Denver-Washington D.C. (c) Cairns-Canberra (d) Rio Gallegos-Buenos Aires.

The speed errors observed in this study are found to be smaller than corresponding errors reported in previous studies (Witte & Wilson, 2004, 2005; Chalko, 2007; Huang *et al*., 2013; Little *et al*., 2013; Steinmetz *et al*. 2014; Bai *et al*., 2015). This is as in this study, the effects of GPS vulnerabilities, such as ionospheric and tropospheric delays, GPS satellite clock and ephemeris error, multipath, and RFI, were not considered. Furthermore, the study was conducted for smooth straight line paths with consistent speed. It has been reported that rapid changes of speed and circular paths can degrade the accuracy of GPS speed measurement (Witte & Wilson, 2004; Huang *et al*., 2013; Steinmetz *et al*. 2014). To this end, further studies need to be conducted to evaluate the effects of various GPS vulnerabilities and movement types on the accuracy of GPS speed measurement in user-controlled scenarios.

4. CONCLUSION

In this study, GPS simulation was used to evaluate the two methods of GPS speed measurement, which are trackpoints and Doppler shift. For the trackpoints method, significant errors were observed, due to positioning errors caused by the GPS receiver's UERE. The errors increased with increasing speed due to increasing length of zig-zag lines connecting the trackpoints, which was caused by the receiver's positioning errors. The Doppler shift method generated much smaller errors for the normal scenario (maximum of 0.238 km/h for speeds of up to 1,800 km/h), as it is insensitive to the UERE of GPS receivers. Decrease of available GPS satellites in the obstruction scenario also caused increase of error for the trackpoints method due to increased PDOP and thus, increased UERE. For the Doppler shift method, the increase of error was much smaller (maximum of 0.254 km/h for speeds of up to 1,800 km/h), indicating that change in GPS satellite geometry has limited effect on this method. Further studies are proposed to evaluate the effect of various GPS vulnerabilities and movement types on the accuracy of GPS speed measurement in user-controlled scenarios.

REFERENCES

Aeroflex (2010). *Avionics GPSG-1000 GPS / Galileo Portable Positional Simulator*. Aeroflex Inc., Plainview, New York.

Aloi, D.N., Alsliety, M. & Akos, D.M. (2011). A methodology for the evaluation of a GPS receiver performance in telematics applications. *IEEE T. Instrum. Meas.*, **56**: 11-24.

Bai, Y., Sun, Q., Du, L., Yu, M. & Bai, J. (2015). Two laboratory methods for the calibration of GPS speed meters. *Meas. Sci. Tech.*, **26**: 015005.

Chalko, T.J. (2007). High accuracy speed measurement using GPS. *NU J. Discovery*, **4**: 1-9.

CNET (2004). *GPSDiag 1.0*. Available online at: http://download.cnet.com/GPSDiag/3000-2130_4-4951103.html (Last access date: 31 January 2010).

Dinesh, S., Wan Mustafa, W.H., Mohd Faudzi, M., Kamarulzaman, M., Hasniza, H., Nor Irza Shakhira, B., Siti Robiah, A., Shalini, S., Jamilah, J., Aliah, I., Lim, B.T., Zainal Fitry, M.A., Mohd Rizal, A.K., Azlina, B. & Mohd Hasrol, H.M.Y. (2010). Evaluation of the effect of radio frequency interference (RFI) on Global Positioning System (GPS) accuracy. *Defence S&T Tech. Bull.*, **3**: 100-118.

Dinesh, S, Mohd Faudzi, M. & Zainal Fitry, M.A. (2012). Evaluation of the effect of radio frequency interference (RFI) on Global Positioning System (GPS) accuracy via GPS simulation. *Defence. Sci. J.*, **62**: 338-347.

Dinesh, S., Shalini, S., Zainal Fitry, M.A. & Siti Zainun, A. (2013). Evaluation of the repeatability of Global Positioning System (GPS) performance with respect to GPS satellite orbital passes. *Defence S&T Tech. Bull.*, **6**: 130-140.

Dinesh, S., Mohd Faudzi, M., Rafidah, M., Nor Irza Shakhira, B., Siti Robiah, A., Shalini, S., Aliah, I., Lim, B.T., Zainal Fitry, M.A., Mohd Rizal, A.K. & Mohd Hasrol Hisam, M.Y. (2014a). Evaluation of the effect of radio frequency interference (RFI) on Global Positioning System (GPS) receivers via GPS simulation. *ASM Sci. J.*,**8**: 11-20.

Dinesh, S., Shalini, S., Zainal Fitry, M.A., Siti Zainun, A., Siti Robiah, A., Mohd Idris, I. & Mohd Hasrol Hisam, M.Y. (2014b). Evaluation of the effect of commonly used materials on multipath propagation of Global Positioning System (GPS) signals via GPS simulation. *Adv. Mil. Tech.*, **9**: 81-95.

Dinesh, S., Shalini, S., Zainal Fitry, M.A., Asmariah, J. & Siti Zainun, A. (2015a). Evaluation of the effect of Global Positioning System (GPS) satellite clock error via GPS simulation. *Defence S&T Tech. Bull.*, **8**: 51-62.

Dinesh, S., Shalini, S., Zainal Fitry, M.A., Asmariah, J. & Siti Zainun, A. (2015b). Evaluation of the trade-off between Global Positioning System (GPS) accuracy and power saving from reduction of number of GPS receiver channels. *Appl. Geomatics*, Under review.

DOD (Department of Defence) (2001). *Global Positioning System Standard Positioning Service Performance Standard, Command, Control, Communications, and Intelligence*. Department of Defence (DOD), Washington D.C.

Gaglione, S. (20015). How does a GNSS receiver estimate velocity? *Inside GNSS*, **10**: 38-41.

Garmin (2007). *GPSmap 60CSx Owner's Manual*. Garmin International Inc., Olathe, Kansas.

Huang, D. (2013). *Evidential Problems with GPS Accuracy: Device Testing*. Master's dissertation, AUT University, Auckland.

Kamarulzaman, M. (2010). *Technical Specification for STRIDE's Mini-Anechoic Chamber*. Science & Technology Research Institute for Defence (STRIDE), Ministry of Defence, Malaysia.

Kaplan, E.D. & Hegarty, C.J. (2006). *Understanding GPS: Principles and Applications*. Artech House, Norwood, Massachusetts.

Kou, Y. & Zhang, H. (2011). Verification testing of a multi-GNSS RF signal Simulator. *Inside GNSS*, **6**: 52-61.

Little, D.M., Rob, J. & Stephen, H. (2013). Accuracy of GPS speed and location data measured in emergency vehicles. *Collis.*, **8**: 88-111.

Pozzobon, O., Sarto, C., Chiara, A.D., Pozzobon, A., Gamba, G., Crisci, M. & Ioannides, R. (2013). Developing a GNSS position and timing authentication testbed: GNSS vulnerability and mitigation techniques. *Inside GNSS*, **8**: 45-53.

Steinmetz, E., Jarlemark, P., Emardson, R., Skoogh, H. & Herbertsson, M. (2014). Assessment of GPS derived speed for verification of speed measuring devices. *Int. J. Instr. Tech.*, **1**: 212-227

USACE (US Army Corps of Engineers) (2011). *Engineer Manual EM 1110-1-1003: NAVSTAR Global Positioning System Surveying.* US Army Corps of Engineers (USACE), Washington D.C.

USCG (US Coast Guard) (2015). *GPS NANUs, Almanacs, & Ops Advisories*. Available online at: http://www.navcen.uscg.gov/?pageName=gpsAlmanacs (Last access date: 9 March 2015).

Witte, T.H. & Wilson, A.M. (2004). Accuracy of non-differential GPS for the determination of speed over ground. *J. Biomech.*, **37**: 1891-1898.

Worley, S. (2007). GPS Errors & Estimating Your Receiver's Accuracy. Available online at: http://edu-observatory.org/gps/gps_accuracy.html (Last access date: 29th January 2010).

Zhang, J., Zhang, K., Grenfell, R. & Deakin, R. (2006). On the relativistic Doppler effect for precise velocity determination using GPS. *J. Geodesy*, **80**: 104-110.

A REVIEW OF ELECTRODEPOSITION TECHNIQUES AND VARIABLES FOR PRODUCTION OF NICKEL-COBALT / ALUMINA ($Ni\text{-}Co/Al_2O_3$) COMPOSITE COATINGS

Nik Hassanuddin Nik Yusoff[1*], Othman Mamat[2] & Mahdi Che Isa[1]

[1]Marine Materials Research Group, Maritime Technology Division (BTM), Science & Technology Research Institute for Defence (STRIDE), Ministry of Defence, Malaysia
[2]Mechanical Engineering Department, Universiti Teknologi Petronas (UTP), Malaysia

[*]Email: nhassanuddin.nyusoff@stride.gov.my

ABSTRACT

This paper provides a review of the electrodeposition process that is used to produce nickel-cobalt / alumina ($Ni\text{-}Co/Al_2O_3$) composite coatings. The electrodeposition techniques, consisting of direct current, pulse current and pulse reverse current, sediment electrodeposition, and CO_2 bath, are described. The effects of electrodeposition variables, including applied current density, deposition time, particle concentration and use of surfactants, are also explained. The paper then discusses the limitations of previous studies, such as lack of focus on the effectiveness of this coating in corrosive and erosive environments, and the effects of alumina particles on coating microstructures. It also suggests longer exposure to corrosive media for more significant corrosion study. Further research needs to be conducted in order to improve the corrosion and erosion resistance of $Ni\text{-}Co/Al_2O_3$ in harsh environments, such as marine conditions.

Keywords: *Nickel-cobalt / alumina ($Ni\text{-}Co/Al_2O_3$) composite coatings; electrodeposition; corrosion and erosion resistance; microhardness and wear rate; particle concentration.*

1. INTRODUCTION

Corrosion is a naturally occurring phenomenon commonly defined as the deterioration of substance (usually a metal) or its properties because of a reaction with its environment. Corrosion can cause dangerous and expensive damage to everything from automobiles, home appliances and drinking water systems to pipelines, bridges, energy production and public buildings. The impact of corrosion on society has been profound directly and indirectly. According to Cramer *et al*. (2005), Ahmad (2006) and Duquette *et al.* (2011), the direct cost of metallic corrosion is estimated to be USD 276 bil. on an annual basis. On average, the total cost of corrosion in industrial and developed countries was estimated to be about 3 to 5% of the gross domestic product (GDP) and this figure was estimated to be more than 6% for developing countries.

In addition to corrosion attacks, marine structures also face aggressive environments in terms of erosion. The presence of turbulence produces particle movement, which is a causing factor for erosion. Systems or equipment that are involved with the transport of particles or laden fluid, such as in offshore oil and gas productions, are also exposed to corrosion and erosion attacks. Thus, the specification and use of materials that combine erosion and corrosion resistances with high mechanical strength is a fundamental requirement in industrial applications, leading it to be the focus of interest in numerous researches (Rayes *et al*., 2013).

Ceramic coatings are excellent candidates for providing protection against corrosion attack. These coatings are widely used in industries as thermal barriers and wear resistant coatings. Zirconia,

dicalcium silicate, silica zirconia and calcium titanate are conventional thermal barrier coating materials, while alumina, titania and zirconia are examples of wear resistant coating materials (Das *et al*., 2003). Ceramic coatings are usually applied using thermal spraying processes, such as plasma spraying, combustion flame spraying, high velocity oxygen flame spraying and detonation gun processes. These processes offer an easy and convenient way of depositing a coating onto almost any surface (Venkataraman *et al*., 2006; Toma *et al*., 2008;). However, despite the excellent mechanical properties and corrosion behaviour of ceramic coatings, the thermal spraying process has limitations when it comes to complex structures, such as inside pipelines and their accessories, such as bends, elbows, tees and valves (Farrokhzad *et al*., 2013).

Alternatively, the electrodeposition technique offers several advantages, such as precisely controlled near room temperature operation, low energy requirements, capability to coat complex component geometries, low cost, and simple scale-up (Saha & Khan, 2010). The ability of the technique to coat various types of materials, such as oxide, nitride, carbide and metallic, in a metal matrix allows it to provide coatings for multiple applications (Berçot *et al*. 2002; Liang *et al*., 2009; Boonyongmaneerat *et al*., 2010; Bakhit & Akbari 2013). The advantages of this technique has encouraged researchers to further explore its potentials.

In recent years, there have been increasing interests focused on electrodeposited nickel-cobalt (Ni-Co) and Ni-Co based metal matrix composite (MMC) coatings due to their superior properties, such as higher hardness (Srivastava *et al*., 2006; Shi *et al*., 2006; Ranjith & Paruthimal Kalaignan, 2010; Srivastava *et al*., 2010), improved anti-wear, better corrosion resistance and oxidation resistance (Cai *et al*., 2015), as compared with pure Ni and Ni based composite coatings. The properties of Ni-Co or Ni-Co based composite coatings are mainly dependent on the incorporated particles and microstructures of the Ni-Co matrix (Kuo *et al*., 2004; Low *et al*., 2006; Sui *et al*., 2007; Nguyen *et al*., 2013; Cai *et al*., 2015).

Table 1 summarises the previous studies on composite coatings applied using the electrodeposition technique. Based on these studies, it was found that the highest nanoparticle concentration in the coating was reported to be less than 30%vol. The average %vol was reported to be just around 10%vol regardless of particle type and matrix. The low concentration of ceramic particles in the coatings have limited their mechanical performances as compared to ceramic coatings.

Table 1: Previous studies on composite coating applied using the electrodeposition technique. DC: direct current, PC: pulse current, PRC: pulse reverse current, Sc CO_2: supercritical CO_2, SCD: sediment coelectrodeposition, SiC: silica carbide, CeO: cerium oxide, TiO_2: titania, C: carbon.

Particles	Matrix	Particle concentration		Method	Curr.Density (A/dm^2)	Surfactant	Ref.
		Solution (g/l)	Deposit (vol%)				
SiC	Ni Ni-Co	5 4	2.0-8.1	SCD	3	Saccharin	Bakhit & Akbari (2014)
SiC	Ni-Co	5-20	8.1-5.7	SCD	1-4	-	Bakhit *et al.* (2014)
Al_2O_3 (0.3 μm)	Ni	10	17.4-16.8	Sc CO2	5	$C_{12}EO_8$	Chiu *et al.* (2014)
Al_2O_3-TiO_2	Ni	25.5 38.25	9.2-11.8	DC	2 -3	-	Farrokhzad et al. (2014)
Al_2O_3	Ni	20	-	DC	2-6	-	Góral *et al.* (2014)
Gamma Al_2O_3	Ni	10-50	2.8-15.4	PC	-	-	(Gupta *et al.* 2014)
CeO_2	Zn	20	-	DC PC	2 0.01-10 Hz	-	Nemes *et al.* (2014)

CeO_2	Ni-B	0-15	4.79	DC	50	-	Shakoor *et al*. (2014)
Al_2O_3 (0.3 µm)	Ni	1-20	13-18	SCD	6.5-34	-	Sun *et al*. (2014)
SiC	Ni-Co	0-20	8	SCD	1-4	SDS	Bakhit & Akbari (2013)
Al_2O_3- TiO_2	Ni	25.5 38.25	9.2-11.8	DC	1-3	-	Farrokhzad *et al*. (2013)
Fly Ash	Ni	1-50	12.5	DC	2-4	-	Nguyen *et al*. (2013)
Nano SiC micro SiC	Ni-Co	5	8.1 59.4	DC SCD	1-4	-	(Bakhit & Akbari 2012)
Al_2O_3	Ni	-	7.5	PC	2	-	Mohan *et al*. (2012)
SiC	Ni	1-10	28	SCD	1-4	TMAH	Narasimman *et al*. (2011)
TiO_2	Ni	5-15	7	DC	5	HPB	Parida *et al*. (2011)
TiO_2	Ni	0-50	8	DC	5	-	Baghery *et al*. (2010)
C	Ni	-	3.4	Sc CO2	5	-	Chung & Tsai (2010)
TiO_2	Zn	1	0.25	PC	0-19	-	Frade *et al*. (2010)
Al_2O_3	Ni	0.5 mol/l	4.3	DC	0.5-3	-	Saha & Khan (2010)
Al_2O_3	Ni	5-30	11.7	DC	1-9	HPB	Gül *et al*. (2009)
Al_2O_3	Ni	20	-	DC	2	-	Ciubotariu *et al*. (2008)
Al_2O_3	Ni-Co	80	6.5	PRC	2.22	-	Chang *et al*. (2008)
Al_2O_3	Ni-Co	20-60	-	PC	1-10	-	Tian & Cheng (2007)
Al_2O_3	Ni-Co	0-80	5.2	PRC	2	LCM	Chang *et al*. (2006)
Al_2O_3	Ni-Co	20-140	10	DC	1-6	-	Wu *et al*. (2004)
Al_2O_3	Ni	5	26.8	DC	3	-	Kuo *et al*. (2004)

Among the various inert particles, alumina (Al_2O_3) particles have many superior properties, such as low price, good chemical stability, and high microhardness and wear resistance at high temperatures. Hence, Al_2O_3 coatings are widely used for shipboards and submarines, textile industry and machinery to give protection and support to their structures (Gell *et al*., 2001; Wang & Leon 2007). The presence of Al_2O_3 particles in Ni-Co based metal matrix could increase the microhardness of the coating. These hard ceramic particles provide greater hardness through dispersion strengthening of the coating (Farrokhzad *et al*., 2013; Farrokhzad *et al*., 2014). However, a lot of factors should be considered to obtain superior coating properties, such as particle characteristics, electrolyte composition including additives, temperature, pH, surfactant type and concentration, current density, hydrodynamics (laminar, mixed and turbulent regimes), and electrode geometry (Low *et al*., 2006).

This paper reviews the electrodeposition techniques that are used to produce Ni-Co/Al_2O_3 coatings, and the electrodeposition variables that influence the coating performance. It then discusses further research that needs to be conducted in order to improve the corrosion and erosion resistance of Ni-Co/Al_2O_3 coating in harsh environments, such as marine conditions.

2. ELECTRODEPOSITION TECHNIQUES

The most commonly used electrodeposition technique is the direct current (DC) technique. This technique uses an electrochemical cell as show in Figure 1, which consists of anode and cathode electrodes, electrolyte, and DC power supply. The currents flow from the anode to the cathode through the electrolyte. During the process, free metal ions in the electrolyte will transfer to the cathode to gain the electrons and form a solid metal (Mansoor *et al.* 2013). The simple setup of this technique has encouraged researchers to conduct various researches related to this technique as shown in Table 1.

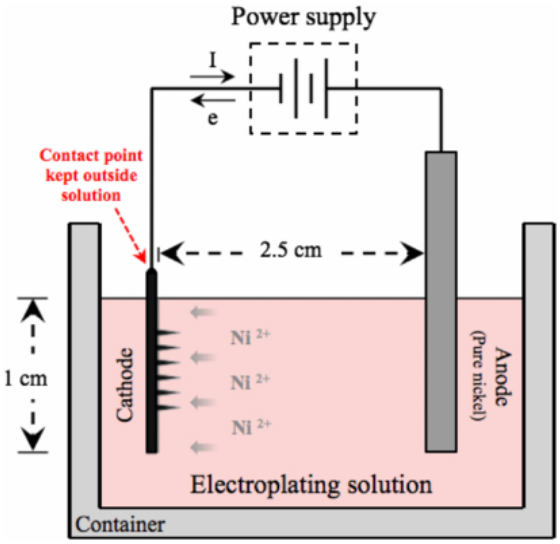

Figure 1. Schematic diagram of the electrochemical setup for the electrodeposition process (Mansoor *et al.*, 2013).

Some studies have also been conducted on the electrode arrangement in the bath. The conventional electrodeposition technique positions the electrodes vertically. However, a few researchers have suggested positioning the electrodes horizontally, with the cathode placed below to the anode. This type of arrangement is known as the sediment electrodepositing technique (Narasimman *et al*., 2011). This technique would allow the particles to settle down easily as sediment on the cathode surface with the support of gravitational and electrophoretic forces. Figure 2 shows a schematic image of the applied force during the deposition process. The gravitational and electrophoretic forces act vertically in the same direction, while the in conventional technique, the electrophoretic force is disturbed by the gravitational force in the perpendicular direction. The cell arrangement used by Narasimman *et al.* (2011) is shown in Figure 3. Working with Ni-SiC coating, they found that the percentage of SiC content in the coating increased as compared to the conventional technique. Feng *et al*. (2008) reported that Ni-Al_2O_3 coatings produced using this technique provide better microhardness and

lower wear rate than Ni-Al_2O_3 coatings produced using the conventional technique. Bakhit *et al*.(2014), who investigated the effect of the electrodeposition technique on microhardness and corrosion properties, also found that sediment electrodeposition increases the SiC content in the Ni-Co matrix and improves the microhardness of nanocomposite coatings (Bakhit & Akbari, 2012).

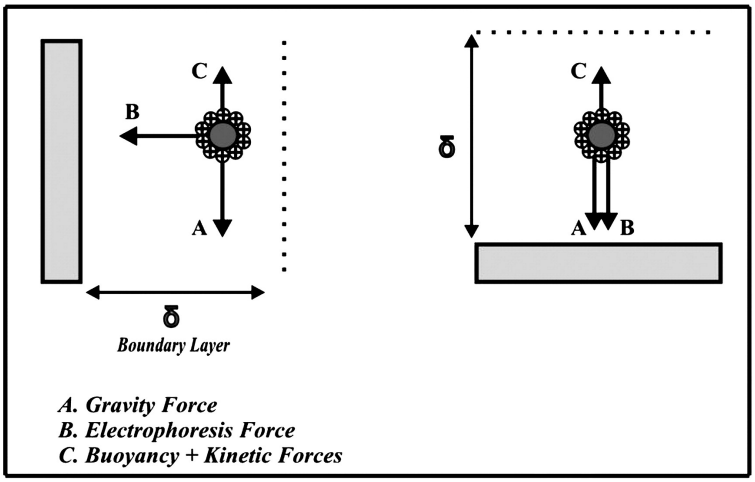

Figure 2: Schematic diagram of the applied forces for an immersed particle in the (L) conventional and (R) sediment electrodepositing techniques (Bakhit & Akbari, 2012).

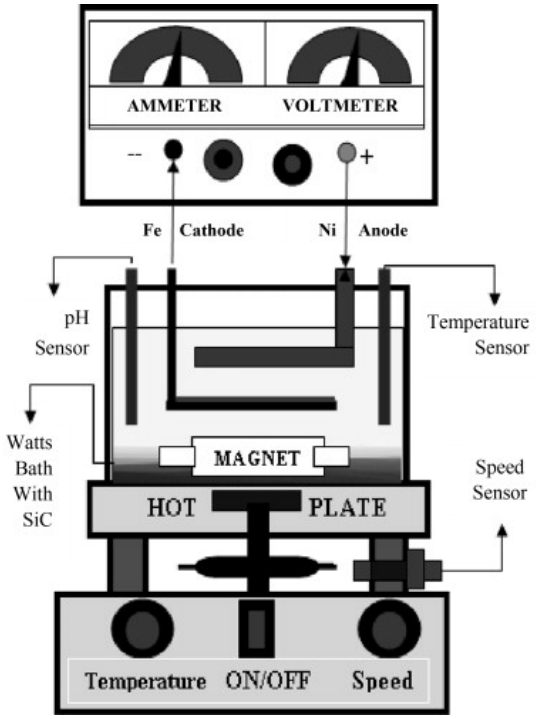

Figure 3: The cell arrangement used for the sediment electrodeposition technique reported by Narasimman *et al*. (2011).

Other techniques frequently used for the electrodeposition process include pulse current and reverse pulse current. In the pulse current technique, the current supply or potential alternates between two different values, while the pulse reverse current technique uses an alternating current between the anodic and cathodic current densities. These techniques are used to control the electron transfer

through the electrolyte by controlling the current distribution. Regulating the current would remove the negatively charged layer that is constructed during the plating process (Chandrasekar & Pushpavanam, 2008). Chang *et al*. (2008) found that Ni-Co/Al_2O_3 coatings produced using this technique are uniform, compact and possess finer grain. Similar findings were reported by Mohan *et al*. (2012) for Ni/nanoAl_2O_3 coatings and Nemes *et al*. (2014) for Zn/CeO_2 coatings. In addition, Bahrololoom & Sani (2005) reported that pulse current provides better mechanical properties to Ni-Al coatings. They also investigated the relationship between frequency and duty cycle of pulse currents with the microhardness and wear behaviour of the coatings. They found the hardness of the coating increased when low duty cycle and frequency were used. These results are in good agreement with the findings of studies conducted using Zn-TiO_2 coatings (Youssef *et al*., 2008; Frade *et al*., 2010).

Zheng & An (2008) fabricated Zn-Ni/Al_2O_3 coatings using an ultrasound horn in the electrolyte to produce ultrasonic streaming and cavitation bubbles. They found that increasing the ultrasonic power from 0 to 0.7 W/cm^2 would increase the Al_2O_3 content in the coating from 4.5 to 8.9 wt.% and could reduce the agglomeration of the Al_2O_3 particles. The presence of ultrasonic streaming is believed to catalyse the movement of the Al_2O_3 nanoparticles towards the cathode, while the cavitation bubbles deagglomerate the nanoparticle. However, as the ultrasonic power is further increased, the coating performance reduces, with high porosity and reduced Al_2O_3 content. Bakhit & Akbari (2013) also used this method in their research involving deposition of Ni-Co/SiC composite coatings. Other researchers also agree with the advantages provided by the ultrasonic method (Kuo *et al*., 2004; Parida *et al*., 2011; García-Lecina *et al*., 2012; Gupta *et al*., 2014).

Another technique that been discussed among the researchers is the addition of CO_2 in the electrolyte. CO_2 is emulsified in the electrolyte with pressure of more than more than 10 MPa to increase the solubility of H_2 produced during the electrodeposition process (Figure 4). The presence of CO_2 in the water forms carbonic acid, which increases the H^+ content in the solution (Chung & Tsai, 2010). As a result, the coatings produced have better hardness and low porosity, as reported by Chung *et al*.(2008) and Chiu *et al*.(2014).

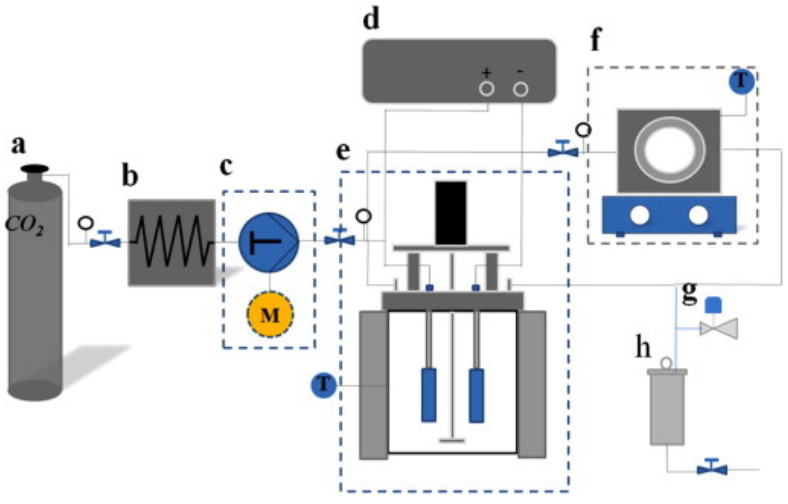

a. CO_2 cylinder ; *b*. cooler ; *c*. high pressure pump ; *d*. power supply ; *e*. electroplating vessel with electric-magnetic driven agitator ; *f*. vessel for view of micro-emulsion formation ; *g*. back pressure regulator ; *h*. separator

Figure 4: Schematic diagram of the recirculating high pressure system for electroplating in supercritical CO_2 fluid (Chung *et al*., 2008).

3. ELECTRODEPOSITION VARIABLES

In addition to the electrodeposition techniques, the mechanical properties of the produced coatings are influenced by several deposition variables, which include applied current density, deposition duration, particle concentrations and particle type (Farrokhzad *et al*., 2014).

Wu *et al*. (2004) studied the effect of current density on Ni-Co/Al_2O_3 coatings. The highest volume percentage of Al_2O_3 was obtained at current density of 3 A/dm^2. The study on Ni-Al_2O_3 coatings conducted by Goral *et al*. (2014) found that microhardness increases when current density is increased from 2 to 6 A/dm^2. Simultaneously, this parameter also provides more uniform particle distribution. Current density also gives the same effect to Ni-SiC coatings, as reported by Bakhit *et al*. (2014). The optimum current density used to obtain the highest particle content in the coating was 3 A/dm^2. In contrast, Sun *et al*. (2014) reported that the lowest current density used (6.5 A/dm^2) provided a slightly higher Al content as compared to current density of 34 A/dm^2, but the difference was less than 1%.

Farrokhzad *et al*. (2014) studied the effect of deposition time on the coating characteristics of Ni/Al_2O_3-TiO_2. They found that the coating prepared at 120 min of deposition time was thicker than the coating prepared at 90 min of deposition time. However, duration time had no significant effect on he microhardness of the coatings. While not many papers discuss the effect of deposition time, some researchers prefer to vary the duration in order to get the suitable thickness of coatings for their studies (Bakhit & Akbari 2013; Gupta *et al*., 2014; Bakhit *et al*., 2014).

Another approach used to improve coating properties is by varying the ceramic particle concentration in the electrolyte. Farrokhzad *et al*. (2014) reported that molarities of Al_2O_3 and TiO_2 particles is proportional to the particle volume in the coating. However, Gul *et al*. (2009) found that the increase of volume of Al_2O_3 in the coating is not comparable to the increase of concentration of Al_2O_3 particles in the electrolyte; a six times increment of Al_2O_3 in the electrolyte only increased the Al_2O_3 concentration in the coating by less than three times. Nguyen *et al*. (2013) also reported similar results; by increasing the fly ash concentration in the electrolyte from 20 to 50 g/l, it could produce coatings with 2.5% higher particle concentration. The concentration of matrix particles in the electrolyte also influences the ceramic particles in the coatings. Kuo *et al*. (2004) increased the concentration of Ni^{2+} (by changing the concentration of $Ni(NH_2SO_3)_2$) in the electrolyte. As result, they managed to increase the Al_2O_3 particles in the coating from 8.4 to 26.8 vol%. Conversely, low Ni^{2+} concentrations would encourage H^+ reduction, which produces coatings with high porosity.

The presence of a surfactant could develop positive charges on the particle surface to prevent agglomeration and improve particles stability in the electrolyte. Chen *et al*. (2006) used hexadecylpyridinium bromide (HPB) as a surfactant in Ni-Al_2O_3 coatings. The increase of HBP to 300 mg/l enhanced Al_2O_3 content by up to 14.7 vol%. Similar results were also reported by Gul *et al*. (2009) and Narasimman *et al*. (2011) by using SiC particles. Surfactants are also used in the sediment electrodeposition technique to decrease electrolyte viscosity and thus, gravitational force and diffusion coefficient improve the deposition process (Parida et al. 2011). Chiu *et al*. (2014) used an octa (ethylene oxide) dodecyl ether ($C_{12}EO_8$) surfactant to emulsify the electrolyte in presence of CO_2. The emulsified electrolyte increases the solubility of H_2. Hence, the formation of H_2 gases bubble could be minimised to produce a smoother surface (Chung & Tsai 2010). Commonly used surfactants are hexadecylpyridinium bromide (HBP) (Chen *et al*., 2006; Gül *et al*., 2009; Parida *et al*., 2011), tetramethyl ammonium hydroxide (TMAH) (Narasimman et al. 2011), polyglycol (Faraji *et al*., 2013), $H(CH_2CH_2O)_8O$–(CH2)12H (Chung et al. 2008), cetyltrimethyl ammonium bromide (CTAB) (Kuo *et al*., 2004) and sodium dodecyl sulfate (SDS) (Bakhit & Akbari, 2013, 2014).

4. DISCUSSION

Composite coating performance has improved over time in terms of mechanical properties and corrosion resistance. However, some improvements are needed with the intention of making this coating reliable for harsh environments. Applications in marine environments expose materials to corrosive conditions and erosive medium. Thus, the use of materials that combine erosion and corrosion resistance with high mechanical strength is a requirement in industrials applications (Rayes *et al*., 2013).

While the improvement of Ni-Co/Al_2O_3 coating properties has shown good achievement to proof its ability as a protective coating, there is a lack of studies on the effectiveness of this coating in erosive environments. Most researches conducted separate between corrosion and erosion effects. Rayes *et al*. (2013) describe the erosion-corrosion as an acceleration of the deterioration rate of metal due to the combined effect of erosion and electrochemical attacks. The combined effect could enhance the damages not only to the coating, but also to the substrate through the combined interaction between the two processes. Erosion could strip the coating and catalyse the corrosion attack. On the other hand, corrosion occurs first to catalyse the erosion process. This mechanism leads the greater damage to the coating and substrate (Rayes *et al*., 2013; Islam & Farhat, 2013; Li *et al*., 2015).

The presence of ceramic particles in the metal matrix also gives different results among the researchers in terms of their corrosion behaviour. Some of the researchers claim that ceramic particles could enhance the corrosion resistance of the coatings (Bakhit *et al*., 2014), while others report different findings (Chiu *et al*., 2014; Sun *et al*. 2014). They verified that the corrosion behaviour of the coatings are not only influenced by the embedded particles, but also other factors. The coating microstructure plays a big role in providing corrosion protection (Hassanuddin *et al*., 2011). The presence of permeable defects, such as pores, cracks and grain boundary gaps, could allow the electrolyte to penetrate and interact with the metal surface, which catalyses the corrosion attack (Ctibor *et al*., 2007; Yusoff *et al*., 2013). The interaction between the electrolyte and substrate exhibits galvanic corrosion either to the coating or to the substract itself depending on nobility of the materials. That is the reason why several researchers have tried to reduce the porosity in their coatings (Yan *et al*., 2003; Haslam *et al*., 2005; Sun *et al*., 2009). However, previous studies on Ni-Co/Al_2O_3 coatings did not discuss this effect very well.

The penetration of the electrolyte through the permeable defects is sluggish due to the small space or capillary. As a result, electrochemistry impedance spectroscopy (EIS) tests for corrosion could give different values over the time and require a longer testing period. Nevertheless, most of the corrosion studies were conducted in a day or two, which believed not be sufficient to model the real process.

Another issue rising from the literature is the low concentration of the ceramic particles in the coatings. Kuo *et al*.(2004) found that lower electrolyte concentrations tend to decrease the agglomerated Al_2O_3 particle size. The Al_2O_3 particles would disperse effectively in the electrolyte solution. As a result, it would create more opportunity for loose Al_2O_3 particles to attach onto the electrodes or substrate (Kuo *et al*., 2004). The increase of Al_2O_3 particles could provide better mechanical performance, especially microhardness and wear resistance (Habib *et al*., 2006). Kuo *et al*. (2004) also changed the Ni^{2+} concentration in order to control the electrolyte concentration, as compared to researchers who used Al_2O_3 concentration as the focus of their study (García-Lecina *et al*., 2012; Gupta *et al*., 2014; Farrokhzad *et al*., 2014). However, the effect of Ni^{2+} concentration with the presence other metallic elements, such as Co^{2+}, and inert particle, such as Al_2O_3 , has not been studied.

5. CONCLUSION

This paper has reviewed several electrodeposition techniques that have been used to produce Ni-Co/Al_2O_3 composite coatings. Direct current is the most commonly used technique due to its simple setup. Other techniques that can be used are pulse current and pulse reverse current, sediment electrodeposition, and CO_2 bath. All the techniques discussed have their own advantages to improve the coating properties. In addition, process variables, including applied current density, deposition time, particle concentration and use of surfactants, also give great effect to the coating performance.

Although the electrodeposition of composite coatings has been established, some improvements are still needed with the intention of making this coating reliable for severe environments. For this purpose, a corrosion-erosion study for Ni-Co/Al_2O_3 coatings should be conducted. Furthermore, increase of Al_2O_3 content is a key to produce coatings with excellence performance.

REFERENCES

Ahmad, Z. (2006). *Principles of Corrosion Engineering and Corrosion Control.* Butterworth-Heinemann, Hungary.

Duquette, D.J., Schafrik, R. E., Asphahani, A.I., Bierwagen, G.P., Butt, D.P., Frankel, G.S., Newman, R.C., Rosenbloom, S.N., Schwartz, L.H., Scully, J.R., Tortorelli, P.F., Trejo, D., Untereker, D.F. and Urquidi-Macdonald, M., (2011). *Research Opportunities in Corrosion Science and Engineering*. The National Academies Press, Washington, DC.

Baghery, P., Farzam, M, Mousavi, A.B. and Hosseini, M. . (2010). Surface & Coatings Technology Ni – TiO 2 nanocomposite coating with high resistance to corrosion and wear. *Surf. Coat. Tech.*, **204**: 3804–3810.

Bahrololoom, M.E. & Sani, R. (2005). The influence of pulse plating parameters on the hardness and wear resistance of nickel–alumina composite coatings. *Surf. Coat. Tech.*, **192**: 154–163.

Bakhit, B. & Akbari, A. (2012). Effect of particle size and co-deposition technique on hardness and corrosion properties of Ni–Co/SiC composite coatings. *Surf. Coat. Tech.*, **206**: 4964–4975.

Bakhit, B. & Akbari, A. (2013). Synthesis and characterization of Ni–Co/SiC nanocomposite coatings using sediment co-deposition technique. *J. Alloy Compd.*, **560**: 92–104.

Bakhit, B. & Akbari, A. (2014). A comparative study of the effects of saccharin and β-SiC nano-particles on the properties of Ni and Ni–Co alloy coatings. *Surf. Coat. Tech.*, **253**: 76–82.

Bakhit, B., Akbari, A., Nasirpouri, F. and Hosseini, M.. (2014). Corrosion resistance of Ni-Co alloy and Ni-Co/SiC nanocomposite coatings electrodeposited by sediment codeposition technique. *Appl. Surf. Sci.,* **307**: 351-359. .

Cai, F., Jiang, C., Fu, P. and Ji, V.. (2015). Effects of Co contents on the microstructures and properties of electrodeposited NiCo–Al composite coatings. *Appl. Surf. Sci.*, **324**: 482–489.

Chandrasekar, M.S. & Pushpavanam, M. (2008). Pulse and pulse reverse plating—Conceptual, advantages and applications. *Electrochim. Acta*, **53**: 3313–3322.

Chang, L.M., An, M.Z., Guo, H.F. and Shi, S.Y.. (2006). Microstructure and properties of Ni–Co/nano-Al2O3 composite coatings by pulse reversal current electrodeposition. *Appl. Surf. Sci.*, **253**: 2132–2137.

Chang, L.M., Guo, H.F. & An, M.Z. (2008). Electrodeposition of Ni-Co/Al2O3 composite coating by pulse reverse method under ultrasonic condition. *Mater. Lett.*, **62**: 3313–3315.

Chen, L., Wang, L., Zeng, Z. and Zhang, J. (2006). Effect of surfactant on the electrodeposition and wear resistance of Ni–Al2O3 composite coatings. *Mater. Sci. Eng. A*, **434**: 319–325.

Chiu, S.Y., Chung, S.T., Lin, C.Y. and Tsai, W.T. (2014). Electrodeposition of Ni-Al2O3 composite coatings employing supercritical CO2 baths. *Surf. Coat. Tech.*, **247**: 68–73.

Chung, S.T., Huang, H.C., Pan, S.J., Tsai, W.T., Lee, P.Y., Yang, C.H. and Wu, M.B.(2008). Material characterization and corrosion performance of nickel electroplated in supercritical CO2 fluid. *Corros. Sci.*, **50**: 2614–2619.

Chung, S.T. & Tsai, W.T. (2010). Effect of pressure on the electrodeposition of nanocrystalline Ni–C in supercritical CO2 fluid. *Thin Solid Films*, **518**: 7236–7239.

Ciubotariu, A.C., Benea, L., Varsanyi, M.L., Dragan, V.,. (2008). Electrochemical impedance spectroscopy and corrosion behaviour of Al2O3–Ni nano composite coatings. *Electrochim. Acta*, **53**: 4557–4563.

Cramer S.D. & Covino, B.S. (2005). *ASM Handbook, 13th Ed.* ASM International, USA.

Ctibor, P., Neufuss, K., Zahalka, F. and Kolman, B. (2007). Plasma sprayed ceramic coatings without and with epoxy resin sealing treatment and their wear resistance. *Wear*, **262**: 1274–1280.

Das, S., Bandyopadhyay, T.K., Ghosh, S., Chattopadhyay, A.B. & Bandyopadhyay, P.P. (2003). Processing and characterization of plasma-sprayed ceramic coatings on steel substrate: Part II. On coating performance. *Metall. Mater. Trans. A*, **34**: 1919–1930.

Faraji, S. Abdul Rahim, A., Mohamed, N., Sipaut, C.S. & Raja, B. (2013). Corrosion resistance of electroless Cu–P and Cu–P–SiC composite coatings in 3.5% NaCl. *Arab J. Chem.*, **6**: 379–388.

Farrokhzad, M.A., Saha, G.C. & Khan, T.I. (2014). Three-body wear performance of co-electrodeposited cermet coatings. *Wear*, 313, 34–42.

Farrokhzad, M.A., Saha, G.C. & Khan, T.I. (2013). Wear performance of co-electrodeposited cermet coatings. *Surf. Coat. Tech.*, **235**: 75–85.

Feng, Q. Li, T., Yue, H., Qi, K., Bai, F. & Jin, J. (2008). Preparation and characterization of nickel nano-Al2O3 composite coatings by sediment co-deposition. *Appl. Surf. Sci.*, **254**: 2262–2268.

Frade, T., Bouzon, V., Gomes, A. & Pereira, M.I.S. (2010). Pulsed-reverse current electrodeposition of Zn and Zn-TiO2 nanocomposite films. *Surf. Coat. Tech.*, **204**: 3592–3598.

García-Lecina, E.,García-Urrutia, I., Díez, J.A., Morgiel, J. & Indyka, P. (2012). A comparative study of the effect of mechanical and ultrasound agitation on the properties of electrodeposited Ni/Al 2O 3 nanocomposite coatings. *Surf. Coat. Tech.*, **206**: 2998–3005.

Góral, A., Nowak, M., Berent, K. & Kania, B. , (2014). Influence of current density on microstructure and properties of electrodeposited nickel-alumina composite coatings. *J. Alloy Compd.*, **615**: S406–S410.

Gül, H. Kılıç, F., Aslan, S., Alp, A. & Akbulut, H. (2009). Characteristics of electro-co-deposited Ni–Al2O3 nano-particle reinforced metal matrix composite (MMC) coatings. *Wear*, **267**: 976–990.

Gupta, A., Barkam, S., Lahiri, D., Balasubramaniam, R. & Balani, K. (2014). Effect of alumina dispersion on microstructural and nanomechanical properties of pulse electrodeposited nickel–alumina composite coatings. *J. Mater. Sci. Technol.*, **30**: 808–813.

Habib, K.A., Saura, J.J., Ferrer, C., Damra, M.S., Giménez, E. and Cabedo, L. , (2006). Comparison of flame sprayed Al2O3/TiO2 coatings: Their microstructure, mechanical properties and tribology behavior. *Surf. Coat. Tech.*, 201, 1436–1443.

Haslam, J.J., Farmer, J.C., Hopper, R.W. & Wilfinger, K.R. (2005). Ceramic coatings for a corrosion-resistant nuclear waste container evaluated in simulated ground water at 90 °C . *Metal Mater. Trans. A*, **36**: 1085–1095.

Hassanuddin, N. Ghazali, M.J., Muchtar, A., Isa, M.C. & Daud, A.R., (2011). Effects of Al_2O_3-13% TiO_2 coating particle size on commercial mild steel via plasma spray method. *Key Eng. Mat.*, **462-463**: 645–650.

Islam, M.A. & Farhat, Z.N. (2013). The synergistic effect between erosion and corrosion of API pipeline in CO2 and saline medium. *Tribol. Int.*, **68**: 26–34.

Kuo, S.L., Chen, Y.C., Ger, M.D. & Hwu, W.H. , (2004). Nano-particles dispersion effect on Ni/Al2O3 composite coatings. *Mater. Chem. Phys.*, **86**: 5–10.

Li, S., Zuo, Y. & Ju, P. (2015). Erosion–corrosion resistance of electroplated Co-Pd film on 316L stainless steel in a hot sulfuric acid slurry environment. *Appl. Surf. Sci.*, **331**: 200–209.

Liang, X.S., Ouyang, J.H., Li, Y.F. & Wang, Y.M. , (2009). Electrodeposition and tribological properties of Ni–SrSO4 composite coatings. *Appl. Surf. Sci.*, **255**: 4316–4321.

Low, C.T.J., Wills, R.G.A. & Walsh, F.C., (2006). Electrodeposition of composite coatings containing nanoparticles in a metal deposit. *Surf. Coat. Tech.*, 201, 371–383.

Mansoor, I., Liu, Y., Häfeli, U.O. & Stoeber, B. , (2013). Arrays of hollow out-of-plane microneedles made by metal electrodeposition onto solvent cast conductive polymer structures. *J. Micromech. Microeng.*, **23**: 85011.

Mohan, S., Saravanan, G. & Bund, A. (2012). Role of magnetic forces in pulse electrochemical deposition of Ni nanoAl 2 O 3 composites. *Electrochim. Acta*, **64**: 94–99.

Narasimman, P., Pushpavanam, M. & Periasamy, V.M. (2011). Synthesis, characterization and comparison of sediment electro-codeposited nickel–micro and nano SiC composites. *Appl. Surf. Sci.*, **258**: 590–598.

Nemes, P.I., Lekka, M., Fedrizzi, L. & Muresan, L.M. (2014). Influence of the electrodeposition current regime on the corrosion resistance of Zn–CeO2 nanocomposite coatings. *Surf. Coat. Tech.*, **252**: 102–107.

Nguyen, V.C., Lee, C.Y., Chen, F.J., Lin, C.S. & Chang, L. (2013). An electroplating technique using the post supercritical carbon dioxide mixed watts electrolyte. *Surf. Coat. Tech.*, **232**: 234–239.

Nguyen, V.H. Ngo, T.A.T., Pham, H.H. and Nguyen, N.P. (2013). Nickel composite plating with fly ash as inert particle. *T. Nonferr. Metal Soc.*, **23**: 2348–2353.

Parida, G. Chaira, D., Chopkar, M. and Basu, A. (2011). Synthesis and characterization of Ni-TiO2 composite coatings by electro-co-deposition. *Surf. Coat. Tech.*, **205**: 4871–4879.

Ranjith, B. & Paruthimal Kalaignan, G. (2010). Ni–Co–TiO2 nanocomposite coating prepared by pulse and pulse reversal methods using acetate bath. *Appl. Surf. Sci.*, **257**: 42–47.

Rayes, M.M. El, Abdo, H.S. & Khalil, K.A., (2013). Erosion - corrosion of cermet coating. *Int. J. Electrochem. Sci.*, **8**: 1117–1137.

Saha, R.K. & Khan, T.I., (2010). Effect of applied current on the electrodeposited Ni–Al2O3 composite coatings. *Surf. Coat. Tech.*, 205, 890–895.

Shakoor, R.A., Kahraman, R., Waware, U.S., Wang, Y. & Gao, W., (2014). Synthesis and properties of electrodeposited Ni–B–CeO2 composite coatings. *Mater. Design*, **59**: 421–429.

Shi, L., Sun, C.F., Gao, P., Zhou, F. and Liu, W.M. (2006). Electrodeposition and characterization of Ni–Co–carbon nanotubes composite coatings. *Surf. Coat. Tech.*, **200**: 4870–4875.

Srivastava, M., Selvi, V.E., Grips,V.K.W & Rajam,V., (2006). Corrosion resistance and microstructure of electrodeposited nickel–cobalt alloy coatings. *Surf. Coat. Tech.*, **201**: 3051–3060.

Srivastava, M., William Grips, V.K. & Rajam, K.S. (2010). Electrodeposition of Ni–Co composites containing nano-CeO2 and their structure, properties. *Appl. Surf. Sci.*, **257**: 717–722.

Sui, J.H., Gao, Z.Y., Cai, W. and Zhang, Z.G. , (2007). Corrosion behavior of NiTi alloys coated with diamond-like carbon (DLC) fabricated by plasma immersion ion implantation and deposition. *Mater. Sci. Eng. A*, **452-453**: 518–523.

Sun, C., Hui, R., Qu, W. and Yick, S., (2009). Progress in corrosion resistant materials for supercritical water reactors. *Corros. Sci.*, **51**: 2508–2523.

Sun, Y., Flis-Kabulska, I. & Flis, J. (2014). Corrosion behaviour of sediment electro-codeposited Ni-Al2O 3 composite coatings. *Mater. Chem. Phys.*, **145**: 476–483.

Tian, B.R. & Cheng, Y.F. (2007). Electrolytic deposition of Ni–Co–Al2O3 composite coating on pipe steel for corrosion/erosion resistance in oil sand slurry. *Electrochim. Acta*, **53**: 511–517.

Toma, F.L., Berger, L.M., Naumann, T. & Langner, S., (2008). Microstructures of nanostructured ceramic coatings obtained by suspension thermal spraying. *Surf. Coat. Tech.*, **202**: 4343–4348.

Venkataraman, R., Ravikumar, B., Krishnamurthy, R. & Das, D.K. , (2006). A study on phase stability observed in as sprayed Alumina-13 wt.% Titania coatings grown by detonation gun and plasma spraying on low alloy steel substrates. *Surf. Coat. Tech.*, **201**: 3087–3095.

Wang, M. & Leon, L.S., (2007). Effects of the powder manufacturing method on microstructure and wear performance of plasma sprayed alumina-titania coatings. *Surf. Coat. Tech.*, **202**: 34–44.

Wu, G., Li, N., Zhou, D. and Mitsuo, K., (2004). Electrodeposited Co–Ni–Al2O3 composite coatings. *Surf. Coat. Tech.*, **176**:157–164.

Yan, D., He, J., Li, X., Liu, Y., Dong, Y. & Liu, H. (2003). The corrosion behavior of plasma-sprayed Ni/Al–Al2O3 and Ni/Al–Al2O3+13 wt.% TiO2 graded ceramic coatings in 5%HCl solution. *Surf. Coat. Tech.*, **176**: 30–36.

Youssef, K.M., Koch, C.C. & Fedkiw, P.S. (2008). Influence of pulse plating parameters on the synthesis and preferred orientation of nanocrystalline zinc from zinc sulfate electrolytes. *Electrochim Acta*, **54**: 677–683.

Yusoff, N.H.N., Ghazali, M.J., Isa, M.C., Daud, A.R. & Muchtar, A. (2013). Effects of powder size and metallic bonding layer on corrosion behaviour of plasma-sprayed Al2O3-13% TiO2 coated mild steel in fresh tropical seawater. *Ceram Int*, **39**: 2527–2533.

Zheng, H.Y. & An, M.Z., (2008). Electrodeposition of Zn–Ni–Al2O3 nanocomposite coatings under ultrasound conditions. *J. Alloy Compd.*, **459**: 548–552.

A REVIEW OF SOOT PARTICLE MEASUREMENT IN LUBRICATING OIL

Fadzli Ibrahim[1,2], Wan Mohd Faizal Wan Mahmood[1*], Shahrir Abdullah[1] & Mohd Radzi Abu Mansor[1]

[1]Department of Mechanics and Materials Engineering, Faculty of Engineering and Built Environment, Universiti Kebangsaan Malaysia (UKM), Malaysia
[2]Mechanical and Aerospace Technology Division, Science & Technology Research Institute for Defence (STRIDE), Ministry of Defence, Malaysia

[*]Email: wmfaizal@eng.ukm.my

ABSTRACT

This paper reviews the most common techniques available for measurement of soot-in-oil particularly for diesel engine lubricating oil. This includes insolubility test, nanoparticle tracking analysis, infrared spectrometric analysis, thermogravimetric analysis, spot test and light extinction measurement. Each method is described systematically, covering the basic principles of operation, their applications and any issues regarding the measurement process. The main concern for each method in the field is on irregularity in output details due to lack of standard analytical procedures for distinguishing between elemental and organic carbons. Combining or complementing these methods can provide a better soot-in-oil measurement.

Keywords: *Soot-in-oil; soot formation; diesel engine; soot measurement; engine emission*.

1. INTRODUCTION

Emissions from vehicles, particularly from diesel engines, have become an essential issue for decades. Even though numerous efforts have been taken, it still not absolutely solved. Unburnt hydrocarbons (HC), oxides of carbon (COx), oxides of nitrogen (NOx), oxides of sulphur (SOx) and solid carbon particulates are the major emissions during the combustion process in diesel engines (Ganesan, 2004). Among all of these emissions, soot particles is one of the products that contaminate engine oils, which will decrease overall engine performance (Woschni & Huber, 1991; Ladommatos *et al.*, 1996; Mainwaring, 1997; Gautam *et al.*, 1999; George *et al.*, 2007a, b). These harmful particles also cause premature oil change and wastage of lubricants for up to billions of tonnes per year, resulting in environmental pollution (Gómez-Rico *et al.*, 2003) and critical impact to human wellbeing (Brunekreef & Holgate, 2002; Kagawa, 2002; Englert, 2004; Kim *et al.*, 2015).

Due to these global problems, most of the countries around the globe are closely monitoring emissions from vehicles, and as a result, the regulations are become more stringent every year. ECOpoint Inc. (2015) reported that most of the pioneer countries in practicing emission regulations, such as Europe and USA (Wan Mahmood, 2011), keep improving their direction by implementing Euro 6 and Tier 4 standards consecutively, starting from 2014. Other countries such as China, Japan and India will do the same according to their own standards.

Together with stricter rules enforced by governments, researchers as well as manufacturers also play an important role in building a better environment. Currently, they have improved diesel engine technology by introducing various approaches, including NOx reduction techniques (Zelenka *et al.*, 2000), improvement of diesel fuel, spraying method and post treatment of exhaust emission (Wei & Na, 2011), portable emission measurement system (PEMS) (Giechaskiel *et al.*, 2013), improvement of oil additives (Hu *et al.*, 2013), and reducing soot by using microwave heating (Al-Wakeel *et al.*, 2012). Although all of these techniques have efficiently applied, the problems of emissions are still far from being completely resolved. However, even tiny enhancements in emission control technology will contribute to greater influence on environmental pollution as well as the global economic condition (Reitz, 2013; Johnson, 2014).

It is well understood that small sized soot particles, generated from engine combustion, have more dangerous effects, not only for human health but also for engine performance. Smaller soot particles increase the potential of engine oil in the crankcase sump to be contaminated. This is due to the higher possibility of smaller particles flowing through the crevice volume between the piston and cylinder wall during the engine cycle (Pulkrabek, 2004; Bredin *et al.*, 2012). Hence, it is important to measure soot properties and characteristics (Xi & Zhong, 2006).

This paper reviews measurement methods for soot-in-oil, particularly for diesel engine lubricating oil. Various methods are discussed in detail, including their operating principle and current issues. Each technique will be summarised accordingly based on their sampling method, particle extraction, diagnostic and particle characteristics. Then, future recommendations are suggested to present possible efforts that can be used in reducing soot-in-oil problems.

2. SOOT FORMATION AND PROPERTIES

Fundamentally, the molecular structure of fuels starts to change when in high temperature conditions, growing as a poly-aromatic hydrocarbon (PAH). Every PAH will react with each other to form larger molecules for soot nucleation, known as nuclei. Surface growth process on the nuclei will develop larger particles, known as primary particles. Then, coagulation (or coalescence) occurs to combine the primary particles as a single spherically shaped particle or agglomerated particles. At any time through this process, oxidation occurs when the temperature reaches

1,300 K, where the carbons or hydrocarbons are transformed into combustion products (Amann & Siegla, 1981; Haynes & Wagner, 1981; Richter & Howard, 2000; Dederichs, 2004; Tree & Svensson, 2007; Eastwood, 2008). Knowledge of these whole soot formation processes is imperative in order to decide how to prepare and conduct the appropriate soot-in-oil measurement techniques.

Soot particle size is visualised in Figure 1, which shows the particle mass and number weighted size distributions. It is shown that the maximum number of soot particles exist during nuclei mode before it continues decreasing in subsequent modes. This mode consists of particles in the diameter range of 0.005 to 0.05 μm (nanoparticles). Significant particle mass appears in the accumulation mode, within the diameter range of 0.1-0.3 μm (between ultrafine and fine particles). This is where the agglomeration and adsorption processes take place. The coarse mode is where particle mass and weight are reduced, containing about 5-20% of the particle mass. The particles from previous modes are deposited onto the cylinder and exhaust system surfaces, causing the reduction (Kittelson, 1998).

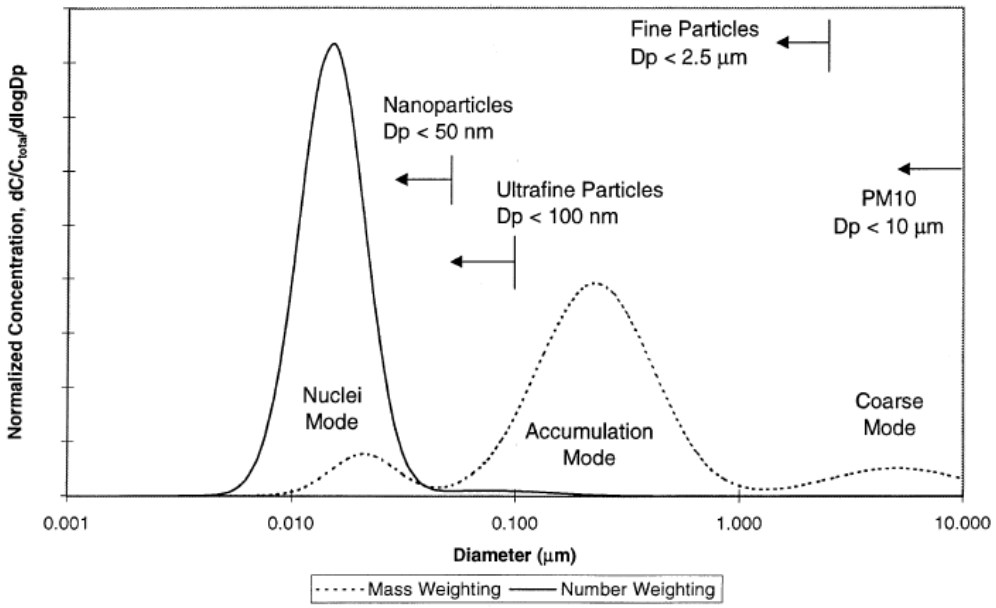

Figure 1: Typical engine exhaust size distribution for mass and number weightings (Kittelson, 1998).

By understanding how soot particles are formed and react, several techniques are established to determine the essential soot characteristics, including (a) mass distribution, (b) particle number, (c) surface concentration, (d) volume fraction, (e) density, and (f) particle size. Each technique applies different basic principles, which contribute to different results.

3. SOOT MEASUREMENT TECHNIQUES

Generally, there are three different locations for soot particles to be measured, which are in the exhaust emission, combustion chamber (both in the combustion flame and deposited on the cylinder wall) and contaminated soot-in-oil, as shown in Figure 2. Figure 3 shows the classification of soot measurement techniques based on operating principle, which are filtering technique, chemical analysis, optical technique, using microbalance instruments, charging method, and a combination of these techniques.

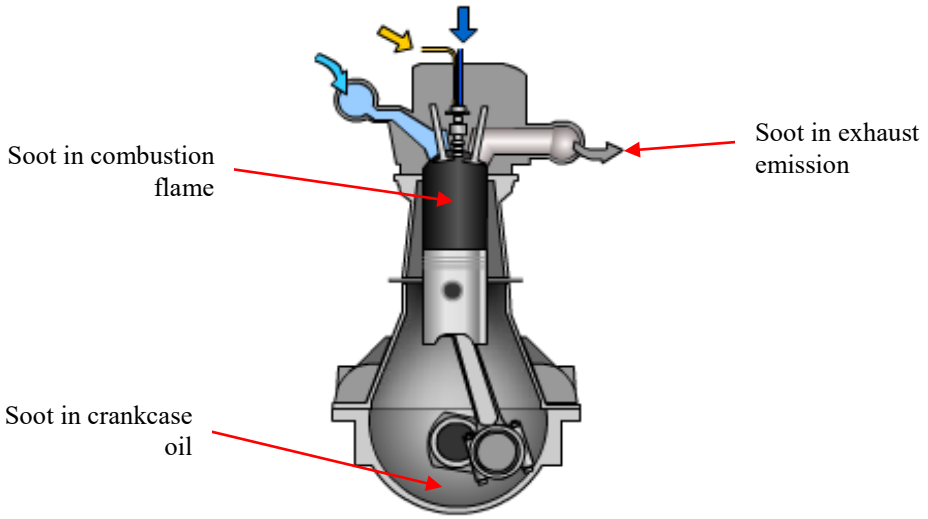

Figure 2: Different types of soot in internal combustion engine (Brain, 2015).

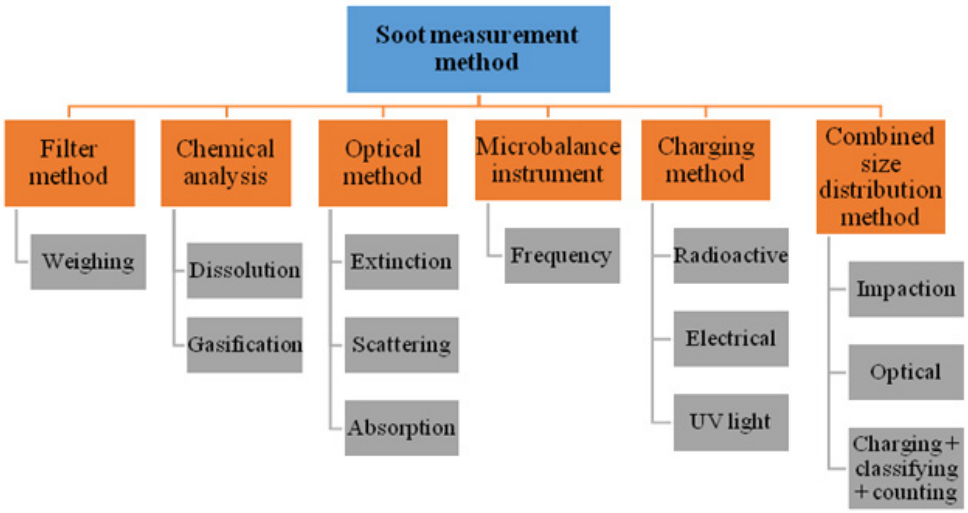

Figure 3: Soot measurement techniques classification by Giechaskiel *et al.* (2013).

While it has been reported that the modern developed techniques provide better response time (McMurry, 2000) and higher portability (Petrovic *et al.*, 2011), in some cases, traditional methods, such as chemical analysis, are still desired in order to utilise more powerful analytical procedures in dedicated research laboratories (Kulkarni *et al.*, 2011). In this section, the most common methods for measuring soot-in-oil will be discussed in detail, comprising their working principle as well as their advantages and current issues.

3.1 Insolubility Test

Insolubility test, also known as pentane and toluene insolubles, high speed insolubles, or total solids, is one of the common tests used to measure soot-in-oil. First, the oil sample needs to be diluted with a solvent. Then, the sample with different density is separated by means of centrifuge or filtering method. If the sample is centrifuged, the mass or volume (depending on the test protocol) of the higher density materials that remains at the bottom of the centrifuge tube is measured as insolubles in the oil. On the other hand, if the filtering method is used, an insoluble material in the oil is calculated by the weight difference between the new and used filters. The advantage of this method is good repeatability in the measurement process. However, after performing the test, proper disposal of the solvent used is needed in order to ensure that the environmental requirements are fulfilled (Seifert & Desjardins, 1995).

Yunkers (1998) applied this method as an indicator of the lubricant oil efficiency. He found that the test was actually measures the already deposited soot within engine instead of total soot dispersed.

3.2 Nanoparticle Tracking Analysis (NTA)

NTA is a technique to analyse the particle size concentration in an oil sample diluted with heptane. It has become an increasingly popular technique due to its low operating cost relative to other technique such as Transmission Electron Microscope (TEM) (La Rocca *et al.*, 2014). This system, as shown in Figure 4, firstly records the path of the nanoparticles which are illuminated by a laser beam. All the analysis parameters need to be set up according to the measurement requirements. Then, the tracking method is performed on the centre of each identified particle and the hydrodynamic diameter of the individual particles is calculated by analysing the particles' displacement over time (Malvern Instruments Ltd, 2015).

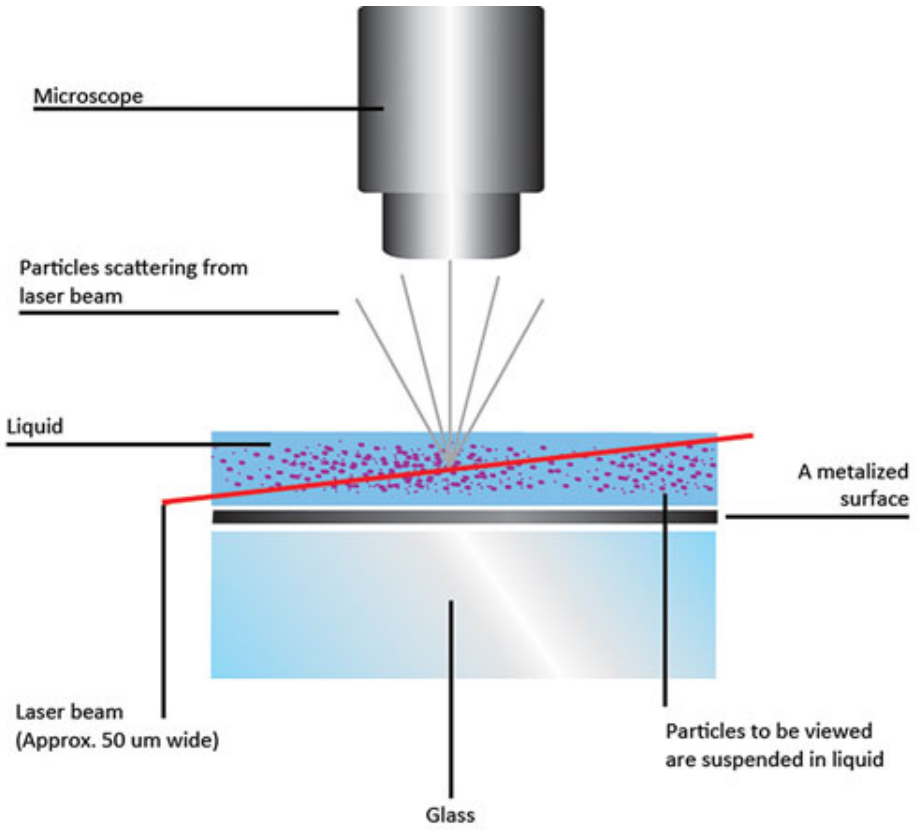

Figure 4: Nanoparticle tracking analysis (NTA) setup (Malvern Instruments Ltd, 2015).

The research conducted by La Rocca *et al.* (2013) was aimed at investigating the centrifugation effect on particle distribution. The results showed that centrifugation modifies the distribution of size and shape of agglomerated particles, but not primary particles. Another research conducted by La Rocca *et al*. (2014) confirms that both NTA and TEM methods are needed to complement each other since NTA has advantage of particles visualisation, while TEM, as a characterisation technique, is necessary to provide images of soot particle shape and structure. Soot agglomerates in this research were found to be in the range of 50 to 300 nm, with an average size of 120 nm.

3.3 Infrared Spectrometric Analysis (ISA)

Figure 5 shows common arrangement of an ISA system. This method is regularly used to measure oxidation, nitration and glycol levels in diesel lubricating oil, and in some cases, the quantity of soot can also be measured. Theoretically, this method quantifies soot by knowing the absorption bands associated with a substance in the

infrared spectrum. Instead of percentage of soot present in the sample, the results acquired with this technique are usually described as absorption/cm. Some issues regarding to this method are the spectral base line offset and the subtraction of the spectra of a reference oil sample, causing the accuracy of the results to be questionable (Seifert & Desjardins, 1995).

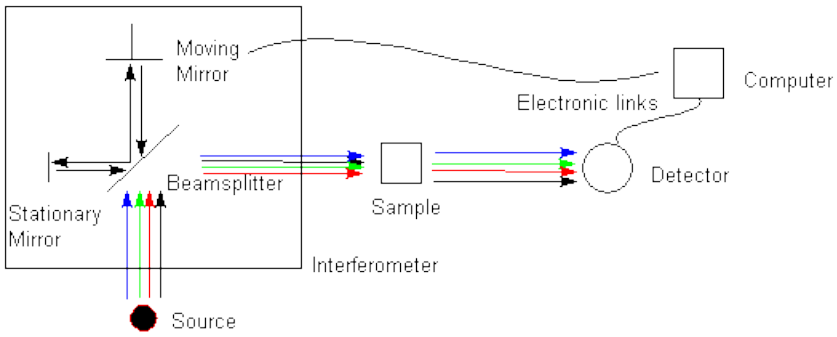

Figure 5: Infrared spectrometric analysis (ISA) system (Oregon State University, 2013).

Gaddam & Vander Wal (2013) in their work used the ISA technique with a specific system, a Fourier transform infrared-Attenuated total reflectance spectroscopy (FTIR-ATR), together with an X-ray photoelectron spectroscopy (XPS) to chemically characterise the soot in a spark-ignition direct-injection (SIDI) engine. Uy *et al.* (2014) employed this method to compare soot quantity and quality between gasoline and diesel engines. They found that the structural and chemical differences between both gasoline and diesel soot affected the polarity and hardness of the soot surface, which cause the wear mechanism in both engines.

3.4 Thermogravimetric Analysis (TGA)

TGA is a method that is commonly used for research purposes, but is not the best choice for commercial use due to its cost constraint. It is considered as an accurate method for measuring soot in lubricating oil. A sample of oil is heated at certain temperature rate in a nitrogen atmosphere. As the weight level of the sample keeps decreasing due to the volatile fraction taken off, the temperature is raised up by replacing the nitrogen in the air. Oxidation of samples will occur until its weight is stable. Then, the soot's weight is measured by deducting the weight of the sum of the volatile and ash components from the weight of the original sample (Seifert & Desjardins, 1995).

Bredin *et al.* (2011) found that approximately 30–40% of soot contents are underestimated, with more than 5% (w/w) of the soot-in-oil combinations examined lost during the analysis. Hence, improvement in oil analysis method is a vital to provide increased accuracy of soot determination.

3.5 Spot Test

This test is relatively simple in procedure, but yet not commonly practiced in soot particle analysis. A sample of oil is dropped on a strip of filter paper, after which it self-dried. The strip is then eluted in solvent to isolate the fractions of chemical species that are soluble in the particular solvents. Perhaps the only reason why this method is not commonly used is because it does not provide a straight forward quantitative measurement of soot concentration, but only a qualitative measure subject to operator interpretation (Seifert & Desjardins, 1995).

Some researchers use this method, which also known as blotter paper test in order to evaluate the effect of soot particle to engine's components wear either for diesel and biodiesel engine (Troyer, 1999; Raadnui & Meenak, 2003; Fitch & Sabrin, 2006).

3.6 Light Extinction Measurement (LEM)

Besides measuring the soot deposited on the cylinder wall, the LEM method can also be used to measure soot concentration in oil. Using the principle which is based on the Beer-Lambert Law (Chun *et al.*, 2010), this technique analyses soot on the diluted oil sample. The general property of lubricating oil as an absorptive material provides the ratio of transmitted light, which is proportional to the soot concentration. Hence, when the light intensity on the sample is held constant, measurements of the light beam intensity through linearly growing thickness of the sample would determine the soot concentration (Seifert & Desjardins, 1995). Previous works in determining the weight concentration of soot in used diesel engine oil has proven that this method can provide fast and accurate results, and requires no special reference oils or standards to perform the analysis (Yunkers, 1998).

3.7 Discussion

The soot measurement techniques discussed in this paper are summarised in Table 1 in terms of measurement principle and process, and soot characteristic. Each method has its specific advantages and disadvantages. While the insolubility test has good repeatability, a proper disposal system is needed after performing the test. The ISA method has an issue with the accuracy of the results, while the spot test only provides a qualitative measurement, which leads to inconsistency in researcher interpretation. The recent developments of new methods, such as NTA, seem able to fill-up the gap of soot-in-oil measurement problems. By complementing with TEM analysis, this particular technique provides accurate measurement and tracking of soot particles.

Table 1: Summary of the soot measurement techniques discussed in this paper.

Measurement system	Measurement principle	Measurement process			Soot characteristic
		Sampling / Source	Extraction / Classification	Diagnose / Characterisation	
Insolubility test	Chemical dissolution	Oil sample is diluted with a solvent	Sample with different density is separated by means of centrifuge or filtering method	Measure mass or volume of remaining / insoluble particles	Soot quantity
NTA	Chemical dissolution	Oil sample is diluted with heptane	Track the motion of each particle from frame to frame from the light scattered	Rate of particle movement is related to a sphere equivalent hydrodynamic radius	Soot size
Spot test	Chemical dissolution	Oil sample dropped on filter paper until self-dried	Isolate the fractions of chemical species that are soluble in the solvents	Qualitatively measured by operator's interpretation	Soot concentration
ISA	Absorption bands	Oil sample is beamed under infrared spectrum	Vibration of molecules at different frequencies	Measure the absorption bands in the infrared spectrum	Soot quantity
TGA	Gravimetric weighing	Continuously weigh a sample as it is heated to certain temperatures	Various components of the sample are decomposed	Measure weight percentage of each resulting mass change	Soot quantity
LEM	Absorption bands	Oil sample filled in a cell is moved through a light beam	A light beam passes through linearly increasing thickness of sample	Perform a series of measurements of the light intensity	Soot concentration

However, these measurement methods encounter problems of inconsistency in output details. This is due to lack of standard analytical procedures for distinguishing between elemental and organic carbons. Hence, different results can be acquired from different laboratories for the similar sample. Therefore, special attention is required exclusively for measurements of the carbon-containing portion of the particles.

5. CONCLUSION

This paper reviewed the most common techniques available for soot-in-oil analysis. The basic principle of each method together with their applications and current issues were discussed. As every measurement technique have their own advantages and disadvantages, combining or complementing these methods can provide a better soot-in-oil measurement. Furthermore, it is crucial to develop methods that are able to face more complicated measurement challenges nowadays. Every measurement and characterisation of soot-in-oil should provide faster response time to generate results with comparatively high levels of accuracy and repeatability. In addition, methods that offer low operational and maintenance cost will provide more advantageous.

REFERENCES

Al-Wakeel, H. B., Abdul Karim, Z. A., Al-Kayiem, H. H. & Mat Jamlus, M. H. (2012). Soot Reduction Strategy : A Review. *J Appl Sci*, **23**(12): 2338–2345.

Amann, C. A. & Siegla, D. C. (1981). Diesel Particulates — What They Are and Why. *Aerosol Sci Tech*, **1**(1): 73–101.

Bredin, A., Larcher, A.V. & Mullins, B. J. (2011). Thermogravimetric analysis of carbon black and engine soot — Towards a more robust oil analysis method. *Tribol Int*, **44**(12): 1642–1650.

Bredin, A., O'Leary, R. A. & Mullins, B. J. (2012). Filtration of soot-in-oil aerosols: Why do field and laboratory experiments differ? *Sep Purif Technol*, **96**: 107–116.

Brunekreef, B. & Holgate, S. T. (2002). Air pollution and health. *The Lancet*, **360**: 1233–1242.

Chun, L., Chen, C., Yipeng, S. & HuaiChun, Z. (2010). Review of soot measurement in hydrocarbon-air flames. *Sci China Ser E*, **53**(8): 2129–2141.

Dederichs, A. S. (2004). *Flamelet Modelling of Soot Formation in Diffusion Flames*. PhD Thesis, Lund University, Lund, Sweden.

Eastwood, P. (2008). *Particulate Emissions from Vehicles*. John Wiley & Sons, England.

ECOpoint Inc. (2015). *Emission Standards*. Available online at: https://www.dieselnet.com/standards [Last access date: 2nd March 2015].

Englert, N. (2004). Fine particles and human health — a review of epidemiological studies. *Toxicol Lett*, **149**: 235–242.

Fitch, J. C. & Sabrin, G. (2006). Review of degradation mechanisms leading to sludge and varnish in modern turbine oil formulations (Paper ID JAI13504). *ASTM Int J*, **3**(8).

Gaddam, C. K. & Vander Wal, R. L. (2013). Physical and chemical characterization of SIDI engine particulates. *Combust Flame*, **160**: 2517–2528.

Ganesan, V. (2004). *Internal Combustion Engines* (*2nd Ed.*). McGraw-Hill, Singapore.

Gautam, M., Chitoor, K., Durbha, M. & Summers, J. C. (1999). Effect of diesel soot contaminated oil on engine wear — investigation of novel oil formulations. *Tribol Int*, **32**: 687–699.

George, S., Balla, S. & Gautam, M. (2007). Effect of diesel soot contaminated oil on engine wear. *Wear*, **262**: 1113–1122.

George, S., Balla, S., Gautam, V. & Gautam, M. (2007). Effect of diesel soot on lubricant oil viscosity. *Tribol Int*, **40**(2007): 809–818.

Giechaskiel, B., Schiefer, E., Schindler, W., Axmann, H. & Dardiotis, C. (2013). Overview of Soot Emission Measurements Instrumentation : From Smoke and Filter Mass to Particle Number. *SAE Int J Engines*, **6**(1): 10–22.

Gómez-Rico, M. F., Martín-Gullón, I., Fullana, A., Conesa, J. A. & Font, R. (2003). Pyrolysis and combustion kinetics and emissions of waste lube oils. *J Anal Appl Pyrol*, **68-69**: 527–546.

Haynes, B. S. & Wagner, H. G. (1981). Soot formation. *Prog Energ Combust*, **7**: 229–273.
Hu, E., Hu, X., Liu, T., Fang, L., Dearn, K. D. & Xu, H. (2013). The role of soot particles in the tribological behavior of engine lubricating oils. *Wear*, **304**: 152–161.
Johnson, T. (2014). Vehicular Emissions in Review. *SAE Int J Engines*, **7**(3): 1207–1227.
Kagawa, J. (2002). Health effects of diesel exhaust emissions - a mixture of air pollutants of worldwide concern. *Toxicology*, **181-182**: 349–353.
Kim, K., Kabir, E. & Kabir, S. (2015). A review on the human health impact of airborne particulate matter. *Environ Int*, **74**: 136–143.
Kittelson, D. B. (1998). Engines and Nanoparticles: a Review. *J Aerosol Sci*, **29**(5/6): 575–588.
Kulkarni, P., Baron, P. A. & Willeke, K. (2011). Introduction to Aerosol Characterization. *In, Aerosol Measurement : Principles, Techniques and Applications (3rd Ed.)*, John Wiley & Sons, England, pp. 3–10.
La Rocca, A., Di Liberto, G., Shayler, P. J. & Fay, M. W. (2013). The nanostructure of soot-in-oil particles and agglomerates from an automotive diesel engine. *Tribol Int*, **61**: 80–87.
La Rocca, A., Di Liberto, G., Shayler, P. J., Parmenter, C. D. J. & Fay, M. W. (2014). Application of nanoparticle tracking analysis platform for the measurement of soot-in-oil agglomerates from automotive engines. *Tribol Int*, **70**: 142–147.
Ladommatos, N., Balian, R., Horrocks, R. & Cooper, L. (1996). The Effect of Exhaust Gas Recirculation on Soot Formation in a High-Speed Direct-injection Diesel Engine. *SAE Technical Paper No. 960841*, 1–11.
Mainwaring, R. (1997). Soot and Wear in Heavy Duty Diesel Engines. *SAE Technical Paper No. 971631*, 47–64.
Malvern Instruments Ltd. (2015). *Nanoparticle Tracking Analysis*. Available online at: http://www.malvern.com/en/products/technology/nanoparticle-tracking-analysis/default.aspx [Last access date: 20th February 2015].
Marshall Brain. (2015). *How Diesel Engines Work*. Available online at: http://auto.howstuffworks.com/diesel.htm [Last access date: 10th March 2015].
McMurry, P. H. (2000). A review of atmospheric aerosol measurements. *Atmos Environ*, **34**: 1959–1999.
Oregon State University. (2013). *FTIR Spectroscopy*. Available online at: http://chemistry.oregonstate.edu/courses/ch361-464/ch362/irinstrs.htm [Last access date: 10th March 2015].
Petrovic, V. S., Jankovic, S. P., Tomic, M. V., Jovanovic, Z. S. & Knezevic, D. M. (2011). The Possibilities for Measurement and Characterization of Diesel Engine Fine Particles - A Review. *Therm Sci*, **15**(4): 915–938.
Pulkrabek, W. W. (2004). *Engineering Fundamentals of the Internal Combustion Engine (2nd Ed.).* Pearson Prentice Hall, USA.
Raadnui, S. & Meenak, A. (2003). Effects of refined palm oil (RPO) fuel on wear of diesel engine components. **254:** 1281–1288.
Reitz, R. D. (2013). Directions in internal combustion engine research. *Combust Flame*, **160**(1): 1–8.
Richter, H. & Howard, J. B. (2000). Formation of polycyclic aromatic hydrocarbons and their growth to soot — a review of chemical reaction pathways. *Prog Energ Combust*, **26**: 565–608.
Seifert, W. W. & Desjardins, J. B. (1995). Measurement of Soot in Diesel Engine Lubricating Oil. *SAE Technical Paper No. 951023*, 1–6.
Tree, D. R. & Svensson, K. I. (2007). Soot processes in compression ignition engines. *Prog Energ Combust*, **33**: 272–309.
Troyer, D. (1999). Get ready for more soot: Is your soot monitoring program up to the EPA's new challenge? *Practicing oil analysis magazine (July-August)*, 17–22.
Uy, D., Ford, M. A., Jayne, D. T., O'Neill, A. E., Haack, L. P., Hangas, J., Jagner, M. J., Sammut, A. & Gangopadhyay, A.K. (2014). Characterization of gasoline soot and comparison to diesel soot: Morphology, chemistry, and wear. *Tribol Int*, **80**: 198–209.
Wan Mahmood, W. M. F. (2011). *Computational Studies of Soot Paths to Cylinder Wall Layers of a Direct Injection Diesel Engine*. PhD Thesis, The University of Nottingham, Nottingham, United Kingdom.

Wei, W. & Na, L. (2011). Study on Exhaust Emission and Its Control Techniques in Diesel Engine. *Fourth Int Conf Intell Comput Tech Autom*, 710–713.

Woschni, G. & Huber, K. (1991). The Influence of Soot Deposits on Combustion Chamber Walls on Heat Losses in Diesel Engines. *SAE Technical Paper No. 910297*, 1–8.

Xi, J. & Zhong, B. (2006). Soot in Diesel Combustion Systems. *Chem Eng Technol*, **29**(6): 665–673.

Yunkers, D. N. (1998). *Fuel Soot Monitoring by Light Extinction Measurement (LEM)*. Report, Analyst Inc., Stafford, Texas.

Zelenka, P., Egert, M. & Cartellieri, W. (2000). Ways to meet future emission standards for heavy Sports Utility Vehicles - SUV. *FISITA W Automot Congr*, 1–15.

THE IMPORTANCE OF FORENSIC MICROBIOLOGY IN CBRNe INVESTIGATIONS

Gian Marco Ludovici[1], Orlando Cenciarelli[1,2], Mariachiara Carestia[1,2], Andrea Malizia[1,2], Annalaura Tamburrini[1], Valentina Gabbarini[1], Alessandro Sassolini[1], Daniele Di Giovanni[1,2], Sandro Mancinelli[1,3], Leonardo Palombi[1,3], Pasquale Gaudio[1,2], Carlo Bellecci[1,2] & Teresa Rinaldi[1,4,5*]

[1]International Master Courses in Protection Against CBRNe Events, Department of Industrial Engineering - School of Medicine and Surgery, University of Rome Tor Vergata, Italy
[2]Department of Industrial Engineering, University of Rome Tor Vergata, Italy
[3]Department of Biomedicine and Prevention, School of Medicine and Surgery, University of Rome Tor Vergata, Italy
[4]Biology and Biotechnology Department 'Charles Darwin' (BBCD), University of Rome La Sapienza, Italy
[5]Major of the Italian Army (Reserve), Italy

[*]Email: teresa.rinaldi@uniroma1.it

ABSTRACT

Forensic microbiology came into the spotlight after the anthrax attack in September 2001 in the US. It is a new discipline that is able to trace the origin of a biological agent using a range of biological analyses, and it is based on the fast and accurate detection and identification of microorganisms found at a biological crime scene. In this paper, we will discuss the importance of forensic microbiology in CBRNe investigations. The technologies that are used for forensic microbiology, along with the most significant cases in which this discipline was successfully applied will also be described.

Keywords: *Chemical, biological, radiological, nuclear & explosives (CBRNe) investigations; forensic microbiology; genomic epidemiology; metagenomics; biological agents.*

1. INTRODUCTION

The first question that arises when an unusual disease outbreak appears is: is it a natural outbreak or a deliberate release of a biological agent? It is not possible to answer this question before having identified the organism responsible for the outbreak. Further complicating matters, a microorganism potentially usable for an intentional bioweapon release could be the same that causes natural outbreaks all over the world (Rambhia *et al.*, 2011). After preliminary studies of samples, in the case of a natural outbreak, genomic epidemiology will be required. On the other hand, in the case of a crime, or chemical, biological, radiological, nuclear & explosives (CBRNe) attack, we can refer to the application of forensic microbiology.

We can define forensic microbiology as the application of biological science in the investigation of legal matters in a way that scientific knowledge and technology are used with the aim of finding the culprit. Indeed, the molecular techniques are the same for both genomic epidemiology and forensic microbiology. However, in the first case, it is a medical problem managed by the health care structures, while in the second case, an investigation also occurs to identify the culprit responsible for the deliberate release of a pathogen (Aggarwal *et al*., 2011).

In this second scenario, the deliberate release of a biological agent can be overt, such as the case of anthrax spores delivered by letters (Atlas, 2002; Cenciarelli *et al.*, 2013), or covert, which is the worst

situation because the disease could spread for days or weeks before discovering that it is a biological attack, leaving epidemiologists and law enforcement officials without the possibility to investigate the crime scene. In all cases of biological outbreaks, an effective infectious disease surveillance system is essential.

In this paper, we will discuss the importance of forensic microbiology in CBRNe investigations. The technologies that are used for forensic microbiology, along with the most significant cases in which this discipline was successfully applied will also be described.

2. FORENSIC MICROBIOLOGY

When an unusual outbreak occurs, public health and law enforcement personnel face great difficulty in differentiating between a natural infection and one resulting from an intentional attack. Forensic microbiology is dedicated to analysing evidences from a bioterrorism act or biocrime, or inadvertent release of a microorganism for attribution purposes. This scientific discipline is relatively new, coming into the spotlight with the anthrax case in September 2001 in the US. The scientific techniques available to permit the unequivocal identification of the microorganism responsible of an outbreak, and discriminating if it is a natural episode or intentional in a very fast way is fundamental for subsequent actions, especially because the microorganisms listed as biological agents usually cause natural outbreaks all over the world (Rambhia *et al.*, 2011).

Nevertheless, the application of this discipline has a bottleneck, which is the availability of international deoxyribonucleic acid (DNA) databases of microorganisms, in particular of those considered as biological agents (Tian & Zheng, 2014). To fill this gap, an ongoing project of the European Biodefense Laboratory Network (EBLN) of the European Defence Agency aims to update its biological agents database. This coordinated work involves biodefense institutions from European countries to improve the capabilities of forensic microbiologists through the construction of a shared database and integrating genome sequencing with metagenomics analysis (Ruifu & Keim, 2012).

Forensic microbiology is effective only if there is basic scientific information on microbiological evolution, genetics, ecology and physiology. This is particularly true for *Bacillus anthracis*, because the studies of natural isolates are extremely important for the comprehension of its evolution. It is noteworthy that its chromosomal genome shows an extremely low genetic diversity between different lineages. In fact, it is defined as a “closed genome” because comparing the sequences of a large number of strains, the pool of genes shared by all strains is the same (core genome) and no dispensable genes are acquired in evolution (dispensable genome) (Tettelin *et al.*, 2005). This feature is also shared by other bacterial species defined as biological agents. Contrariwise, other bacterial species, such as *Streptococcus agalactiae*, in addition to the core genome also have a dispensable genome (Medini *et al.*, 2005). *Bacillus anthracis* is part of the *Bacillus cereus* group (*sensu stricto*), together with *Bacillus cereus and Bacillus thuringiensis* (Read *et al.*, 2003).

The virulence of *Bacillus anthracis* is based on the presence of two plasmids: pXO1, which is the coding for the tripartite lethal toxin; and pXO2, which is the coding for the protective capsule. Recent observations point to evolutionary variability based on the capacity of sharing of plasmids between bacteria (Rasko *et al.*, 2007; Hu *et al.*, 2009), and sharing of plasmids between a pathogen and a harmless strain, which could transform a non-pathogenic strain to a strain capable of causing the anthrax disease (Salter, 2011).

Figure 1 shows examples of *Bacillus anthracis* plasmids isolated in *Bacillus cereus* strains causing anthrax-like illness. A patient in the US showed symptoms similar to inhalation anthrax, but he was actually infected by a *Bacillus cereus* strain (G9241) harbouring two plasmids. One of them was 99.6% identical to the *Bacillus anthracis* pXO1 plasmid, and the second, called pBC218, encodes the polysaccharide capsule cluster (Hoffmaster *et al.*, 2004). In 2003, two fatal cases involving metalworkers were investigated using molecular analysis and it was demonstrated that they were

infected by a *Bacillus cereus* strain with the *Bacillus anthracis* pXO1 plasmid (Avashia *et al.*, 2007). Shahcheraghi & Ayatollahi (2013) found a similar strain in Iran. In 2010, in Africa, a chimpanzee died of anthrax caused by a strain harbouring two plasmids identical to the anthrax virulence plasmids, pXO1 and pXO2, and a new plasmid, but with a chromosome more similar to *Bacillus thuringiensis* and *Bacillus cereus* than to *Bacillus anthracis* (Klee *et al.*, 2010). In all these sporadic cases, even if there were not outbreaks, the genome sequences had helped to decipher the origin of the natural strains causing the fatal anthrax disease.

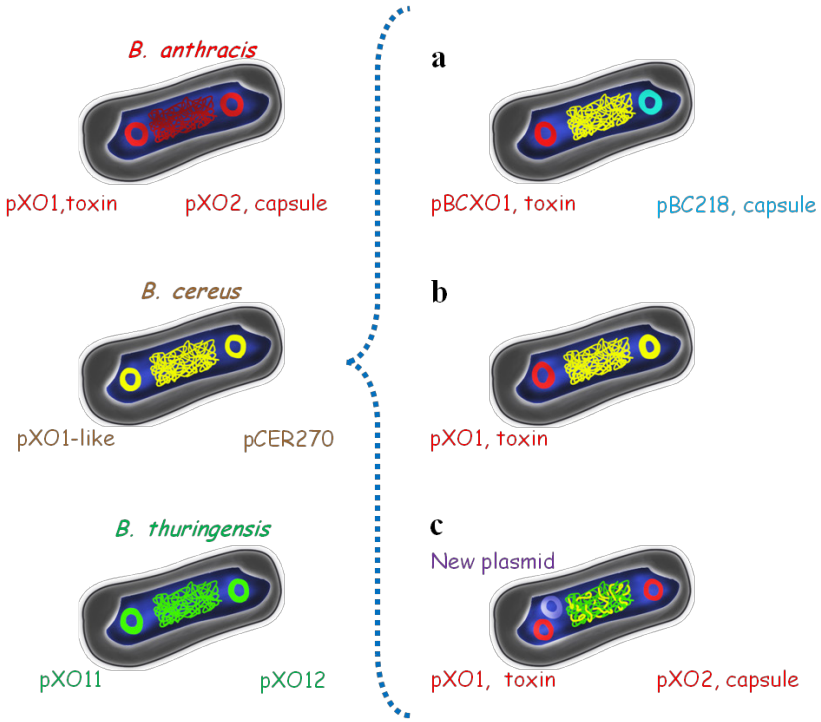

Figure 1: Schematic examples of *Bacillus anthracis* plasmids isolated in *Bacillus cereus* strains causing anthrax-like illness. Red, yellow and green: genomes and plasmids of *Bacillus anthracis*, *Bacillus cereus* and *Bacillus thuringiensis* respectively. Blue and light blue: new plasmids. (a) A *Bacillus cereus* strain (G9241) harbouring two plasmids: one of them, pBCXO1 is 99.6 % identical to the *Bacillus anthracis* pXO1 plasmid, and the second, called pBC218, encodes the polysaccharide capsule cluster (Hoffmaster *et al.*, 2004). (b) A *Bacillus cereus* strain with the *Bacillus anthracis* pXO1 plasmid (Avashia *et al.*, 2007; Shahcheraghi & Ayatollahi, 2013). (c) A *Bacillus* strain harbouring two plasmids identical to the anthrax virulence plasmids, pXO1 and pXO2, and a new plasmid, but with a chromosome more similar to *Bacillus thuringiensis* and *Bacillus cereus* than to *Bacillus anthracis* (Klee *et al.*, 2010).

The advent of synthetic biology and dual-use research open the possibility to modify an innocuous microorganism and turn it into a biological agent (Suk *et al.*, 2011; Tucker, 2012). In a hypothetical use of a genetically engineered microorganism as a biological agent, only with genome sequence would it be possible to decipher intentional genetic manipulations. This would be another potential indication that the microorganism had been deliberately or accidentally released.

3. TECHNOLOGIES FOR FORENSIC MICROBIOLOGY

The essential technologies used in microbial investigations, described here, have taken advantage of the improvement of sequencing, which is becoming cheaper and faster:

- **Sequencing:** With the advent of next generation sequencing (NGS) technology, the analysis of collected samples is fast and relatively cheap, and it is commonly used to analyse biological evidence samples collected from crime scenes (Pattnaik & Jana, 2005; Ruifu, 2012; Budowle *et al.*, 2014). By applying NGS technology, multiple results can be obtained simultaneously; microsatellite typing, single nucleotide polymorphisms (SNPs) and mitochondrial DNA sequencing. In this review, we will not discuss the field of human genetic forensics, but rather we will underline that the same type of biological techniques can be used in different complex investigations. In fact, during an outbreak, NGS allows the sequencing of the genome of an isolated bacterium or virus in hours, and by comparing this sequence with genomic databases, it is possible to identify the origin of the bacterial strain or virus. The availability of international reference strain collections of pathogenic organisms, which affect humans or animals, is of extreme value for timely recognition of an outbreak as natural or intentional (Fillo *et al.*, 2011; De Santis *et al.*, 2011; Irenge & Gala, 2012; Sjodin *et al.*, 2013; Girault *et al.*, 2014).

- **Molecular phylogenetics:** It is the combination of molecular evolutionary analysis and the statistical framework developed for the forensic study of nucleic acid samples. The advancement of sequencing technologies has taken phylogenetic analysis to a new life. Some viruses, such as hepatitis C virus, poliovirus and influenza, mutate incredibly quickly (Parvin *et al.*, 1986; Jorba *et al.*, 2008). By sequencing virus samples from different individuals, and then comparing the differences, such as polymorphisms in their genomes, scientists can trace their evolution and place them on a family tree. Phylogenetic forensics can be applied not only for legal proceedings, but also in biodefence (Bhattacharya, 2014).

- **Metagenomics**: It is the study of a collection of genetic material from a mixed community of organisms. Even the study of the interaction between the skin human microbiota and the environment, which is highly dynamic, has been proposed to be useful for forensic identification, since human microorganisms and microbial communities are constantly transferred between surfaces (Fierer *et al.*, 2010). Moreover, random whole metagenomic sequencing approaches can be employed for comparative analysis and discrimination between soils for application in forensic science (Khodakova *et al.*, 2014). In this context, the sequence of the genetic material of microorganisms found in a crime scene can be quickly obtained by determining the bacterial strains present (Brenig *et al.*, 2010).

The described techniques are widely applied to trace the first patient of an outbreak or a source of contamination. The methods, which combine traditional evolutionary-biological practices with modern sequencing technology, is being increasingly used and accepted in criminal and civil investigations, and also for biodefence. The importance of genomics as a tool in epidemiological investigation is now widely accepted. For example, molecular phylogenetic analyses are being used increasingly in epidemiological investigation of outbreaks and transmission cases because it is possible to trace back the source of contamination (Bhattacharya, 2014; Kupferschmidt, 2011).

The following studies are considered examples of the use of genomic epidemiology, which is based on the principle that the microevolutionary events occurring within a pathogen genome over the course of an outbreak can be used as markers of transmission:

- In 2006, an outbreak of *Mycobacterium tuberculosis* was reported in Canada. Genomic investigation based on bacterial whole-genome sequencing and social network analysis established that socio-environmental factors (likely crack cocaine use) caused the

simultaneous expansion of two extant lineages of *Mycobacterium tuberculosis* (Gardy *et al.*, 2011).

- In 2008, a multidrug-resistant *Acinetobacter baumannii* hospital outbreak occurred and genomic epidemiology was used to investigate this case (Lewis *et al.*, 2010).

- In 2010, a cholera epidemic in Haiti that originated from a *Vibrio cholerae* strain was found to belong to a single monophyletic group present in Nepal. Epidemiological investigations concluded the strain was carried by a UN peacekeeper from Nepal (Hendriksen *et al.*, 2011; Lantagne *et al.*, 2014).

- In 2011, an outbreak of an enterohemorrhagic *Escherichia coli* hit the north of Germany. At the very beginning, this outbreak was suspected to be a bioterrorism attack, but the genome sequence, performed in five hours per isolate, established that the strain was of natural origin (Grad *et al.*, 2012; Qin *et al.*, 2011; Rasko *et al.*, 2011; Scheutz *et al.*, 2011).

- In 2014, the sequence of 99 Ebola virus genomes from 78 patients in Sierra Leone allowed to characterise the patterns of viral transmission. This West African variant diverged from the central African lineages around 2004, and crossed from Guinea to Sierra Leone in May 2014 (Cenciarelli *et al.*, 2014, 2015; Gire *et al.*, 2014).

4. CASE STUDIES

In July 1993, a liquid suspension of *Bacillus anthracis* was aerosolised from the roof of a building in Kameido, Tokyo, Japan by the religious group Aum Shinrikyo. At that time, multiple-locus variable-number tandem repeated analysis found that all the isolates were identical to a strain used in Japan to vaccinate animals against anthrax (Takahashi *et al.*, 2004). Fortunately, no cases of anthrax were registered because this strain, Sterne 34F2, lacked the pX02 plasmid (Keim *et al.*, 2001).

In 1998, the use of molecular phylogenetic analysis was successfully applied on the hepatitis C virus, with rapidly evolving ribonucleic acid (RNA). It was found that an anesthetist was responsible for the infection of 275 of his patients with the virus (González-Candelas *et al.*, 2013).
In 2001, after the anthrax case in US, through the sequence of the *Bacillus anthracis*, it was found that the most likely source was an US Army laboratory, where the strain was identified as the *Bacillus anthracis* Ames strain. This was the first case in which the FBI asked for the entire sequence of a microorganism to solve a case. Indeed, thanks to this case, there was an influx of US government funding and the advent of cheaper and faster sequencing technologies (Kupferschmidt, 2011; Rasko *et al.*, 2011).

This was a clear example of an overt attack; the spores were sent by letters, implying a deliberate action and excluding the hypothesis of a natural contamination. Nevertheless, the analysis of the *Bacillus anthracis* genome was fundamental to determine that this strain was uncommon in nature, limiting the investigation to the people who had access to this laboratory strain. The peculiarity of this strain was that it had four mutations that were created in the U.S. Army Medical Research Institute of Infectious Diseases (USAMRIID) for testing experimental anthrax vaccines. Out of 1,070 *Bacillus anthracis* isolates obtained from different facilities and analysed by researchers, only eight contained all these four mutations and the genomes matched with the RMR-1029 strain constructed at the USAMRIID (Koblentz & Tucker, 2010).

In 2009, an anthrax outbreak emerged among heroin users in Scotland, and expanded into England and Germany in 2010. It re-emerged with additional cases in Germany, Denmark, France and Great Britain in 2012-2013, causing 62 cases and 27 deaths. Phylogeographic analysis demonstrated that the *Bacillus anthracis* strain was closely related to strains from Turkey (strain A. Br. 008/009), and not to isolates from Scotland or Afghanistan (the presumed origin of the heroin). The investigation

conducted was focused on clarifying if this outbreak was related to bioterrorist activities, a biocrime or a natural event due to a random contamination. The findings of the investigation suggested accidental contamination along the drug trafficking route through cutting of substances or animal hides used to smuggle heroin into Europe, but the forensic attribution of this event is still ongoing (Price, 2012; Berger *et al.*, 2014).

Additionally no biological agent was found using the available techniques in the seized heroin, but only in biological samples. Analyses oriented to identify and genotype *Bacillus anthracis* are ongoing for heroin samples seized since 1988. These results will be able to confirm or rule out the presence of the bacteria and eventually its genotype, but will not be able to refine the final attribution of the event (Berger *et al.*, 2014). Conversely, metagenomics, as the study of genetic material recovered directly from environmental samples, could support these results in terms of profiling of environmental genetic biodiversity of *Bacillus anthracis* strains causing the attribution for the forensic process.

5. CONCLUSION

Forensic microbiology, in recent years, especially due to the deliberate use of *Bacillus anthracis* spores in the US in 2001, has been put in the foreground. With the development of techniques that are more economical and faster, such as metagenomics and NGS, forensic microbiology is able to trace the origin of biological agents, and specifically to consider whether the agent is of natural origin or if it is deliberately used for terrorist purposes. For this, forensic microbiology is of particular importance in CBRNe investigations, in order to evaluate a rapid and more effective response to emergencies.

ACKNOWLEDGMENT

Special acknowledgement for the realisation of this work goes to the International Master Courses in Protection Against CBRNe Events (http://www.mastercbrn.com).

REFERENCES

Aggarwal, P., Chopra, A. K., Gupte, S., & Sandhu, S. S. (2011). Microbial forensics: An upcoming investigative discipline. *J. Indian Acad. Forensic Med.,* **33**: 2.

Atlas, R. M. (2002). Bioterrorism: from threat to reality. *Annu. Rev. Microbiol*, **51**: 167-185.

Avashia, S. B., Riggins, W. S., Lindley, C., Hoffmaster, A., Drumgoole, R., Nekomoto, T., Jackson, P. J., Hill, K. K., Williams, K., Lehman, L., Libal, M. C., Wilkins, P. P., Alexander, J., Tvaryanas, A., & Betz, T. (2007). Fatal pneumonia among metalworkers due to inhalation exposure to Bacillus cereus containing Bacillus anthracis toxin genes. *Clin. Infect. Dis.*, **44**: 414-416.

Berger, T., Kassirer, M., & Aran, A. A. (2014). Injectional anthrax-new presentation of an old disease. *Euro Surveill.*, **19**: 20877.

Bhattacharya, S. (2014). Science in court: Disease detectives. *Nature*, **506**: 424-426.

Brenig, B., Beck, J., & Schütz, E. (2010). Shotgun metagenomics of biological stains using ultra-deep DNA sequencing. *Forensic Sci. Int. Gen.*, **4**: 228-231.

Budowle, B., Connell, N. D., Bielecka-Oder, A., Colwell, R. R., Corbett, C. R., Fletcher, J., Forsman, M., Kadavy, D. R., Markotic, A., Morse, S. A., Murch, R. S., Sajantila, A., Schmedes, S. E., Ternus, K. L., Turner, S. D., & Minot, S. (2014). Validation of high throughput sequencing and microbial forensics applications. *Investig. Genet.*, **5**: 9.

Cenciarelli, O. Pietropaoli, S, Frusteri, L., Malizia, A., Carestia, M., D'Amico, F., Sassolini, A., Di Giovanni, D., Tamburrini, A.,Palombi, L., Bellecci, C. & Gaudio, P. (2014). Biological

emergency management: the case of Ebola 2014 and the air transportation involvement. *J. Microb. Biochem. Technol.*, **6**:247- 253.

Cenciarelli, O., Pietropaoli, S., Malizia, A., Carestia, M., D'Amico, F., Sassolini, A., Di Giovanni, D., Rea, S., Gabbarini, V., Tamburrini, A., Palombi, L., Bellecci, C., & Gaudio, P. (2015). Ebola virus disease 2013-2014 outbreak in West Africa: An analysis of the epidemic spread and response. *Int. J. Microbiol.*, article ID 769121.

Cenciarelli, O., Rea, S., Carestia, M., D'Amico, F., Malizia, A., Bellecci, C., Gaudio,

P., Gucciardino, A. & Fiorito, R. (2013). Bioweapons and bioterrorism: A

review of history and biological agents. *Defence S&T Tech. Bull.*, 6:111-129.

De Santis, R., Ciammaruconi, A., Faggioni, G., Fillo, S., Gentile, B., Di Giannatale, E., Ancora, M., & Lista, F. (2011). High throughput MLVA-16 typing for Brucella based on the microfluidics technology. *BMC Microbiol.*, **11**: 60.

Fierer, N., Lauber, C. L., Zhou, N., McDonald, D., Costello, E. K., & Knight, R. (2010). Forensic identification using skin bacterial communities. *Proc. Natl. Acad. Sci. U.S.A.*, **107**: 6477-6481.

Fillo, S., Giordani, F., Anniballi, F., Gorgé, O., Ramisse, V., Vergnaud, G., Riehm, J. M., Scholz, H. C., Splettstoesser, W. D., Kieboom, J., Olsen, J., Fenicia, L., & Lista, F. (2011). Clostridium botulinum group I strains genotyping by 15 loci Multi Locus VNTR Analysis (MLVA). *J. Clin. Microbiol*., **49**: 4252-4263

Gardy, J. L., Johnston, J. C., Sui, S. J. H., Cook, V. J., Shah, L., Brodkin, E., Rempel, S., Moore, R., Zhao, Y., Holt, R., Varhol, R., Birol, I., Lem, M., Sharma, M. K., Elwood, K., Jones, S. J. M., Brinkman, F. S. L., Brunham, R. C., and & Tang, P. (2011). Whole-genome sequencing and social-network analysis of a tuberculosis outbreak. *N. Engl. J. Med.*, **364**: 730-739.

Girault, G., Thierry, S., Cherchame, E., & Derzelle, S. (2014). Application of high-throughput sequencing: discovery of informative SNPs to subtype Bacillus anthracis. *Adv. Biosci. Biotechnol.*, **5**: 669.

Gire, S. K., Goba, A., Andersen, K. G., Sealfon, R. S., Park, D. J., Kanneh, L., Jalloh, S., Momoh, M., Fullah, M., Dudas, G., Wohl, S., Moses, L. M., Yozwiak, N. L., Winnicki, S., Matranga, C. B., Malboeuf, C. M., Qu, J., Gladden, A. D., Schaffner, S. F., Yang, X., Jiang, P., Nekoui, M., Colubri, A., Coomber, M. R., Fonnie, M., Moigboi, A., Gbakie, M., Kamara, F. K., Tucker, V., Konuwa, E., Saffa, S., Sellu, J., Jalloh, A. A., Kovoma, A., Koninga, J., Mustapha, I., Kargbo, K., Foday, M., Yillah, M., Kanneh, F., Willie, R., Massally, J. L. B., Chapman, S. B., Bochicchio, J., Murphy, C., Nusbaum, C., Young, S., Birren, B. W., Grant, D.S., Scheiffelin, J. S., Lander, E. S., Happi, C., Gevao, S. M., Gnirke, A., Rambaut, A., Garry, R. F., Khan, S. H., & Scheiffelin, J. S. (2014). Genomic surveillance elucidates Ebola virus origin and transmission during the 2014 outbreak. *Science*, **345**: 1369-1372.

González-Candelas, F., Bracho, M. A., Wróbel, B., & Moya, A. (2013). Molecular evolution in court: analysis of a large hepatitis C virus outbreak from an evolving source. *BMC Biol.*, **11**: 76.

Grad, Y. H., Lipsitch, M., Feldgarden, M., Arachchi, H. M., Cerqueira, G. C., FitzGerald, M., Godfrey, P., Haas, B. J., Murphy, C. I., Russ, C., Sykes, S., Walker, B. J., Wortman, J. R., Young, S., Zeng, Q., Abouelleil, A., Bochicchio, J., Chauvin, S., DeSmet, T., Gujja, S., McCowan, C., Montmayeur, A., Steelman, S., Frimodt-Møller, J., Petersen, A. M., Struve, C., Krogfelt, K. A., Bingen, E., Weill, F., Lander, E. S., Nusbaum, C., Birren, B. W., Hung, D. T., & Hanage, W. P. (2012). Genomic epidemiology of the Escherichia coli O104: H4 outbreaks in Europe, 2011. *Proc. Natl. Acad. Sci. U.S.A.*, **109**: 3065-3070.

Hendriksen, R. S., Price, L. B., Schupp, J. M., Gillece, J. D., Kaas, R. S., Engelthaler, D. M., Bortolaia, V., Pearson, T., Waters, A. E., Upadhyay, B. P., Shrestha, S. D., Adhikari, S., Shakya, G., Keim, P. S., & Aarestrup, F. M. (2011). Population genetics of Vibrio cholerae from Nepal in 2010: evidence on the origin of the Haitian outbreak. *MBio*, **2**: e00157-11.

Hoffmaster, A. R., Ravel, J., Rasko, D. A., Chapman, G. D., Chute, M. D., Marston, C. K., De, B. K., Sacchi, C. T., Fitzgerald, C., Mayer, L. W., Maiden, M. C. J., Priest, F. G., Barker, M., Jiang, L., Cer, R. Z., Rilstone, J., Peterson, S. N., Weyant, R. S., Galloway, D. R., Read, T. D., Popovic, T., & Fraser, C. M. (2004). Identification of anthrax toxin genes in a Bacillus cereus associated with an illness resembling inhalation anthrax. *Proc. Natl. Acad. Sci. U.S.A.*, **101**: 8449-8454.

Hu, X., Van der Auwera, G., Timmery, S., Zhu, L., & Mahillon, J. (2009). Distribution, diversity, and potential mobility of extrachromosomal elements related to the Bacillus anthracis pXO1 and pXO2 virulence plasmids. *Appl. Environ. Microb.*, **75**: 3016-3028.

Irenge, L. M., & Gala, J. L. (2012). Rapid detection methods for Bacillus anthracis in environmental samples: a review. *Appl. Microbiol. Biotechnol.*, **93**: 1411-1422.

Jorba, J., Campagnoli, R., De, L., & Kew, O. (2008). Calibration of multiple poliovirus molecular clocks covering an extended evolutionary range. *J. Virol.*, **82**: 4429-4440.

Keim, P., Smith, K. L., Keys, C., Takahashi, H., Kurata, T., & Kaufmann, A. (2001). Molecular investigation of the Aum Shinrikyo anthrax release in Kameido, Japan. *J. Clin. Microbiol.*, **39**: 4566-4567.

Khodakova, A. S., Smith, R. J., Burgoyne, L., Abarno, D., & Linacre, A. (2014). Random whole metagenomic sequencing for forensic discrimination of soils. *PloS one*, **9**: e104996.

Klee, S. R., Brzuszkiewicz, E. B., Nattermann, H., Brüggemann, H., Dupke, S., Wollherr, A., Franz, T., Pauli, G., Appel, B., Liebl, W., Couacy-Hymann, E., Boesch, C., Meyer, F., Leendertz, F. H., Ellerbrok, H., Gottschalk, G., Grunow, R., & Liesegang, H. (2010). The genome of a Bacillus isolate causing anthrax in chimpanzees combines chromosomal properties of B. cereus with B. anthracis virulence plasmids. *PloS one*, **5**: e10986.

Koblentz, G. D., & Tucker, J. B. (2010). Tracing an attack: the promise and pitfalls of microbial forensics. *Survival*, **52**: 159-186.

Kupferschmidt, K. (2011). Outbreak detectives embrace the genome era. *Science,* **333**: 1818-1819.

Lantagne, D., Nair, G. B., Lanata, C. F., & Cravioto, A. (2014). The cholera outbreak in Haiti: where and how did it begin?. In *Cholera Outbreaks* (pp. 145-164). Springer Berlin Heidelberg.

Lewis, T., Loman, N. J., Bingle, L., Jumaa, P., Weinstock, G. M., Mortiboy, D., & Pallen, M. J. (2010). High-throughput whole-genome sequencing to dissect the epidemiology of Acinetobacter baumannii isolates from a hospital outbreak. *J. Hosp. Infect.*, **75**: 37-41.

Medini, D., Donati, C., Tettelin, H., Masignani, V., & Rappuoli, R. (2005). The microbial pan-genome. *Curr. Opin. Genetics Dev.*, **15**: 589-594.

Parvin, J. D., Moscona, A., Pan, W. T., Leider, J. M., & Palese, P. (1986). Measurement of the mutation rates of animal viruses: influenza A virus and poliovirus type 1. *J. Virol.*, **59**: 377-383.

Pattnaik, P., & Jana, A. M. (2005). Microbial forensics: applications in bioterrorism. *Environ. Forensics*, **6**: 197-204.

Price, E. P., Seymour, M. L., Sarovich, D. S., Latham, J., Wolken, S. R., Mason, J., Vincent, G., Drees, K. P., Beckstrom-Sternberg, S. M., Phillippy, A. M., Koren, S., Okinaka, R.T., Chung, W., Schupp, J. M., Wagner, D. M., Vipond, R., Foster, J. T., Bergman, N. H., Burans, J., Pearson, T., Brooks, T., & Keim, P. (2012). Molecular epidemiologic investigation of an anthrax outbreak among heroin users, Europe. *Emerg. Infect. Dis.*, **18**: 1307.

Qin, J., Cui, Y., Zhao, X., Rohde, H., Liang, T., Wolters, M., Li, D., Campos, C. B., Christner, M., Song, Y., & Yang, R. (2011). Identification of the Shiga toxin-producing Escherichia coli O104: H4 strain responsible for a food poisoning outbreak in Germany by PCR. *J. Clin. Microbiol.*, **49**: 3439-3440.

Rambhia, K. J., Ribner, A. S., & Gronvall, G. K. (2011). Everywhere you look: select agent pathogens. *Biosecur. Bioterror*, **9**: 69.

Rasko, D. A., Rosovitz, M. J., Økstad, O. A., Fouts, D. E., Jiang, L., Cer, R. Z., Kolstø, A., Gill, S. R., & Ravel, J. (2007). Complete sequence analysis of novel plasmids from emetic and periodontal Bacillus cereus isolates reveals a common evolutionary history among the B. cereus-group plasmids, including Bacillus anthracis pXO1. *J. Bacteriol.*, **189**: 52-64.

Rasko, D. A., Worsham, P. L., Abshire, T. G., Stanley, S. T., Bannan, J. D., Wilson, M. R., Langham, R. J., Decker, R. S., Jiang, L., Read, T. D., Phillippy, A. M., Salzberg, S. L., Pop, M., Van Ert, M. N., Kenefic, L. J., Keim, P. S., Fraser-Liggett, C. M., & Ravel, J. (2011). Bacillus anthracis comparative genome analysis in support of the Amerithrax investigation. *Proc. Natl. Acad. Sci. U.S.A.*, **108**: 5027-5032.

Read, T. D., Peterson, S. N., Tourasse, N., Baillie, L. W., Paulsen, I. T., Nelson, K. E., Tettelin, H., Fouts, D. E., Eisen, J. A., Gill, S. R., Holtzapple, E. K., Økstad, O. A., Helgason, E., Rilstone, J., Wu, M., Kolonay, J. F., Beanan, M. J., Dodson, R. J., Brinkac, L. M., Gwinn, M., DeBoy, R. T., Madpu, R., Daugherty, S. C., Durkin, A. S., Haft, D. H., Nelson, W. C., Peterson, J. D.,

Pop, M., Khouri, H. D., Radune, D., Benton, J. L., Mahamoud, Y., Jiang, L., Hance, I. R., Weidman, J. F., Berry, K. J., Plaut, R. D., Wolf, A. M., Watkins, K. L., Nierman, W. C., Hazen, A., Cline, R., Redmond, C., Thwaite, J. E., White, O., Salzberg, S. L., Thomason, B., Friedlander, A. M., Koehler, T. M., Hanna, P. C., Kolstø, A., & Hanna, P. C. (2003). The genome sequence of Bacillus anthracis Ames and comparison to closely related bacteria. *Nature*, **423**: 81-86.

Ruifu, Y. (2012). Microbial forensics: a powerful tool for pursuing bioterrorism perpetrators and the need for an international database. *J. Bioterror. Biodef.,* **3**: 1-8.

Ruifu, Y. & Keim, P. (2012). Microbial forensics: a powerful tool for pursuing bioterrorism perpetrators and the need for an international database. *J. Bioterr. Biodef.*, **S3**:007.

Salter, S. J. (2011). You cannot B. cereus. *Nat. Rev. Microbiol.*, **9**: 83-83.

Scheutz, F., Nielsen, E. M., Frimodt-Moller, J., Boisen, N., Morabito, S., Tozzoli, R., Nataro, J. P., & Caprioli, A. (2011). Characteristics of the enteroaggregative Shiga toxin/verotoxin-producing Escherichia coli O104: H4 strain causing the outbreak of haemolytic uraemic syndrome in Germany, May to June 2011. *Euro Surveill.*, **16**: 19889.

Shahcheraghi, S. H., & Ayatollahi, J. (2013). pXO1-and pXO2-like Plasmids in Bacillus cereus and B. thuringiensis. *Jundishapur J. Microbiol.*, **6**: e8482.

Sjödin, A., Broman, T., Melefors, Ö., Andersson, G., Rasmusson, B., Knutsson, R., & Forsman, M. (2013). The need for high-quality whole-genome sequence databases in microbial forensics. *Biosecur. Bioterror*, **11**: 78-86.

Suk, J. E., Zmorzynska, A., Hunger, I., Biederbick, W., Sasse, J., Maidhof, H., & Semenza, J. C. (2011). Dual-use research and technological diffusion: reconsidering the bioterrorism threat spectrum. *PLoS Pathog,* 7(1), e1001253.

Takahashi, H., Keim, P., Kaufmann, A. F., Keys, C., Smith, K. L., Taniguchi, K., Inouye, S., & Kurata, T. (2004). Bacillus anthracis Bioterrorism Incident, Kameido, Tokyo, 1993. *Emerg. Infect. Dis.*, **10**: 117.

Tettelin, H., Masignani, V., Cieslewicz, M. J., Donati, C., Medini, D., Ward, N. L., Angiuoli, S. V., Crabtree, J., Jones, A. L., Durkin, A. S., Deboy, R. T., Davidsen, T. M., Mora, M., Scarselli, M., Margarit Y Ros, I., Peterson, J. D., Hauser, C. R., Sundaram, J. P., Nelson, W. C., Madupu, R., Brinkac, L. M., Dodson, R. J., Rosovitz, M. J., Sullivan, S. A., Daugherty, S. C., Haft, D. H., Selengut, J., Gwinn, M. L., Zhou, L., Zafar, N., Khouri, H., Radune, D., Dimitrov, G., Watkins, K., O'Connor, K. J. B., Smith, S., Utterback, T. R., White, O., Rubens, C. E., Grandi. G., Madoff, L. C., Kasper, D. L., Telford, J. L., Wessels, M. R., Rappuoli, R., & Fraser, C. M. (2005). Genome analysis of multiple pathogenic isolates of Streptococcus agalactiae: implications for the microbial "pan-genome". *Proc. Natl. Acad. Sci. U.S.A.*, **102**: 13950-13955.

Tian, D., & Zheng, T. (2014). Comparison and Analysis of Biological Agent Category Lists Based On Biosafety and Biodefense. *PloS one*, **9**: e101163.

Tucker, J. B. (Ed.). (2012). *Innovation, Dual-use, and Security: Managing the Risks of Emerging Biological and Chemical Technologies*. MIT press, Cambridge, Massachusetts.